ULTRA LOW-SPEED ANEMOMETRY

by

Robin J. Kung & G. J. Binder

Prepared under

Grant DA-AMC-28-043-65-G20

Distribution of this document is unlimited

Fluid Dynamics and Diffusion Laboratory
College of Engineering
Colorado State University
Fort Collins, Colorado

June 1967

CER66-67RJK49

ABSTRACT

An investigation of low-speed (0-2 ft/sec) anemometers is presented. First the design, the characteristics, and the calibration of a very low-speed micro wind tunnel are described. Then the principle, operation and performance of three different anemometers at these low speeds are discussed. These instruments are :

1) the hot-spot anemometer, based on the measurement of the travelling time of a hot cloud,
2) the drag anemometer which consists of a small plate mounted to the moving coil mechanism of a micro-ammeter, and
3) a constant temperature hot-wire anemometer.

The comparison of the merits and disadvantages of these instruments shows that in most instances the hot-wire anemometer is superior to the two other anemometers.

ACKNOWLEDGMENTS

The author wishes to express his sincere appreciation to his major professor, Dr. Gilbert J. Binder, Assistant Professor of Civil Engineering, Colorado State University, for his guidance during the course of this study. His valuable advice and contributions made this thesis possible.

Moreover, Dr. E. J. Plate, Associate Professor of Civil Engineering, and Dr. L. C. Bartel, Associate Professor of Physics, members of the writer's research committee, reviewed this thesis and gave many helpful comments and suggestions; for these, the author is indeed grateful.

In addition, a number of other persons played important roles in the preparation of this thesis. To them the writer wishes to express his sense of indebtedness and to offer his appreciation: to Mr. J. T. Lin of the Civil Engineering Department of Colorado State University, who helped in the collection of data; Miss Hanae Akari, who traced the figures; Mrs. Joella Matthews, who typed the text; Mr. Duayne Barnhart and Mrs. Lilah Roberts, who assisted in the reproduction of the final paper.

Financial support for research was provided by the Integrated Army Meteorological Wind Tunnel Research Program under Grant DA-AMC-28-043-65-G20 and is here gratefully acknowledged.

Finally the author's most deeply felt thanks go to his wife, Theresa, for her understanding, when research required many hours away from home, and for her patience, while this thesis was in progress.

TABLE OF CONTENTS

TABLE OF CONTENTS - Continued

TABLE OF CONTENTS - Continued

TABLE OF CONTENTS - Continued

LIST OF TABLES

LIST OF FIGURES

LIST OF FIGURES - Continued

LIST OF FIGURES - Continued

LIST OF SYMBOLS

Symbol	Definition	Dimensions
A	Cross section area of tunnel	ft^2
A_1	Area of control section	ft^2
A_2	Area of test section	ft^2
a	Distance between hot-spot wire and resistance thermometer	inch
b	Temperature coefficient of electric resistance of wires	$^0F^{-1}$
C	Conversion constant	
C_p	Specific heat at constant pressure	joules/gm^{0}C
d	Wire diameter	inch
E	Hot-wire anemometer output	volt
$E(U)$	Hot-wire anemometer output at velocity U	volt
E_w	Voltage across wire	volt
e	Bucked hot-wire anemometer output	mv
g	Acceleration of gravity	ft/sec^2
H	Heat	cal
h	Heat transfer coefficient	watt/in^2 ^{0}F

LIST OF SYMBOLS - Continued

Symbol	Definition	Dimensions
Δh	Dynamic head in mm of Hg	mm
I	Hot-wire current	amp
I_o	Balance current of drag anemometer in absence of flow	amp
$I(U, \beta)$	Balance current of drag anemometer in velocity U and angle of attack β	amp
K	Thermal conductivity	watts/in.°F
ℓ	Wire length	inch
Nu	Nusselt number	
n	Speed of a rotating wheel	RPM
Pr	Prandtl number	
Δp	Pressure difference	lb/ft^2
R_e	Reynolds number	
R_g	Wire resistance at room temperature	ohm
R_o	Wire resistance at 0°C or 32°F	ohm
R_w	Working resistance of hot wire	ohm
r	Radius of heat cloud	inch
s	Radius of sphere	inch
t	Transient time of heat pulse	sec
U	Velocity	ft/sec

Symbol	Definition	Dimensions
V_1	Local velocity at control section	ft/sec
$\overline{V}_1$	Mean velocity at control	ft/sec
V_2	Local velocity at test section	ft/sec
$\overline{V}_2$	Mean velocity at test section	ft /sec
V_{c1}	Velocity at center of control section	ft/sec
V_{c2}	Velocity at center of test section	ft/sec
y	Rising distance of a heat cloud	cm
α	Thermal diffusivity	ft^2/sec
α	Ratio of mean velocity to the velocity at center	
β	Angle of attack	degree
γ	Angle of attack	degree
θ	Temperature	^0F
θ_g	Gas temperature	^0F
θ_w	Wire temperature	^0F
ρ	Wire density	gm/cm^3
ρ_{air}	Density of air	$slug/ft^3$
ρ_{Hg}	Density of mercury	$slug/ft^3$
σ^{-1}	Wire resistivity	ohm - inch
τ	Time constant of resistance thermometer	sec

Chapter I

INTRODUCTION

The investigation of mountain lee waves undertaken at the Fluid Dynamics and Diffusion Laboratory of Colorado State University required the measurement of very low velocities in air typically less than 2 ft/sec. In order to perform these measurements, an appropriate instrument was first developed and the calibration of this instrument would later have to be checked from time to time.

The large wind tunnel of the laboratory was first used to carry out the task of developing an anemometer. When the instrument had to be calibrated, the need for a primary velocity standard arose. Since the differential pressure produced by a pitot tube placed in an air stream of less than 2 ft/sec is too small to be accurately measured even with the most sensitive pressure gage, it was necessary to devise another technique. This primary velocity was then obtained by measuring the time it would take a soap bubble or smoke puff to travel a certain distance. This technique was very time consuming. In addition, the wind speed in the tunnel was not perfectly stable at velocities below 2 ft/sec and it was very difficult to set it at a precise value. Finally, it appeared somewhat wasteful to tie up this large wind tunnel just to place a small anemometer in it.

These considerations pointed to the need of a special wind tunnel for the purpose of low-speed anemometer testing and calibration. This wind tunnel could be quite small in size and therefore inexpensive to build.

This study divides then into two main parts. The first one describes the production of low speed flow veins and measurements of the reference velocity herein, one section being devoted to the initial experiments performed in the large wind tunnel and another section to the design and performance of the special purpose tunnel. In the second part are reported the investigations of three low-speed anemometers which were carried out in these wind tunnels.

PART ONE

LOW-SPEED WIND TUNNELS

Chapter II

THE LARGE WIND TUNNEL AND THE PRIMARY VELOCITY MEASUREMENT

2.1 The Large Wind Tunnel (10)

The large wind tunnel of the Fluid Dynamics and Diffusion Laboratory at Colorado State University has a test section 88-ft. long with a normal cross-sectional area 6 x 6 ft. (Figure 1).

The tunnel was designed for either closed or open loop operation for velocities ranging from 0--120 ft/sec. The fan and driving motor were, however, designed especially to provide good velocity control above 2 ft/sec. To produce velocities below this value, the speed or RPM control had to be set to the minimum and the pitch control of the fan had to be adjusted. But this adjustment is rather coarse, so that it is almost impossible to find the right setting to produce even approximately a given velocity between 0 and 2 ft/sec.

In order to improve the control of the wind speed in this range, which precisely is the range of interest of this study, two fine wire screens (50 meshes/in., 16% open area) were introduced up and downstream of the test section. The hope was that the large pressure drop across them would require the fan to be run at an RPM sufficiently above the minimum, so as to permit the use of the fan speed control for the setting of the velocity. These two screens improved the control over the wind speed below 2 ft/sec somewhat but not enough for the requirements of this investigation.

2.2 Primary Velocity Measurements

Since the dynamic head produced in a pitot tube by a velocity of 1 ft/sec is only about 4×10^{-4} mm of mercury, it could not be measured with reasonable accuracy with the "Equibar" pressure transducer since the lowest full scale of this instrument is 10^{-2} mm Hg and the accuracy of the instrument is 3% of full scale. Therefore, another technique had to be devised for the determination of the primary velocity against which the instruments under investigation could be checked.

After several trials, it was found that the best technique was to use soap bubbles and to measure their distance travelled during a certain interval of time. The bubble generator consisted of a nozzle into which a soap solution and helium were fed simultaneously. The helium supply tubing was pulsed by a cam driven clamp, the tubing itself providing the restoring force. The cam was mounted on a DC motor whose supply voltage provided the control of the pulse frequency, i.e., the rate of bubble formation.

Helium had to be used because a heavier gas-like air produced bubbles which dropped almost vertically at the low speeds mentioned. As may be seen in Fig. 2, the helium soap bubbles had a rising trajectory, but their rate of ascent was slow enough to permit determination of the horizontal velocity.

These bubbles were released in front of a grid of vertical white threads spaced 1/2 in. apart. A strobe light and a camera completed the equipment. When the bubbles were released and the strobe light was operating, time exposures were taken (Tri-x film was used). Such a photograph is shown in Fig. 2. What is actually seen is not the bubble itself but the light reflections of it.

The velocity could easily be determined from such photographs by dividing the horizontal distance between two successive images of a bubble by the time interval given by the strobe.

Although this technique is workable, it is time consuming and tedious, especially the waiting time necessary to get the films developed. It was, indeed, only with the photographs in hand that one could decide whether the desired velocities were obtained. It should be mentioned that the adjustment of the bubble generator was not as simple a matter as it would appear; photographs of the bubbles were not obtained at the first try either for they offer almost no contrast and reflections were only strong enough when the strobe light hit them from some particular angle.

Chapter III

DESIGN AND CALIBRATION OF A VERY LOW SPEED WIND TUNNEL

After the large wind tunnel had been used for some time for the investigation of the hot spot and the drag anemometers, a more efficient experimental method became more of a necessity with every day of testing. because the desired low velocities were not readily obtained and the primary velocity determination was laborious. The construction of a special purpose wind tunnel which would produce stable and controllable velocities between 0 and 2 ft/sec., and which would permit a simple, quick and independent determination of these velocities was then decided.

3.1 Principle and Design

3.1.1 Principle - The principle of the special very low speed wind tunnel (to which we shall from now on simply refer as micro-tunnel) is to expand a flow vein where the velocity is large enough to be measurable with a pitot tube into another vein of large diameter and low wind speed. The micro-tunnel is thus essentially composed of small cross sectional area A_1 followed by a test section of large cross-sectional area A_2 . If the average velocities in these sections are $\overline{V}_1$ and $\overline{V}_2$, respectively, we have from continuity

$$A_1 \overline{V}_1 = A_2 \overline{V}_2 \tag{3-1}$$

and from $A_2 >> A_1$ it follows that $\overline{V}_2 << \overline{V}_1$.

If the velocities V_1 and V_2 in the control and test sections were uniform, we would have

$$\overline{V}_1 = V_1 \text{ and } \overline{V}_2 = V_2$$

and hence,

$$V_2 = \frac{A_1}{A_2} V_1 \quad . \tag{3-2}$$

The velocity anywhere in the test section V_2 could thus very simply be inferred from the measurement of the velocity V_1 in the control section once the areas A_1 and A_2 have been determined.

In practice, however, velocity distributions are not uniform so that the relation between V_2 and V_1 is not as simple as in Eq. 3-2. For most purposes it is sufficient to relate the velocity at a fixed point C_2 in the test section, say V_{c2} , to the velocity at a fixed point C_1 in the control section, say V_{c1} . The function

$$V_{c2} = f(V_{c1}) \tag{3-3}$$

has thus to be determined.

If we let $\alpha_1 = \frac{V_1}{V_{c1}}$ and $\alpha_2 = \frac{\overline{V}_2}{V_{c2}}$ (3-4)

we have then $V_{c2} = \left(\frac{A_1}{A_2}\right)\left(\frac{\alpha_2}{\alpha_1}\right) V_{c1}$ (3-5) which is the desired relationship. α_1 and α_2 are coefficients related to the uniformity of the velocity. In particular, if V_{c1} and V_{c2} are the maximum velocities occurring in the two sections, α_1 and α_2 are smaller or equal to one; the more uniform the velocity distributions, the closer their values are to one.

3.1.2 Design - The primary design requirement for the micro-tunnel was to produce stable velocities in the test section ranging from approximately 0.1 ft/sec. to about 2 ft/sec. The velocity in the control section had to be measurable with a pitot tube, i.e., had to be at least 3 ft/sec. A secondary requirement was to keep the cost as low as possible; the tunnel size had thus to be small and standard materials and parts had to be used.

The tunnel itself was constructed out of standard "Lucite" pipe. The control section has an I.D. of 1" and the test section an I.D. of $5\frac{1}{2}$". The area ratio $\frac{A_2}{A_1}$ is thus approximately 30. The drive motor is a Ford 200 series D. C. motor with a maximum speed of 22,000 RPM. The motor is connected to a conventional D. C. power supply with adjustable output voltage which governs the speed of the motor. Two fans 2 inches in diameter are used. This required a transition from the fan to the control section. A complete sketch of the micro-tunnel is given in Fig. 3. Figure 4 is a photograph of the micro-tunnel and support instruments.

The pitot tube is made from 1/16-in. stainless steel tube. The static pressure tab is mounted on the pipe itself. The pitot tube can be moved along a diameter, and the whole control section can be rotated 90^0 so that velocity profiles can be taken along two perpendicular diameters.

The upstream part of the test section is cut into rings of different widths between which screens can be inserted. These rings are held in place by pins and four long bolts which fasten the main body of test section to control section. This construction permitted the screens to be quickly changed. Figure 5 is a close-up of the micro-tunnel. The motor, transition, control and test sections, the pitot tube and the interchangeable screens are clearly shown on this photograph.

3.1.3 <u>Flow direction</u> - It is easier to maintain a uniform velocity distribution through a contraction than through an expansion. On the other hand, if the fan is placed at the exit, it cannot impart any circular motion to the fluid neither in the test nor in the control section, since these would be upstream. It would therefore be natural to suck the air through the micro-tunnel.

However, velocities of air due to thermal gradients can easily reach 1 ft/sec. If the air was thus directly sucked into the test section, these thermal motions would appear as non-steady, irregular speeds inside the tunnel. This situation could be remedied by placing several fine mesh screens at the entrance. But owing to the pressure drop through these screens, the pressure in the test section would then be much below atmosphere. In order to avoid any large disturbance to the flow in the test section, the latter one would therefore have to be airtight. In particular, the opening, through which the instruments under test are introduced, would have to be airtight and different seals would be necessary for various instruments. This sealing problem could be quite bothersome, especially if a quick calibration were desired.

The blowing of the air through the tunnel was then found to be the better solution. First, the circular motion of the air created by the fan was easily eliminated by placing a honeycomb immediately after the blower Second, the expansion of the vein in the control section into a uniform stream in the test section by a set of screens had only to be solved once and for all. This is discussed in detail in the next section Third, the flow irregularities due to thermal motions outside would no longer be a concern since the flow at the entrance is fast and is in addition passed through screens before reaching the test section. Finally, the test section is very nearly at atmospheric pressure. The pressure drop due to friction over the 8.5 in. length at the low velocities was considered extremely small.

No special provisions for airtightness of the test section were thus necessary; it proved to be sufficient to reduce the opening with scotch tape.

3.2 Screen Arrangement

In addition to the requirements mentioned earlier, it also was desirable to obtain a velocity distribution in the test section as uniform as possible, so as to permit testing of instruments of some size and avoid having to set them precisely at a given point. On the other hand, it also was desirable to keep the total length of the tunnel to a strict minimum. It was, thence, not possible to let the flow vein issuing from the control section expand naturally, since this would roughly have required about a length of ten diameters or 50 in.

Various devices were therefore investigated which would break up the one-inch jet issuing from the control section into a uniform stream $5\frac{1}{2}$ in. in diameter over a short distance. It was anticipated that various devices may have to be tried before an adequate solution would be found. The tunnel was consequently constructed so as to permit easy and quick replacement of these parts. The solutions which were successively tried consisted of a set of non-uniform plus some fine uniform screens, diffusers with fine screens, fine and coarse screens and finally, fine mesh screens only.

3.2.1 <u>Non-uniform screens</u> - The first logical thing to do seemed to fabricate screens with increasing open area ratio from the center outward, which would thus force the flow from the center to the periphery of the pipe. Two 1/4-in. thick lucite disks were perforated with holes ranging from 1/32-in. to 1/4-in. diameter which increased with the radial distance of the holes.

These two non-uniform screens were installed in the micro-tunnel followed by a fine mesh wire screen "S" (50 meshes per inch open area 16%). The uniformity of the flow in the test section was then checked with a hot-wire anemometer. (For details on instrumentation see Chapter VI). The first velocity profile is curve a in Fig. 6.

The ordinate $e = E - E_o$ represents the anemometer reading minus the output for zero velocity. Although the actual calibration of the hot-wire anemometer (HWA) was unknown at this phase of the investigation, it was established that e was the increasing function of velocity. Thus, even though it was not possible to compute the velocity differences corresponding to the humps in curve 6a, there could be no doubt that these irregularities in the HWA output represented non-uniformities in the velocity distribution. Since we were only checking how uniform the velocity distribution was, this raw output data was all that was needed.

In order to see whether the humps in profile 6a were due to the non-uniform screens, these were then successively rotated 180^0 about an axis perpendicular to their plane. The resulting profiles are shown in Fig 6, curves b, c and d. These show that some of the irregularities were due to these screens.

To improve the flow uniformity, three of the fine screens "S" were introduced into the tunnel. The profiles obtained with this set-up show a marked improvement compared to the previous ones. They are clearly independent of the particular orientation of the non-uniform screens.

Next, four S - screens were inserted instead of three. To our surprise, see Fig. 7, the orientation of the non-uniform screens still seemed to affect the velocity profile. What actually happened was that during the change in orientation of the non-uniform screens some of the uniform S - screens were turned also. The differences among profiles a, b, c of Fig. 7 are certainly due to the latter ones. Yet, at that time we did not suspect this to be due to the S - screens.

3.2.2 <u>Diffusers</u> - Next, it was thought that improved uniformity of velocity in the test section might be obtained by breaking up the 1-in. jet in a "diffuser". This device consisted of a short piece of 1-in. pipe which extended the control section into the test pipe, whose downstream end was closed and whose lateral surface was perforated with small holes. Through the diffuser the flow was thus changed from axial to radial.

The first diffuser had 1/8" diameter holes and gave worse results than the non-uniform screen.

The second diffuser had 1/16 " diameter holes. The velocity distribution obtained with two and three fine S - screens are shown on Fig. 8. Besides the near perfect symmetry, one notices the good uniformity obtained with three screens. The problem seemed thus solved, except that the large head loss through the diffuser had reduced the velocity range that could be obtained by one third, so that the diffuser had to be abandoned.

3.2.3 <u>Uniform screens only</u> - Tried next and last were uniform wire screens only. With three or four S-screens (50 meshes per in., 16% open area) the velocity profiles were nearly uniform sometimes. Yet in some cases they had a very pronounced hump. This was rather puzzling, since all the screens were cut out of the same roll of material.

A coarser screen (open area 50%) was substituted for the last fine S-screen without notable result. The distances between the screens had no effect either on the velocity distribution as shown in Fig. 9.

It appeared then that some of the S-screens were the cause of some of the observed oddities. Their orientation was then systematically changed by rotating them one at a time 180^0 about an axis perpendicular to their plane (i.e., the tunnel axis). The results of Fig. 10 demonstrate the marked effect these screens have on the velocity distribution in the test section. The influence of the fourth screen is dominant as shown by the difference in shape of curves a) and b). The first and second screens only have mirror effects on the profile as shown by curves d) and e) compared to c).

All the S-screens seemed to be quite uniform to the naked eye and under the microscope. The skewness of profile b) seems difficult to explain. Yet it is not impossible that there could be a small but systematic change in open area ratio from one part of the screens to the other. The larger head loss through the tighter parts of the screens entails smaller velocities in this region.

It does not appear that the skewness of profile b) can be attributed to the bundling up in irregular fashion of several small jets through the screen holes into a larger jet which was shown by Bradshaw (2) to create uneven velocity distributions behind screens with less than 50% open areas. In our case, indeed, random irregularities were not obtained but a large scale distortion was obtained in the velocity profile.

3.2.4 Conclusion - From the various attempts to produce a uniform velocity distribution in the center region of the test section, it was found that this could be achieved by use of a diffuser and some S-wire screens and use of four of these screens alone if these were properly selected. Since with this later solution, the velocity range that could be covered with the existing motor and fan was adequate while it was appreciably reduced with the diffuser. The final screen arrangement chosen was, of course, that which gave the largest region of uniform velocity in the test section and this is the arrangement of profile c) in Fig. 10.

3.3 Calibration Procedure

Before the micro-tunnel could be used, the relationship between the velocities at points C_1 and C_2 in the control and test section, respectively, had to be determined. It was, of course, quite natural to take C_1 and C_2 at the center of the two sections. The relationship would, of course, hold at any other points where velocities were the same as the centers. Especially if the velocity in the center region of the test sections is uniform, the location of C_2 is no longer critical; and this is why much effort went into finding the arrangement that would produce the best uniformity in velocity.

As shown in section 3.1.1, the relationship between V_{c1} and V_{c2} is determined once the coefficients α_1 and α_2 are known. It should be pointed out that these coefficients themselves depend on the average velocities, say $\alpha_1(\overline{V}_1)$ and $\alpha_2(\overline{V}_2)$. These coefficients can be computed from their definition

$$\alpha = \frac{\overline{V}}{V_c} \qquad \text{and} \qquad \overline{V} = \frac{1}{A}\int_A V\,da \tag{3-6}$$

once the velocity distributions are known. Since V_1 is measurable by the pitot tube, the velocity distributions in the control section can be obtained without difficulty.

However, in order to measure velocity distributions in the test section, a calibrated instrument capable of measuring low velocities was theoritically necessary. But, the purpose of the tunnel was precisely to study and calibrate anemometers at these velocities, so that we were apparently in a vicious circle. This difficulty was surmounted by an iteration procedure as follows:

First, α_2 was assumed equal to one for all velocities (case of a perfectly uniform velocity across the entire section), from which it followed according to Eq. 3-5.

$$V'_{c2} = \left(\frac{A_1}{A_2}\right) \alpha_1 \, V_{c1} \tag{3-7}$$

where V'_{c2} is an approximate value of the velocity in the test section. From this an approximate calibration curve, say C' , for the hot-wire anemometer could be inferred.

Then, by using this first approximation calibration curve C' and a set of profiles of HWA output, a set of new values for α_2 , say $\alpha''_2(\overline{V}_2)$, could be calculated. With these, the new relationship

$$V''_{c2} = \left(\frac{A_1}{A_2}\right) \frac{\alpha_1}{\alpha''_2} V_{c1} \qquad (3\text{-}8)$$

yielded the second approximation calibration curve C'' for the HWA.

The same procedure was repeated until two successive sets of α_2's and calibration curves were identical. These then were the final coefficients and the final calibration curve.

One can easily guess that the more uniform the velocity distributions in the test section, or the closer to one the actual values of α_2 are, the faster the process converges. On the other hand, if the "bucked" HWA output $e = E - E_o$ would be exactly proportional to the velocity

$$V_2 = k\,e \ , \qquad (3\text{-}9)$$

it would follow at once that

$$\alpha_2 = \frac{1}{A_2 e_{c2}} \int_{A_2} e\,da \qquad (3\text{-}10)$$

$$= \frac{\overline{e}_2}{e_{c2}} \ .$$

Consequently, the closer the calibration curve e vs V_2 would be to a proportionality relationship, the faster the convergence would be again. Since these properties could both be approximately established from the profiles e vs V_2 , we were assured that the process would converge rapidly.

3.4 Instrumentation

3.4.1 Velocity measurement in the control section - The dynamic pressure head from the pitot tube in the control section was measured with an "Equibar" Type 120 pressure transducer manufactured by Transonics Inc. The "Equibar" has full scales ranging from 0.01 to 30 mm Hg. It is provided with a meter which permits direct reading and with an output for external recording or reading. The output voltage is 30 mv for full scale (Figure 11).

This output was generally fed into a Moseley (Type 135) x - y Plotter (Figure 11). It provided the y-deflection to the plotter, the x-deflection was set manually proportionately to the radial position of the pilot tube. In this way a direct plot of the dynamic head vs radial distance was obtained and allowed a visual check of the regularity of the results.

From Bernouilli's equation one has

$$V_1 = \sqrt{\frac{2g\ \rho_{Hg} C\ \Delta h}{\rho_{air}}} \tag{3-11}$$

where Δp = pressure differential, lb/ft^2

ρ_{air} = density of air, $slug/ft^3$

ρ_{Hg} = density of mercury, $slug/ft^3$

C = conversion constant = $1/304$

Δh = dynamic head in mm Hg read from the Equibar

g = acceleration of gravity = $32.2\ ft/sec^2$.

For an atmospheric pressure of 24.75 inches of Hg and at room temperature of 25^0 C , $\rho_{air} = 1.895 \times 10^{-3}$ slugs/ft³ and hence,

$$V_1 = 54 \sqrt{\Delta h} \quad . \tag{3-12}$$

As the pitot tube was traversed, its position was determined with a height gage which could be read to the nearest 1/1000 in.

3.4.2 <u>Velocity measurements in the test section</u> - Velocities in the test section were measured with a Disa (Model 55 A01 - Fig. 11) constant temperature hot-wire anemometer (abbreviated HWA). In order to improve the accuracy of the HWA reading, a so-called "bucking" or "zero-suppression" system was used. This is explained in detail in Chapter VI.

The hot-wire probe was traversed through the test section with a depth gage on which the position could be read to the nearest 1/1000 ft.

3.4.3 <u>Data collection</u> - In order to take into account some residual irregularities in the velocity profiles, it was decided to take two profiles along orthogonal diameters for every velocity in both the control and in the test section. Because of convenience, all vertical profiles and then all horizontal profiles were taken.

While a profile was measured in the test section, the output from the pitot tube was recorded on air x-y plotter in order to insure that the flow remained stationary and vise versa. This was necessary because the motor would drift at times. Conversely, when measurements were taken with the pitot tube in the control section, the HWA of the test section was used as reference.

3.5 Results and Computation

3.5.1 Data - The velocity profiles in the control section are shown in Figs. 12 and 13. These profiles are quite uniform and symmetric.

The profiles e vs r for the test section are shown in Figs. 14 and 15. From these figures one sees that the velocity distributions in the test section are thus not exactly symmetric with respect to the section axis. The values of α_2 will thus depend on whether the horizontal or vertical profile is chosen. In order to approximate the true values of α_2, the computations were done with both profiles and the average taken.

3.5.2 Computations

3.5.2.1 Values of α_1

The computation of these coefficients is straight forward since the actual values of the velocities are known.

From equation 3.6 ,

$$\alpha_1 = \frac{\overline{V}_1}{V_{c1}}$$

$$\overline{V}_1 = \frac{1}{A_1} \int_{A_1} V_1 \, dA \qquad (3\text{-}13)$$

$$\overline{V}_1 = \frac{2\pi}{A_1} \int_0^{0.5} V_1 \, r dr \qquad (3\text{-}14)$$

For example, Table 1 is the computations of α_1 for the curve H_2 of Fig. 13. The velocity used at any particular value of r is the average of four measurements taken in pairs on horizontal and vertical diameters.

The values of α_1 are shown in Fig. 16.

3.5.2.2 Values of α_2

Since $$\alpha'_2 = \frac{2\pi}{A_2} \int_0^a rV_2 dr \, , \qquad (3\text{-}15)$$

the computation of α_2 and V_{c2} was according to the iteration method in Section 3.3. For example, Table 2 gives the computation of α_2 and V_{c2} for the data curve H_2 of Fig. 15.

The variations of α_2 and V_{c2} at the various stages of the iteration are given in Table 3. It is seen that the final value is reached after the second iteration.

The final value of α_2 are shown in Fig. 17. The systematic difference between the coefficients computed from the horizontal and vertical profiles are clearly seen on this plot. The true value of α_2 is taken as the mean of the two values for a given V_{c2} and a smooth curve was drawn through these points. The least accurate values of α_2 are those for the lowest velocity, because it depends on the interpretation of the calibration curve between the point of zero velocity and the maximum velocity of this profile.

3.5.3 Calibration curve of micro-tunnel - The calibration curve of the micro-tunnel as calculated from Eq. 3-5 is shown on Fig. 18. This curve gives the velocity at the center - or the center region - in the test section as a function of the velocity at the center of the control section.

3.5.4 Check of micro-tunnel calibration curve - A calibration facility with a rotating arm is available at the FDD Laboratory. By measuring the RPM n and the length of the rotating arm L, the velocity V of probe attached to it may easily be determined:

$$V = \frac{2\pi}{60} nL \quad .$$

The velocity is changed by shifting the driving belt to pulleys of different diameters.

Two difficulties, however, complicate the use of the rotating arm device. First, the sliding contact which is a graphite brush introduces an extraneous resistance of about four ohms into the hot-wire arm of the HWA bridge. This resistance is as large as that of the hot wire itself. It thus decreases the sensitivity of the anemometer and makes the balance of the bridge rather difficult. This difficulty was overcome by letting the cable connecting the hot-wire probe to the instrument wind around the shaft of the rotating arm, so that no sliding contacts were necessary. This was possible because the arm was turning slowly and a few revolutions were sufficient for one measurement.

The second difficulty is also inherent to any rotating device. Indeed, the motion of the probe induces motions in the air of the tank which do not readily die out. These residual velocities of the air show up as rather large fluctuations in the HWA output. In order to get a good average, several measurements have to be taken.

In order to check the calibration curve of the micro-tunnel, a hot wire was calibrated with both the rotating arm device and with the micro-tunnel. Since all points fall on the same line as shown in Fig. 19, the micro-tunnel calibration obtained through the iteration procedure is conclusively confirmed. The accuracy of this calibration may from this check be estimated to be better than $\pm 1\,\%$.

3.6 Conclusion

The micro-tunnel constitutes a very useful and convenient tool for investigating and calibrating low-speed anemometers. The velocity at the center of the test section may be inferred from that at the center of the control section (see Fig. 18) which may be measured with a pitot tube. This velocity may be varied continuously from 0 to 1.6 ft/sec.

PART TWO

LOW-SPEED ANEMOMETERS

Chapter IV

THE HCT-SPOT ANEMOMETER

4.1 Principle and Method of Measurement

The principle of the hot-spot anemometer (abbreviated HSA) is based on the very definition of the velocity as the soap bubble technique is. It consists in "tagging" an air parcel and to clock it at two successive points of passage. In this case an air parcel is heated, whence the name "hot-spot anemometer".

The "hot spot" is generated by sending a short but intense current through a thin wire which is thus heated and which in turn heats the air which passes over it during this time. The passage of the hot spot is detected with a platinum wire thermometer. Here the hot spot was clocked between the instant of its release and its passage over the thermometer. If the distance a between the heat source wire and the thermometer is known, and if the time t between the release of the current pulse and the detection of the hot spot by the thermometer is measured, the velocity V of the air flow is

$$V = \frac{a}{t} \quad . \tag{4-1}$$

This method bears some similarity to the heat-wake velocity measurements of Kovasznay (7) and Sato (11). Both Kovasznay and Sato made use of a sinusoidal heat source current and the velocities were around 14 ft/sec. The HSA discussed here is the same as the one presented by Bauer(11) who, however, used his instrument in much faster flows (47 ft/sec).

The sensor of the HSA is shown in Fig. 20. It consists of a heat source wire and an ultra thin platinum wire which serves as a thermometer, the temperature being sensed by the change in electrical resistance of this wire. These two wires are held parallel and normal to the flow.

The heating current pulse and the subsequent response of the platinum thermometer amplified one thousand times are displayed on the oscillogram of Fig. 21a. Although the vertical scales for the two signals are different, the time scale is the same. The striking feature of this photograph is the great difference in width between the heating pulse and the response curve of the thermometer. The first curve had a duration of about one m sec; whereas, the second extends over about 20 m sec. The causes of this twenty-fold stretch are the thermal inertia of the heating wire, the heat diffusion of the hot cloud during its transit from one wire to the other, and the imperfect time response of the thermometer.

The influence of these effects, as a function of the transit time, is strikingly displayed by the oscillograms of Fig. 22. These are the various responses of the Pt-thermometer to the same pulse and for the same distance as for various velocities. As we have seen, these response curves are not simply shifted to the right (larger transit time) as the velocity is decreased, but the amplitude of the maximum decreases and the curves become broader mainly because of diffusion.

The question which arises then is what is the time of transit of the hot cloud from the heating to the thermometer wire? Is it the time between maxima, the time between the starting points of the two signals, or is it some time in between?

In order to make the time measurements easier, it also was desirable to use an electronic counter, since otherwise one would have to use the oscillograms and measure the time graphically from them. The counter is equipped with "start" and "stop" triggering inputs with separately adjustable levels, i.e., the time measurement may be started and stopped by electric pulses. Since the slopes of the heating pulse are vertical for all practical purposes (see Fig. 23), the starting time is nearly independent of the triggering level. But for the "stop" triggered by the thermometer output, the time will depend on the triggering level. This is best seen as sketch in Fig. 21b, where e_1 and e_2 designate the triggering levels and t_1 and t_2 the corresponding time intervals. The electronic counter could also be triggered on the negative slope since it has a switch with $\pm$ slope.

The slope of the thermometer response curve may be steepened by increasing the amplification. Figure 24 is an oscillogram of the heat pulse and the thermometer output amplified here 10^6 times. It is seen that the positive slope of the thermometer response curve is now almost vertical. The flat portion of this curve is due to the amplifier cut-off. The wiggles between the two pulses are due to the background noise, appreciable now because of the high amplification.

The large amplification provides us thus with a well-defined $\pm$ slope for stopping the time measurement of the counter. With this technique, may the HSA be used without calibration, i.e., are the thermal inertia and diffusion effects small enough to be neglected? Figure 25 shows that this is not the case. If these effects were small these curves should all fall along a 45^0 straight line passing through the origin. Before the hot-spot anemometer can be used without preliminary calibration, these corrections have to be calculated in order to get velocity measurements of acceptable accuracy. The corrections are discussed in the following sections.

The measurements of Figs. 26 and 27 were taken in the large wind tunnel. The reference velocity of the first set of data was provided by a pitot tube. Figure 27 gives results of a low velocity where the primary velocity measurement was by the soap bubble technique.

4.2 Corrections for the Hot-Spot Anemometer

4.2.1 Diffusion of the heat cloud - The data of Fig. 25 were taken with a heat pulse of 0.15 m sec duration. Since the smallest transit time t of the hot cloud is 3 m sec (velocity of 2 ft/sec, a = 0.069 in.) it is also at least twenty times longer than the duration of the pulse. The heating pulse may as a first approximation be considered as an instantaneous point source.

Consider the fluid at rest and assume a large amount of heat generated at time $t = 0$ at the origin of a set of rectangular axes. After an interval of time t, the hot point has grown into a cloud by diffusion. The differential equation of heat diffusion is

$$\nabla^2\theta = \frac{1}{\alpha}\frac{\partial\theta}{\partial t} \tag{4-2}$$

where α is the thermal diffusivity (ft^2/sec.). Assuming spherical symmetry and substituting $\Theta = \theta r$ into equation 4.2,

$$\frac{\partial \Theta}{\partial t} = \alpha \frac{\partial^2 \Theta}{\partial r^2} \quad . \tag{4-3}$$

The boundary conditions are

$$\Theta = \theta_i r \qquad \text{when } t = 0,\ 0 < r \leq s$$

$$\Theta = 0 \qquad \text{when } t = 0,\ r > s$$

$$\Theta = 0 \qquad \text{when } t = 0,\ r = 0$$

where s is the radius of a very small sphere, which is supposed to be suddenly brought to the temperature θ_i at the time $t = 0$. The general solution of Eq. 4-3 is (6)

$$\Theta = \frac{\theta_i}{2\sqrt{\pi \alpha t}} \int_o^s r' \left[e^{-\frac{(r-r')^2}{4\alpha t}} - e^{-\frac{(r+r')^2}{4\alpha t}} \right] dr' \quad . \tag{4-4}$$

By expanding the integrand in powers of r' and assuming s to be small, the following approximate solution is obtained (6):

$$\theta = \frac{\theta_i \, s^3}{b\sqrt{\pi \alpha^3 t^3}} \, e^{-\frac{r^2}{4kt}} \left[1 + \left(\frac{n^2}{kt} - 6 \right) \frac{s^2}{40kt} \right] \quad . \tag{4-5}$$

The initial heat introduced is

$$H_i = \frac{4}{3} \pi s^3 \rho \, C_p \, \theta_i \quad . \tag{4-6}$$

When this expression is substituted into Eq. 4-5 and $s \rightarrow 0$, Eq. 4-5 becomes

$$\theta = \frac{H_i}{\rho \, C_p (4 \pi \alpha t)^{3/2}} \, e^{-\frac{r^2}{4\alpha t}} \quad . \tag{4-7}$$

This equation describes thus the temperature distribution of a three-dimensional hot cloud t seconds after the heat H_i has been introduced at the origin.

Now let us find the relation between the pairs (r_1, t_1) and (r_2, t_2) corresponding to the same temperature θ_o. Hence, by definition

$$\theta_o = \frac{H_i}{\rho C_p (4\pi\alpha t_1)^{3/2}} e^{-\frac{r_1^2}{4\alpha t_1}} \qquad (4\text{-}8)$$

$$\theta_o = \frac{H_i}{\rho C_p (4\pi\alpha t_2)^{3/2}} e^{-\frac{r_2^2}{4\alpha t_2}}$$

from which it follows that

$$\frac{r_1^2}{t_1} - \frac{r_2^2}{t_2} = 6\alpha \ln \frac{t_2}{t_1} \qquad (4\text{-}9)$$

For air at room temperature, $\alpha \approx 2.2 \times 10^{-3}$ ft²/sec. If $\frac{t_2}{t_1}$ is of the order of one, it follows that the right-hand side is of the order of 10^{-3}. If $r_1 \approx 10^{-2}$ ft and $t_1 \approx 10^{-2}$ sec and if r_2 and t_2 are of the same order, one may as a first approximation write

$$\frac{r_1^2}{t_1} = \frac{r_2^2}{t_2} \qquad (4\text{-}10)$$

or

$$r_2 = r_1 \sqrt{\frac{t_2}{t_1}} \; .$$

Let us apply this result to the HSA. If the heating current pulses are identical, then H_i is the same for any heat cloud. In addition, if the triggering level for the stop input to the counter is kept the same, the counting time will always be stopped when the Pt - resistance wire reaches the same temperature.

With these conditions satisfied, suppose that the time t_1 is measured in the absence of flow. t_1 is then the time it takes for the temperature at the position of the Pt-wire, i.e., at a distance $r_1 = a$, where a is the distance between the two wires to reach the temperature θ_o by diffusion alone.

In the presence of flow, the center of the hot cloud is entrained by the velocity U . Now the temperature of Pt-wire reaches the value θ_o after a time t_2 . During this time the center of the cloud will move a distance Ut_2 and because diffusion will spread the temperature θ_o to a distance r_2 . The sum of these two distances is equal to the spacing a between the two wires.

$$Ut_2 + r_2 = a \quad . \tag{4-11}$$

Since according to relation 4.10 ,

$$r_2 = a\sqrt{\frac{t_2}{t_1}} \quad ,$$

it follows that

$$v = \frac{a}{t_2}\left(1 - \sqrt{\frac{t_2}{t_1}}\right) \quad . \tag{4-12}$$

The term $\sqrt{\frac{t_2}{t_1}}$ is the correction term due to diffusion. Let us repeat that t_1 simply is the time measured in the absence of flow, and t_2 the time measured in the presence of flow with the electronic counter, everything else remaining the same, i.e., the heat pulse and the counter settings.

4.2.2 <u>Buoyancy of the heat cloud</u> - Since the heat cloud is lighter than the surrounding air, it has a rising trajectory. Moreover, since different particles of the same cloud are at different temperatures, the buoyancy force acting on them is different. The situation is therefore quite complicated. As a first approximation we shall neglect the deformation of the cloud due to the varying buoyancy.

The rate of ascension of the hot spot was measured in the absence of ambient flow by rotating the two probes so as to have the Pt-wire above the heat source wire. With a storage oscilloscope, oscillograms of heating pulses of various amplitudes and the response of Pt-thermometers were taken for heating pulses of varying amplitude (see Fig. 28). The same experiment was repeated for several wire spacings.

The speed of ascension of the hot spot was then computed from the time it took for the wire to reach the maximum temperature. This speed depends on the amplitude of the heating current pulse, since the hotter the initial temperature the larger the buoyancy force. The results are shown in Fig. 29.

The correction introduced for diffusion has then to be changed in the following way: the distance r_2, which accounts for the diffusion of the heat cloud while it is being corrected, must be changed to the horizontal distance $\sqrt{r_2^2 - y_2^2}$ where y_2 is the rise of the hot spot during the time t_2 . On the other hand, when t_1 is measured, the cloud will have risen a height y_1 , so that the distance r_1 has to be changed to $\sqrt{a^2 + y_1^2}$. This is illustrated in Figs. 30a and 30b. Hence, Eq. 4-11 becomes:

$$Ut_2 + \sqrt{r_2^2 - y_2^2} = a$$

and Eq. 4-10 becomes

$$r_2 = \sqrt{\frac{t_2}{t_1}(a^2 + y_1^2)}$$

so that

$$U = \frac{a}{t_2} - \frac{1}{t_2}\sqrt{\frac{t_2}{t_1}(a^2 + y_1^2) - y_2^2} \quad . \tag{4-13}$$

This relation accounts for both diffusion and buoyancy effects. The values of y_1 and y_2 may be read from Fig. 29.

4.2.3 <u>The time constant of the platinum resistance thermometer</u> - The response of the resistance thermometer element is given by the differential equation (3)

$$t\frac{d\theta}{dt} = \theta - \theta_e \quad . \tag{4-15}$$

θ_e is the original equilibrium temperature of the wire. The constant τ is the time constant of the resistance thermometer. The value of τ can be calculated from

$$\tau = \frac{1}{\frac{K}{\rho C_p}\left(\frac{\pi}{\rho}\right)^2 + \frac{4}{d^2}\frac{h_d}{\rho C_p} - \frac{\sigma^{-1}}{\rho C_p}\left(\frac{4}{\pi d^2}\right)^2 I^2} \quad . \quad (4\text{-}16)$$

For a 0.000025-inch diameter, 90% Pt. -10% Re wire, the time constant is 50 microseconds (page 15, Figure 9b of ref. 3).

In the HSA study, when the distance a between two wires is larger than 0.06" the measured time t_2 is of the order of 10 milli-seconds for the velocities under consideration. The response of the Pt-thermometer is therefore sufficiently fast for the HSA used at low velocities and no correction needs to be introduced for this effect.

4.3 Instrumentations of HSA

The micro-wind tunnel, which was described in Chapter III, was used to calibrate the hot-spot anemometer.

The resistance thermometer (a wire 2.5 10^{-5} in. diameter and 0.06 in. in length, with 900 ohms of 90% Pt.-10% Rh.) was balanced by a Wheatstone bridge (see Fig. 31). A circuit diagram of the Wheatstone bridge is shown in Fig. 32. To balance the bridge, a decade resistance was used (Fig. 31). The terminals of the bridge output were connected to a low level pre-amplifier (Tektronix type 122, max. gain 10^3). In order to obtain gains higher than 10^3, two such amplifiers were used in series. A Hewlett Packard (type 523 B) counter and a Tektronix (type 564) dual beam oscilloscope were used to obtain reliable triggering of the counter. The amplitudes of the triggering signal had to be at least 1 volt.

The heat pulse was produced by a pulse generator through a heat source wire. The heat source wires were 8 ohms 80% Pt.-20% Ir. wire, 0.0004 in. in diameter and 0.07 in. in length. Their resistances were about 8 ohms.

The current-pulse generator was designed at the electronics shop of the F.D.D. laboratory by Mr. C. Finn. Its circuit diagram is shown on Fig. 33. Both the magnitude and the duration of a pulse could be adjusted. The shortest heating pulse (0.15 m sec. duration) of maximum amplitude was used. Since the negative slope of the heat pulse (see Fig. 34) was nearly vertical, it was used for the "start" triggering of the counter.

The block diagram of the HSA instrumentation is shown in Fig. 35.

4.4 Experimental Procedure and Results

After the probes were set in the micro-tunnel and the instruments were warmed up, the triggering levels to the counter had to be adjusted. The heating pulse was set to minimum width and maximum amplitude. The only setting that was subsequently changed was that of the velocity in the micro-tunnel.

The time t_1 , i.e., for $U = 0$, was first measured and then various times t_2 corresponding to different velocities were measured. The time for any particular velocity was determined several times and the average of these values was taken as true value.

The computations of the corrections outlined above are summarized in Tables 4 to 7. The corrected results are shown in Fig. 36. The improvement of these results over those of Fig. 25 is very clear. See the points corrected for diffusion and buoyancy force on one curve which approaches the ideal 45^0 straight line at higher velocities with these corrections. The velocity predicted by the HSA is 10% below the true value at 0.5 ft/sec. This error is smaller for large velocities, but larger for small velocities. One notices on Fig. 36 that most of the points lie below the ideal 45^0 line whereas the uncorrected data curves of Fig. 25 are way above this line. In other words, the data is over-corrected and no reason to explain this fact could be found. One may notice that at low velocities the "correction" is two to three times the magnitude of the resulting velocity. It is clear from Tables 4 to 7 that U is a small difference of two large numbers. The first and second term of

Equation 4-13 for instance 16.63 and 12.5 cm/sec, yields a velocity of 4.13 cm/sec for a true velocity of 6 cm/sec. An error on the correction term results on a three-fold error on the velocity.

The advantage of the HSA that should be stressed is that no calibration is necessary if an accuracy of 10% is sufficient. If the HSA is directly calibrated against a primary standard (such as the micro-tunnel), its accuracy is of the order of a few percent if the flow is horizontal. If the flow direction in a vertical plane is unknown, the performance of this instrument would be less owing to the rising trajectory of the hot spot.

Chapter V

THE DRAG ANEMOMETER

This anemometer was described in the Journal of Scientific Instruments (5). It appeared to be a simple and inexpensive instrument capable of measuring very low velocities and may be of velocity angles.

5.1 Working Principle

The drag anemometer consists of micro-ammeter and a long and thin piece of stainless steel tubing (5.5 in. in length) fixed on the moving coil mechanism onto which a small mica plate (3/4" x 3/4") is glued. A system of counter weights is added to balance the whole moving part (Fig. 37).

If the plate is set into an air stream,the drag on the mica plate produces a torque about the coil axis. The torque balance may then be restored by sending an adequate current through the coil. The intensity of this current is, of course, a function of the velocity and of the angle between the plate and the velocity.

5.1.1 Measurement of wind direction - Let $I(U, \beta)$ designate the current needed to balance the drag anemometer in a flow with mean velocity U and angle of attack β . It is reasonable to assume that the dependence on β is the same for all velocities. Then ,

$$I(U,\beta) - I_o = f(\beta)\, g(U) \quad . \tag{5-1}$$

where I_o is the current required to maintain the needle at the mid-point of the dial plate in the absence of flow or in a flow, but with the plate parallel to it. Also ,

$$I_o = I(U, \pi/2) = I(0, \beta) \tag{5-2}$$

If the angle of attack changes from β to γ and if U remains unchanged, then

$$I(U, \gamma) - I_o = f(\gamma)\, g(U) \quad . \tag{5-3}$$

Next, if we let $\beta + \gamma = \pi/2$, Eq. 5-3 can be rewritten as:

$$I(U, \pi/2 - \beta) - I_o = f(\pi/2 - \beta)\, g(U) \quad . \tag{5-4}$$

Equation 5-1 divided by Equation 5-4 yields

$$\frac{I(U, \beta) - I_o}{I(U, \pi/2 - \beta) - I_o} = \frac{f(\beta)}{f(\pi/2 - \beta)} = F(\beta) \tag{5-5}$$

or

$$\beta = G\left[\frac{I(U, \beta) - I_o}{I(U, \pi/2 - \beta) - I_o}\right] \quad . \tag{5-6}$$

Since all the quantities on which G depends can be measured, once the function G is known, β may be calculated from the measurement of I for two perpendicular orientations of the plate.

Of course, one expects to find that the cosine law approximately holds, i.e.,

$$f(\beta) \approx \cos\beta .$$

Hence, for $\gamma + \beta = \pi/2$

$$f(\pi/2 - \beta) \approx \sin\beta$$

and

$$F(\beta) = \text{cotan}\,\beta$$

$$G(\beta) = \text{cotan}^{-1}\,\beta$$

The angle could, of course, also be determined by determining the position for which the drag is maximum. But this technique would be slow and tedious because the curve $\left[I(U, \beta) - I_o\right]$ vs β would have to be determined point by point. At each position the anemometer has, indeed, to be balanced "by hand" so that the curve $I(U, \beta) - I_o$ vs β cannot be continuously recorded. The method given above only requires the measurement of I for two positions of the plate.

5.1.2 <u>Magnitude measurement</u> - Once the angle of attack is determined by the method of preceding section, the drag anemometer is rotated in order to make $\beta = 0$. The current $I(U, 0)$ is a function of velocity U only, or

$$U = h\left(\frac{I_{\beta = o}}{I_o}\right) \tag{5-7}$$

since I_o is constant. The function h may be determined by direction calibration of the instrument.

5.2 Instrumentation

The instrumention required by this anemometer is extremely simple. The balancing current was supplied by a 3 V battery, was adjusted by a 10K pot, and read on a milliammeter.

The drag anemometer was mounted on a rotating actuator geared to a potentiometer for the angle readings. Use of the rotator facilitated directional calibration.

5.3 Results

Some measurements with the drag anemometer were taken in the large wind tunnel. Figure 38 shows the results of direction measurements. Because of the difficulty of getting readings when the angle of attack β was between 30^0 - 70^0 and because of the instability of the large wind tunnel at low velocities (1.35 ft/sec), these direction measurements did not produce satisfactory results. Figure 39 gives the calibration curve of the drag anemometer in the large wind tunnel. The reference velocities were provided by the HSA as presented in Fig. 25.

The calibration measurements performed in the micro-tunnel were of much better quality.

For a fixed velocity, the angle of attack β was changed from 0^0 to 90^0. Since $\beta + \gamma = 90^0$, $I(U, \beta)$ and $I(U, \gamma)$ could both be obtained at the same time. Figure 40 shows plots of $I(U, \beta)$ vs β and Fig. 41 the universal curve $\dfrac{I(U, \beta) - I_o}{I(U, \gamma) - I_o}$ vs β.

If the angle of attack of flow is unknown, the current $I(U, \beta)$ should first be read, then the anemometer should be rotated 90^0 and the reading of $I(U, \gamma)$ should be taken. Since I_o is a constant, the value of $\dfrac{I(U, \beta) - I_o}{I(U, \gamma) - I_o}$ can be calculated. Then, the angle of attack β can be found by use of the universal curve of Fig. 41.

Figure 42 is the calibration curve of the drag anemometer in terms of wind speed when $\beta = 0$. It should be noted that, since the torque produced by the drag force depends on the area of the plate and on the distance from the plate to the axis of rotation, the instrument must be recalibrated every time the plate is removed or changed.

Figure 43 is the plotting of $I(U, \beta)$ vs. U for different angles of attack β. This figure shows that the drag anemometer is not sensitive to the angle change when β is less than 45^0.

Chapter VI

THE HOT-WIRE ANEMOMETER (HWA)

In Chapter III, the micro-tunnel was calibrated by a constant temperature hot-wire anemometer. The sensitivity of the hot wire was great enough to measure the velocities as low as 0.2 ft/sec. after a "bucking system" was introduced.

6.1 Principles of Operation

In most gases and liquids the heat transfer from cylinders to an air stream obey the following empirical relationship (8):

$$Nu = 0.42\ Pr^{0.2} + 0.57\ Pr^{0.33} + Re^{0.50} \tag{6-1}$$

which holds in the Reynolds number $0.01 < Re < 10,000$ (6-2)

where Nu = Nusselt number defined as $Nu = \frac{\alpha d}{k_g}$

Pr = Prandtl number $= \frac{C_p \mu_g}{k_g}$

Re = Reynolds number $= \frac{\rho_g Ud}{\mu g}$

and α = heat transfer coefficient

k_g = heat conductivity of gas at temperature θ_g

μ_g = absolute viscosity of gas at temperature θ_g

C_p = specific heat of gas at constant pressure

p_g = density of gas at temperature θ_g

U = velocity of gas

d = diameter of wire (cylinder) .

In our study the diameter of the cylindrical wire was 0.0002 in. It follows that 6.1 may be used for the following range of velocities:

$$0.13 < U < 1.3\ 10^5 \text{ ft/sec.} \tag{6-3}$$

For flows of low Reynolds number, another empirical relation from Collins and William (5) is:

$$Nu \left(\frac{\theta f}{\theta_g}\right)^{-0.17} = 0.24 + 0.56\ Re^{0.45} \tag{6-4}$$

while for $0.02 < Re < 44$. Here $\theta_f = \frac{\theta_w + \theta_g}{2} = \theta_g + \frac{\Delta\theta}{2}$

(6-5)

and θ_w is the wire temperature or $\Delta\theta = \theta_w - \theta_g$.

The heat per unit time transferred to the ambient gas from a wire of length ℓ and uniform temperature is $\alpha \pi d \ell\ (\theta_w - \theta_g)$. For thermal equilibrium, the heat generated per unit time by the current through hot wire must be equal to the heat lost per unit time due to heat convection. Therefore:

$$I^2 R_w = C\alpha \pi d \ell\ (\theta_w - \theta_g) \tag{6-7}$$

where I is the current intensity, R_w the resistance of the "hot" wire and C a conversion constant. Since $I^2 R_w$ is obtained in joules per sec. and $\alpha \pi d \ell (\theta_w - \theta_g)$ is obtained in calories per sec. $C = 4.2$.

By definition, $Nu = \frac{\alpha d}{k_g}$ and $I^2 R_w = \frac{E_w^2}{R_w}$.

Equation 6-7 becomes (E_w = voltage across wire)

$$\frac{E_w^2}{R_w} = C \pi k_g \ell (\theta_w - \theta_g) \, Nu \tag{6-8}$$

or

$$Nu = \frac{E_w^2}{C \pi k_g \ell (\theta_w - \theta_g) R_w} . \tag{6-9}$$

If R_o is the wire resistance at 0^0C or 32^0F , then

$$R_g = R_o \quad 1 + b(\theta_g - \theta_o) \tag{6-10}$$

and

$$\theta_o = 0^0C = 273^0 K$$

where R_g = the resistance at gas temperature and

b = temperature coefficient of the electric resistance of wires $5.2 \times 10^{-3} (^0C)^{-1} = 2.89 \times 10^{-3} (^0F)^{-1}$.

If R_w is the working resistance and θ_w is the working temperature of the wire,

$$R_w = R_g + b R_o (\theta_w - \theta_g) . \tag{6-11}$$

For a given wire, fluid and temperatures in particular θ_w = constant, it is seen from Eqs. 6-9 and 6-1 or 6-4 that the voltage across the wire E_w is only a function of the velocity U of the fluid. This is the working principle of the constant temperature anemometer.

The anemometer output E is related to the voltage across the wire E_w by a relation given for each anemometer set. For the Disa hot-wire anemometer, this relation is

$$E_w = \frac{1.04 \times E}{100.622 + R_w} \times R_w \quad . \tag{6-13}$$

Hence,

$$E = E(U) \quad . \tag{6-14}$$

The heat transfer from the hot wire depends not only on the magnitude of the velocity, but also on the flow direction with respect to the wire. In particular, the heat transfer from the wire is maximum and minimum when the fluid velocity is respectively perpendicular and parallel to the wire. If the output of the anemometer set is then plotted (or recorded) vs wire orientation at the minimum of this curve, the projection of the velocity on the plane in which the wire is rotated will be along the wire.

Since the wire can be rotated in any plane, the hot wire can be used to determine the direction of the velocity vector in three-dimensional flow. The minimum of the output curve is much sharper than the maximum, it provides a better definition for the flow direction.

6.2 Instrumentations

The hot-wire anemometer was calibrated in the micro-tunnel (Chapter III).

The wire, which was 0.0002 in. in diameter and 0.06 in. in length, approximately, was soldered on a Disa hot-wire probe (type 55A22). The probe was mounted on a Disa 55A20 holder, and a probe cable 17-ft long was connected to the 55A0A Disa constant temperature anemometer set.

In order to improve the accuracy of the hot-wire anemometer reading, a bucking system was used in order to provide a reading of zero volt at zero velocity. The block diagram of the bucking system is shown in Fig. 44.

The necessity for a bucking system arises from the need to read accurately a small voltage change in large voltages. Indeed, the HWA output E at zero velocity is typically 5 V and it increases to 5.2 V only at a velocity of 1 ft/sec: $E(0) = 5\text{V}$, $E(1\text{ fps}) = 5.2\text{ V}$. If U designates the velocity, and if for simplicity we assume a linear relationship between E and U in the range $(0, 1\text{ fps})$, then

$$U = 5(E - 5) \quad . \tag{6-16}$$

A reading error ΔE on E produces then a relative error on U:

$$\frac{\Delta U}{U} = \frac{\Delta E}{E-5} = \left(\frac{E}{E-5}\right)\frac{\Delta E}{E} \quad . \tag{6-17}$$

For $E = 5.2$ V at a velocity of 1 ft/sec, then

$$\frac{\Delta U}{U} = 26\ \frac{\Delta E}{E} \quad . \tag{6-18}$$

With a conventional cadran type voltmeter, a voltage of 5.2 V would have to be read on the 10 V scale. The resolution on such a scale on a good instrument would be no better than 0.05 V. The uncertainty of the voltage reading would thus entail an uncertainty on U of

$$\frac{\Delta U}{U} = 26 \times \frac{0.05}{5.2} \approx 24\% \quad . \tag{6-19}$$

Alternatively, one easily sees that in order to infer a velocity with less than 1% error from the HWA output, it is necessary to be able to read 5.2 V to the nearest 0.002 V. This is impossible with a conventional voltmeter; but it can be done with a 4-digit digital voltmeter.

This difficulty may also be alleviated by bucking out the zero velocity output. It can be seen from Fig. 44 that with such a system the voltmeter reads the difference e of the HWA output minus the reference or bucking voltage. This reading e is then adjusted so as to obtain a zero reading when the velocity is zero. For a velocity U the voltmeter then registers a voltage of $e = E(U) - E(O)$. For simplicity we assume that the relationship between e and U is linear; e.g.,

$$U = \text{constant} \times e \tag{6-20}$$

so that

$$\frac{\Delta U}{U} = \frac{\Delta e}{e} \quad . \tag{6-21}$$

The accuracy of the velocity is equal to that of the voltage reading and not 26 times as above. Hence, with this "zero-suppression", a conventional millivoltmeter is quite adequate for the measurement of small velocities with a HWA.

In order to improve its stability, the reference voltage supply was connected to a Sorensen 60 cycle AC-power regulator. Thereafter, the bucking voltage varied less than one mV over a period of several hours.

6.3 Results

Several hot wires were calibrated when the room temperature was between 77.5^{0}F and 80^{0}F. The working temperature of all wires was set at 300^{0}F. Figure 45 shows the calibration curves of the wires with resistances of 2.48 ohms, 2.61 ohms, and 3.33 ohms at 32^{0}F.

Figure 46 gives the directional sensitivity of a hot wire at various velocities. The vertical coordinate shows the bucked voltage $e = E - E(0)$. The ordinate of the minima of the three curves has been changed in order to provide a better comparison. The horizontal coordinate is the angle around which the hot wire has been rotated. The direction of the flow can be found from the horizontal coordinate for which the ordinate shows a minimum value for each curve.

In curve c of Fig. 46, it is not difficult to find the minimum value. Curve a of Fig. 46, which is not well defined, is very flat around the minimum value.

Since these curves are symmetric with respect to a vertical passing through their minimum, the abscissa of this minimum is also that of the mid-point of any two points of the curve lying on the same horizontal. With this technique the maximum duration between the various abscissa of the minima is 1.5 degree.

Chapter VII

COMPARISON OF LOW-SPEED ANEMOMETERS

The comparative advantages and disadvantages of the three low-speed anemometers investigated will finally be discussed from various points of view.

7.1 Measuring Capability

Both the DA (drag anemometer) and the HWA (hot-wire anemometer) are capable to determine the magnitude and the direction of the velocity in a gas flow. The HSA (hot-spot anemometer), on the contrary, is only able to measure the magnitude of a horizontal wind due to unsymmetrical effect of buoyancy; this is a serious limitation of HSA at low velocities. Only at higher velocities, 3 ft/sec, this effect becomes negligible.

7.2 Calibration

The HSA instrument is the only one which can be used without direct calibration against a primary low speed standard, if the various corrections are determined experimentally and if a large error may be tolerated below 0.5 ft/sec.

7.3 Sensitivity and Repeatability

All three anemometers read velocities down to 0.2 ft/sec. Because of buoyancy effects, neither the HSA nor the HWA could be used below this limit. With a sufficiently sensitive moving coil micro-ammeter, the drag anemometer would be able to measure velocities below this limit.

The repeatability of the three anemometers is comparable. It should be stressed that the HWA is very sensitive to temperature changes at low velocities. The wire has to be used at the same temperature at which it has been calibrated unless the temperature compensation is taken into account (see reference 9 Lin and Binder).

7.4 Special Resolution

Because of the necessity of the drag plate, being determined by the required sensitivity, the special resolution of the DA is poor. The drag anemometer could not be used in a flow with a large gradient. The sizes of HSA and of the HWA are of the order of one to two mm.

7.5 Remote Readout

The DA has to be balanced by visual observation of the ammeter dial; the experimenter must be able to "see" this dial.

The instrument must be accessible; it cannot be used remotely. In the large wind tunnel, the DA was already difficult to use because mirrors were necessary to observe the position of the dial.

This is absolutely no problem with either of the two other anemometers.

7.6 Automatic Recording

The DA has to be balanced manually and about ten readings (release of ten hot spots) have to be taken to obtain a reliable average with the HSA. Either of these instruments lends itself to automatic recording. The recording of the HWA output on the contrary presents no problem whatever.

This disadvantage of DA and HSA also implies that these instruments are not suitable for measuring in transient flow.

Since no balance has to be adjusted with the constant temperature HWA and only one reading is required, this anemometer is the most convenient to use.

7.7 Ruggedness

All three anemometers are delicate instruments. Because of the ultra-thin wire used as resistance thermometer, the HWA is even more delicate than the other two instruments.

7.8 Complexity of Experimental Set-Up

With the pulsing apparatus, amplifiers, electronic counter, oscilloscope, the HSA requires a quite complex experimental set-up, which is very simple for the two other instruments.

7.9 Cost

The DA is inexpensive and only requires a micro-ammeter for readout.

A constant temperature HWA set is fairly expensive (on the order of two to three thousand dollars) but is nearly self sufficient. The reference power supply is inexpensive and only a millivoltmeter is required.

Whereas the HSA probes and the pulse circuit are inexpensive, the HSA requires an elaborate support instrumentation, which is no problem if it is available but renders the cost prohibitive if it has to be purchased.

Chapter VIII

CONCLUSIONS

From the preceding remarks, it is clear that the best low-speed anemometer is the constant temperature hot-wire anemometer. This instrument is used in the mountain lee wave study mentioned in the introduction.

If an inexpensive instrument was needed for some simple measurements, then the drag anemometer would be adequate.

Finally, if no calibration could be performed and poor accuracy could be tolerated below 0.5 ft/sec, the hot-spot anemometer should be used.

TABLES

TABLE 1. CALCULATION OF α_1 FOR DATA CURVE H_2 OF FIGURE 12

Pts.	r (in.)	V_1 (fps)	$\frac{\pi r^2}{144}$ (10^{-3} ft^2)	$\Delta \frac{\pi r^2}{144}$	$\overline{V}$ (fps)	ΔQ (10^{-3} cfs)
1	0.00	35.4	0			
				2.30	35.40	81.50
2	0.325	35.4	2.30			
				0.77	35.25	27.18
3	0.375	35.1	3.07			
				0.42	34.90	14.65
4	0.400	34.7	3.49			
				0.45	34.25	15.42
5	0.425	33.8	3.94			
				0.45	33.10	15.90
6	0.450	32.4	4.42			
				0.50	29.15	14.57
7	0.475	25.9	4.92			
				0.53	12.95	6.86
8	0.500	0	5.45			
Σ				5.45		176.08

$$\overline{V}_1 = \frac{\Sigma \Delta Q}{A_1} = \frac{176.08}{5.45} = 32.3 \text{ (fps)}$$

$$\alpha_1 = \frac{\overline{V}_1}{V_{c1}} = \frac{32.3}{35.4} = 0.914 .$$

TABLE 2. CALCULATION OF α_2 FOR DATA CURVE H_2 OF FIGURE 15

Pts.	r (ft) (1)	πr^2 (10^{-2} ft^2) (2)	$\Delta\pi r^2$ (10^{-2} ft^2) (3)	$\bar{e}$ (m v) (4)	V_2 (fps) (5)	V_2 avg (fps) (6)	ΔQ = (3) x (6) (10^{-2} cfs) (7)	V_2' (fps) (8)	V_2' avg (fps) (9)	(10^{-2} cfs) (10)	V_2'' (fps) (11)	V_2'' avg (fps) (12)	$\Delta Q''$ = (3) x (12) (10^{-2} cfs) (13)	V_2''' (fps) (14)	V_2''' avg (fps) (15)	$\Delta Q'''$ = (3) x (15) (10^{-2} cfs) (16)
1	0.229	16.5		0	0											
			1.3			0.327	0.425		0.367	0.477		0.370	0.481	0		
2	0.22	15.2		166	0.655			0.735			0.740				0.368	0.478
			1.34			0.788	1.056		0.875	1.173		0.877	1.175	0.736		
3	0.21	13.86		239	0.920			1.015			1.014				0.872	1.168
			1.26			0.989	1.246		1.089	1.360		1.085	1.366	1.008		
4	0.20	12.60		273	1.058			1.160			1.156				1.079	1.359
			1.27			1.076	1.354		1.180	1.494		1.179	1.509	1.150		
5	0.19	11.33		281	1.095			1.200			1.192				1.168	1.470
			1.13			1.100	1.243		1.205	1.361		1.198	1.353	1.186		
6	0.18	10.20		284	1.106			1.210			1.204				1.192	1.347
			1.12			1.106	1.238		1.210	1.355		1.204	1.349	1.198		
7	0.17	9.08		284	1.106			1.210			1.204				1.198	1.342
			1.03			1.110	1.144		1.213	1.250		1.206	1.241	1.198		
8	0.16	0.05		285	1.113			1.216			1.208				1.200	1.236
			0.98			1.108	1.085		1.212	1.189		1.204	1.200	1.202		
9	0.15	7.07		283	1.104			1.207			1.200				1.198	1.174
			1.76			1.110	1.936		1.205	2.120		1.198	2.110	1.194		
10	0.13	5.31		282	1.097			1.203			1.196				1.191	2.096
			2.17			1.091	2.370		1.197	2.595		1.190	2.581	1.188		
11	0.10	3.14		279	1.085			1.190			1.184				1.182	2.564
			2.35			1.075	2.525		1.180	2.772		1.175	2.750	1.176		
12	0.05	0.79		275	1.065			1.170			1.166				1.167	2.740
			0.79			1.065	0.841		1.170	0.924		1.166	0.921	1.158		
13	0	0		275	1.065			1.170			1.166				1.158	0.915
Σ			16.5				164.63			18.070			18.036			

$\overline{V}_2 = \frac{16.463}{16.5} = 0.996$ $\quad \overline{V}_2' = \frac{18.07}{16.5} = 1.096$ $\quad \overline{V}_2'' = \frac{18.036}{16.5} = 1.093$ $\quad \overline{V}_2''' = \frac{17.889}{16.5} = 1.084$

$\alpha_2 = \frac{0.996}{1.065} = 0.934$ $\quad \alpha_2' = \frac{1.096}{1.17} = 0.936$ $\quad \alpha_2'' = \frac{1.093}{1.166} = 0.938$ $\quad \alpha_2''' = \frac{1.084}{1.158} = 0.936$

TABLE 3. THE VARIATION OF α_2 AND V_{c2}

Run	α_2 (1)	V_{c2} (2)	α'_2 (3)	V'_{c2} (4)	α''_2 (5)	V''_{c2} (6)	α'''_2 (7)	V'''_{c2} (8)	α^{iv}_2 (9)
V_1	1	1.648	0.933	1.651	0.934	1.654	0.935	1.655	0.935
V_2	1	1.089	0.908	1.101	0.909	1.103	0.911	1.104	0.911
V_3	1	0.530	0.863	0.532	0.865	0.534	0.866	0.535	0.867
V_4	1	0.402	0.830	0.406	0.833	0.408	0.833	0.408	0.834
V_5	1	0.279	0.798	0.283	0.780	0.286	0.784	0.289	0.783
V_6	1	0.177	0.732	0.180	0.738	0.184	0.743	0.185	0.745
H_1	1	1.498	0.942	1.584	0.944	1.582	0.946	1.581	0.946
H_2	1	1.065	0.934	1.170	0.936	1.166	0.938	1.158	0.936
H_3	1	0.535	0.871	0.543	0.873	0.541	0.874	0.540	0.875
H_4	1	0.387	0.838	0.395	0.840	0.391	0.841	0.391	0.841
H_5	1	0.287	0.787	0.296	0.786	0.295	0.790	0.298	0.793
H_6	1	0.166	0.742	0.170	0.745	0.169	0.740	0.171	0.748

TABLE 4. COMPUTATION OF THE CORRECTIONS OF HSA FOR $a = 0.146$ in.

$a = 0.371$ cm $\quad y_o = 0.121$ cm $\quad a^2 + y_o^2 = 0.1519$ cm^2

U	U	t	a/t	$\frac{t}{t_o}(a^2 + y_o^2)$	y^2	$\frac{\sqrt{(5) - (6)}}{t}$	(4) - (7)	U
(fps)	(cm/sec)	(10^{-3} sec)	(cm/sec)	cm^2	cm^2	(cm/sec)	(cm/sec)	(fps)
(1)	(2)	(3)	(4)	(5)	(6)	(7)	(8)	(9)
0	0	34.12	10.88	0.1519	0.0146	10.88	0	0
0.2	6.10	20.57	18.05	0.0916	0.0143	13.53	4.52	0.148
0.304	9.27	17.49	21.2	0.0778	0.01414	14.44	6.76	0.252
0.391	11.92	14.57	25.5	0.0648	0.0138	15.5	10.00	0.328
0.472	14.4	13.04	28.44	0.0581	0.013	16.3	12.14	0.39
0.55	16.75	11.51	32.22	0.05125	0.0125	17.1	15.12	0.497
0.716	21.82	9.62	38.55	0.0428	0.0117	18.35	20.2	0.663
0.96	29.28	7.75	47.8	0.0345	0.0092	19.25	28.55	0.936
1.204	36.7	6.30	58.85	0.02805	0.00883	22.1	36.75	1.204
1.367	41.7	5.96	62.2	0.02653	0.00844	22.6	39.6	1.30
1.59	48.5	5.10	72.7	0.0227	0.0074	24.3	48.4	1.588

TABLE 5. COMPUTATION OF THE CORRECTIONS OF HSA FOR a = 0.131 in.

$a = 0.333$ cm $y_o = 0.1195$ cm $a^2 + y_o^2 = 0.1251\ cm^2$

U (fps) (1)	U (cm/sec) (2)	t (10^{-3} sec) (3)	a/t (cm/sec) (4)	$\frac{t}{t_o}(a^2+y_o^2)$ cm^2 (5)	y^2 cm^2 (6)	$\frac{\sqrt{(5)-(6)}}{t}$ (cm/sec) (7)	(4) - (7) (cm/sec) (8)	U (fps) (9)
0	0	32.55	10.23	0.1250	0.0143	10.23	0	0
0.198	6.00	20.02	16.63	0.0771	0.01425	12.5	4.13	0.1355
0.271	8.26	16.83	19.78	0.0648	0.0141	13.38	6.48	0.212
0.356	10.85	14.70	22.65	0.0566	0.01355	14.13	8.52	0.279
0.452	13.78	12.82	25.97	0.0493	0.013	14.9	11.07	0.363
0.55	16.75	11.07	30.1	0.0426	0.01236	15.72	14.38	0.472
0.74	22.57	8.90	37.45	0.03424	0.0112	17.08	20.37	0.668
0.96	29.27	7.21	46.2	0.02772	0.00978	18.57	27.69	0.908
1.18	35.96	6.12	54.4	0.02353	0.00865	19.95	34.45	1.13
1.35	41.2	5.28	63.1	0.02031	0.00763	21.3	41.8	1.37
1.66	50.6	4.58	72.7	0.01761	0.00768	21.8	50.9	1.67

TABLE 6. COMPUTATION OF THE CORRECTIONS OF HSA FOR a = 0.069 in.

a = 0.175 cm $\quad y_o$ = 0.1196 cm $\quad a^2 + y_o^2$ = 0.04496 cm^2

U (fps) (1)	U (cm/sec) (2)	t (10^{-3} sec) (3)	a/t (cm/sec) (4)	$\frac{t}{t_o}(a^2 + y_o^2)$ cm^2 (5)	y^2 cm^2 (6)	$\frac{\sqrt{(5) - (6)}}{t}$ (cm/sec) (7)	(4) - (7) (cm/sec) (8)	U (fps) (9)
0	0	19.86	8.83	0.04496	0.0143	8.83	0	0
0.217	6.62	13.97	12.55	0.0316	0.0132	8.71	3.84	0.126
0.273	8.33	9.63	18.2	0.0218	0.0121	10.23	7.97	0.261
0.352	10.73	8.56	20.48	0.0194	0.01142	10.43	10.05	0.3295
0.424	12.92	7.85	22.34	0.01777	0.0105	10.85	11.49	0.377
0.491	14.98	7.05	24.9	0.01596	0.0096	11.30	13.6	0.446
0.55	16.77	6.56	26.7	0.01485	0.0095	11.15	15.55	0.51
0.073	20.53	5.72	30.7	0.01295	0.00859	11.53	19.17	0.629
0.81	24.7	4.86	36.1	0.011	0.00705	12.93	23.17	0.727
0.98	29.9	4.18	41.9	0.00946	0.00612	13.83	28.07	0.92
1.193	36.4	3.55	49.4	0.00983	0.00525	14.86	34.72	1.138
1.34	40.85	3.13	56.0	0.00708	0.00455	16.1	39.9	1.31
1.48	45.15	2.90	60.4	0.00656	0.00422	16.68	43.72	1.465
1.66	50.6	2.69	66.4	0.00609	0.0039	17.4	49	1.61

TABLE 7. COMPUTATION OF THE CORRECTIONS OF HSA FOR a = 0.095 in.

a = 0.2913 cm y_o = 0.1131 $a^2 + y_o^2$ = 0.1713 cm^2

U (fps) (1)	U (cm/sec) (2)	t (10^{-3} sec) (3)	a/t (cm/sec) (4)	$\frac{t}{t_o}(a^2+y_o^2)$ cm^2 (5)	y^2 cm^2 (6)	$\frac{\sqrt{(5)-(6)}}{t}$ (cm/sec) (7)	(4) - (7) (cm/sec) (8)	U (fps) (9)
0	0	12.35	23.6	0.0977	0.0128	23.6	0	0
0.196	5.97	9.92	29.35	0.0785	0.0118	26.1	3.25	0.107
0.29	8.84	8.46	34.4	0.067	0.0109	28.0	6.4	0.21
0.373	11.38	7.64	38.1	0.0605	0.01018	29.4	8.7	0.285
0.409	14.0	6.72	43.4	0.0532	0.00938	31.2	12.2	0.40
0.543	16.56	6.25	46.6	0.0495	0.00879	32.3	14.3	0.47
0.65	19.8	5.71	50.9	0.0452	0.00814	33.7	17.2	0.564
0.77	23.43	5.13	54.9	0.0406	0.00743	35.5	19.4	0.637
0.932	28.4	4.54	64.1	0.0359	0.00662	37.7	26.4	0.87
1.157	35.17	3.85	74.1	0.0305	0.00573	40.9	33.7	1.105
1.34	40.85	3.44	84.6	0.0272	0.00515	43.2	41.4	1.358
1.57	47.85	3.14	92.8	0.02485	0.00467	45.2	47.6	1.56

FIGURES

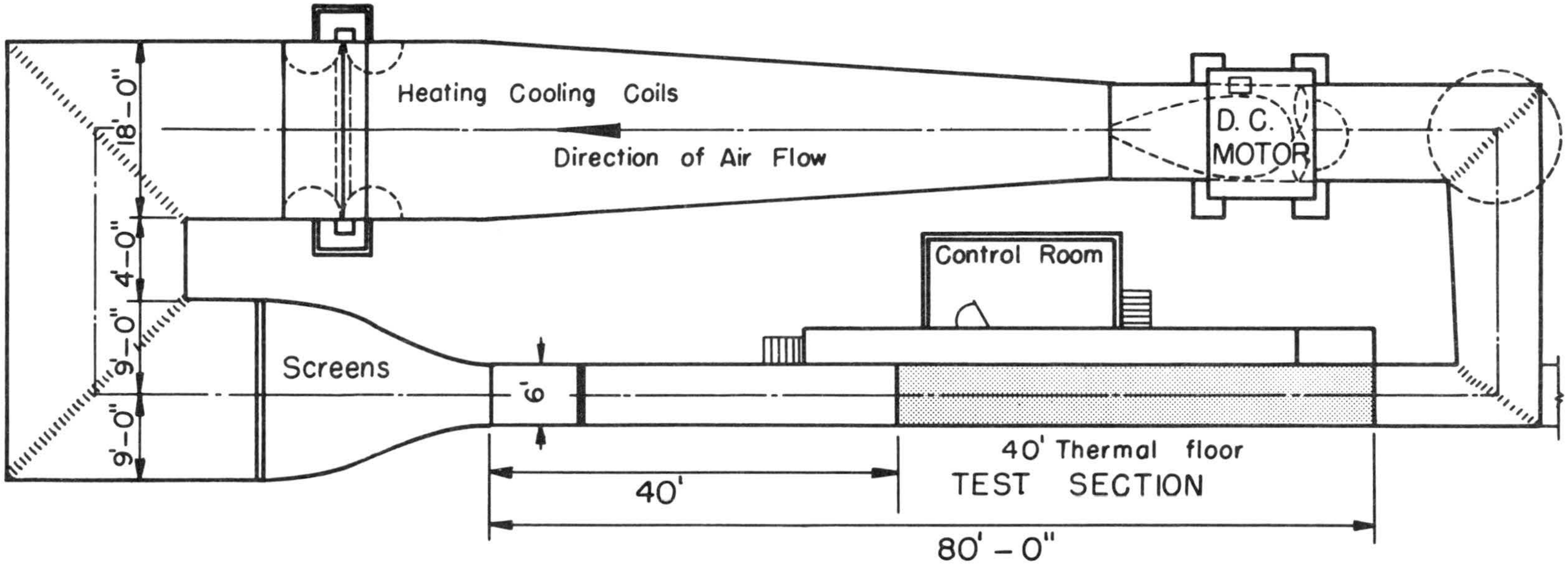

Figure 1. Large wind tunnel

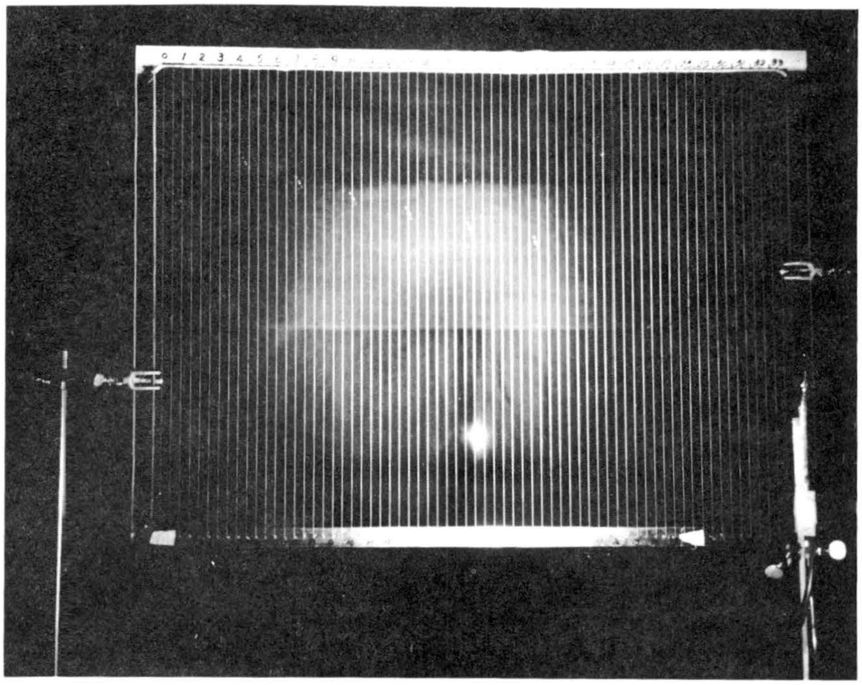

Figure 2. Time exposure photograph of a soap bubble taken with a strobe as light source

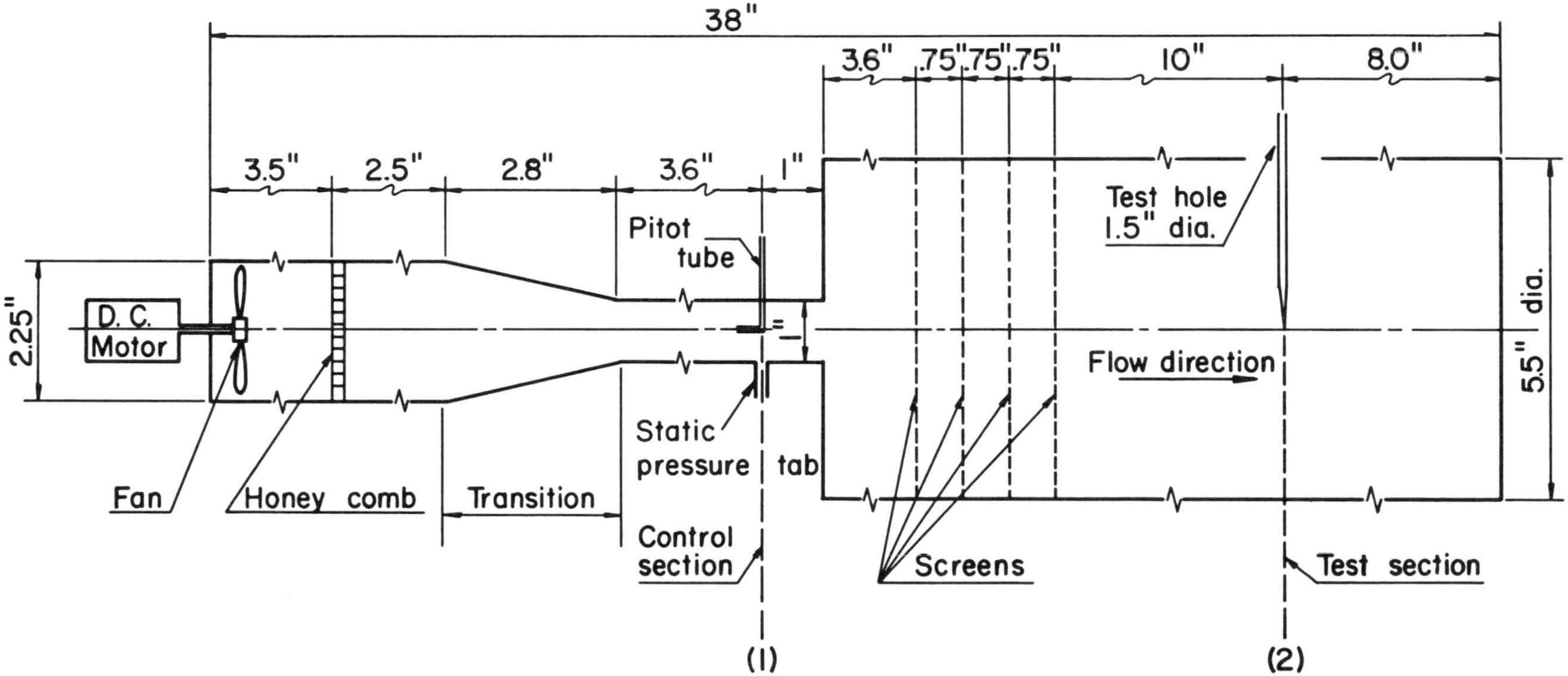

Figure 3. Sketch of the micro-wind tunnel

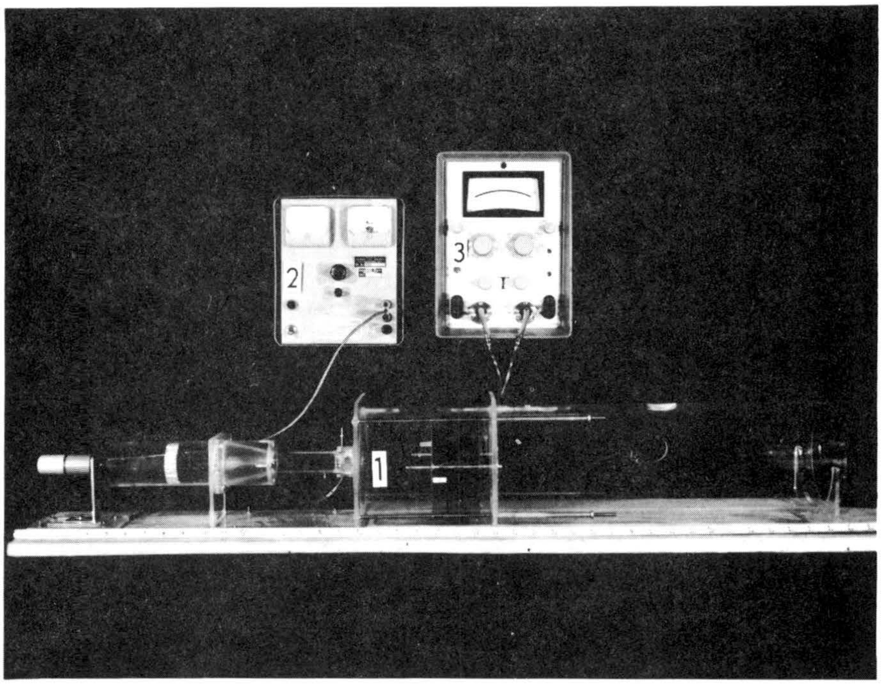

1. Micro-tunnel 2. D. C. power supply for drive motor

3. Equibar pressure transducer

Figure 4. The micro-wind tunnel and support instruments

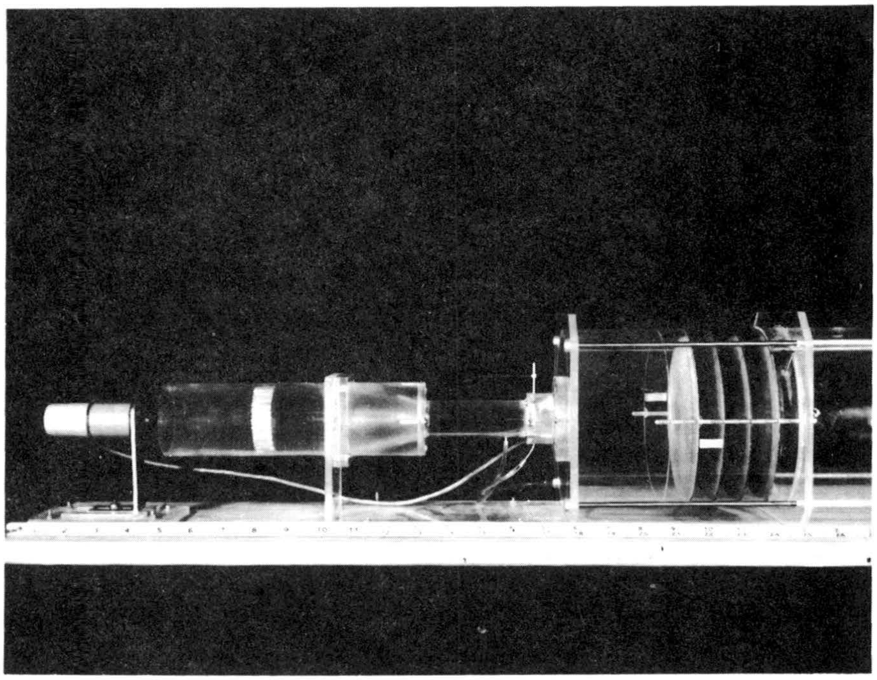

Figure 5. Close-up of micro-tunnel

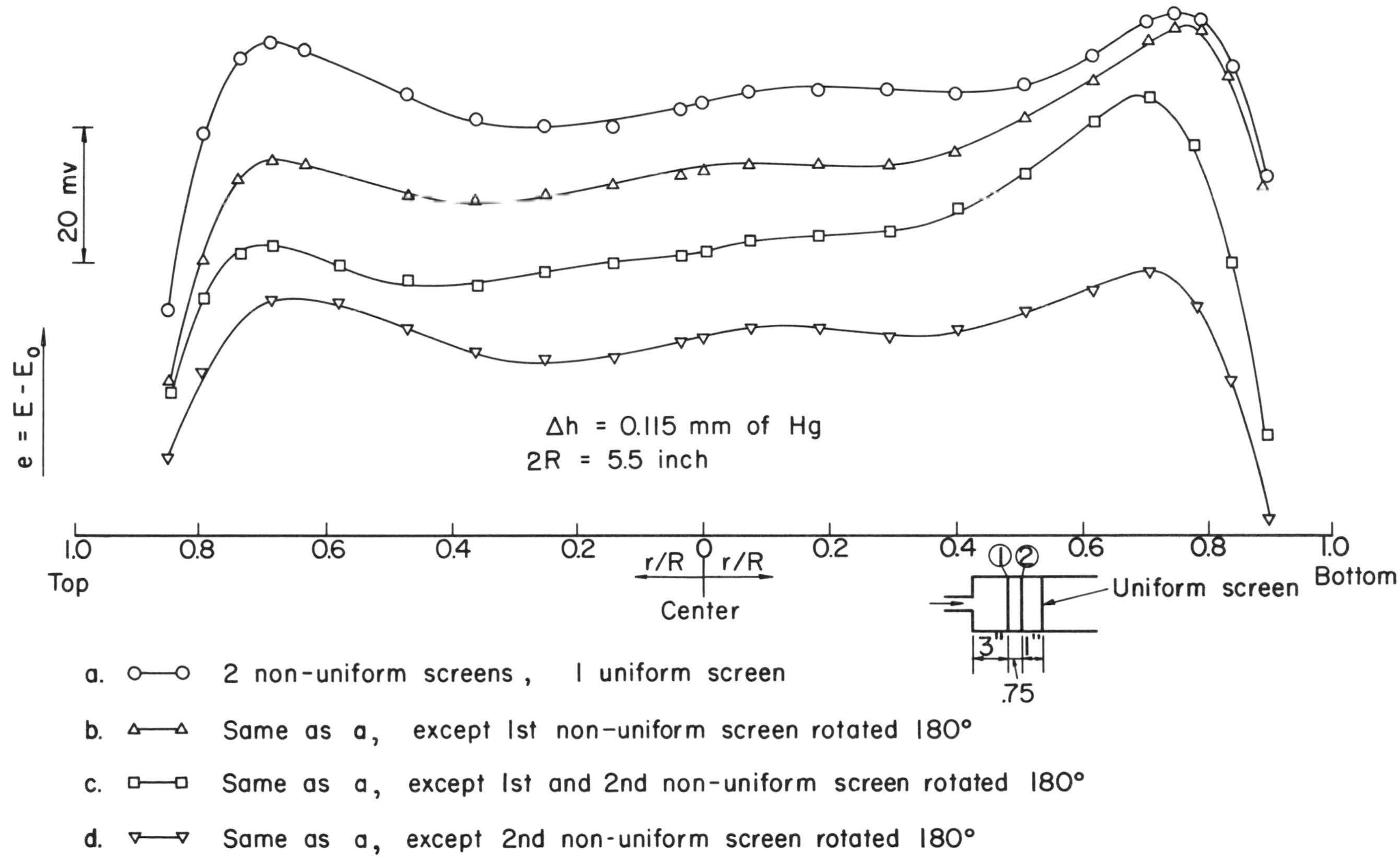

Figure 6. Influence of two non-uniform and one uniform screen on the velocity distribution in the test section

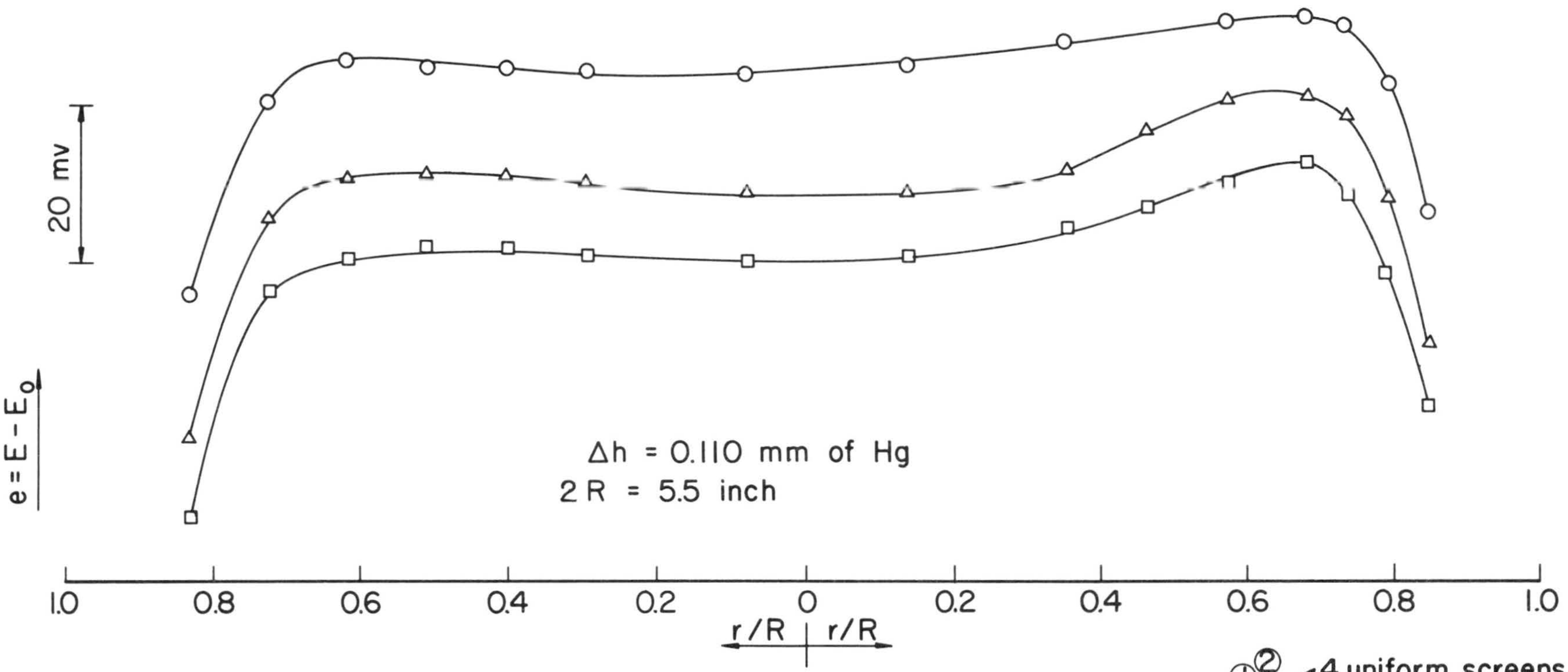

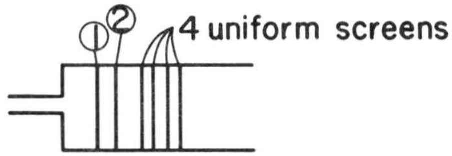

a. ○—○ 2 non-uniform screens, 4 uniform screens

b. △—△ Same as a., except 2nd non-uniform screen rotated 180°

c. □—□ Same as a., except 1st non-uniform screen rotated 180°

Figure 7. Velocity profiles in test section for two non-uniform screens and four uniform screens

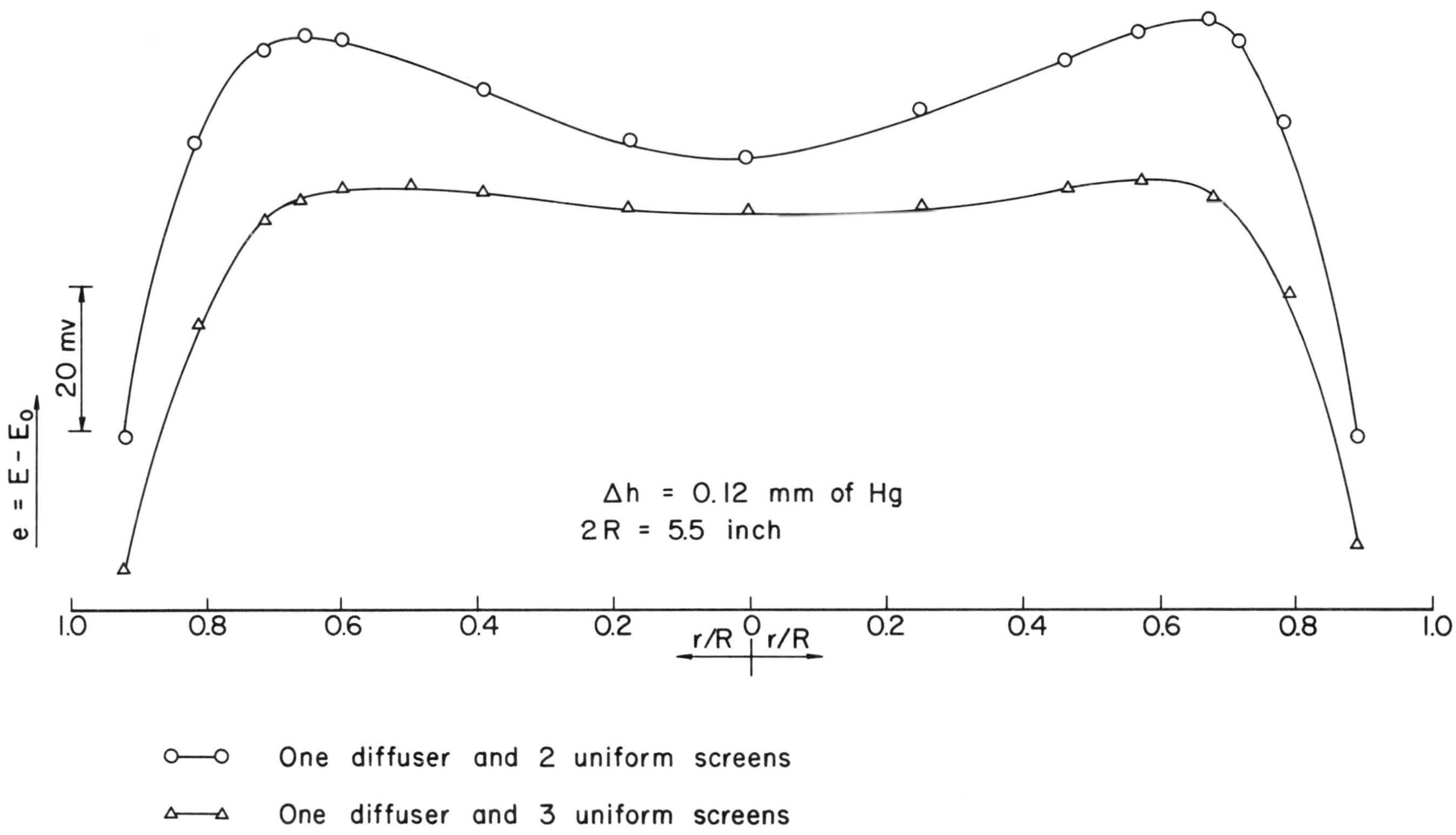

Figure 8. Velocity profiles at test section with diffuser

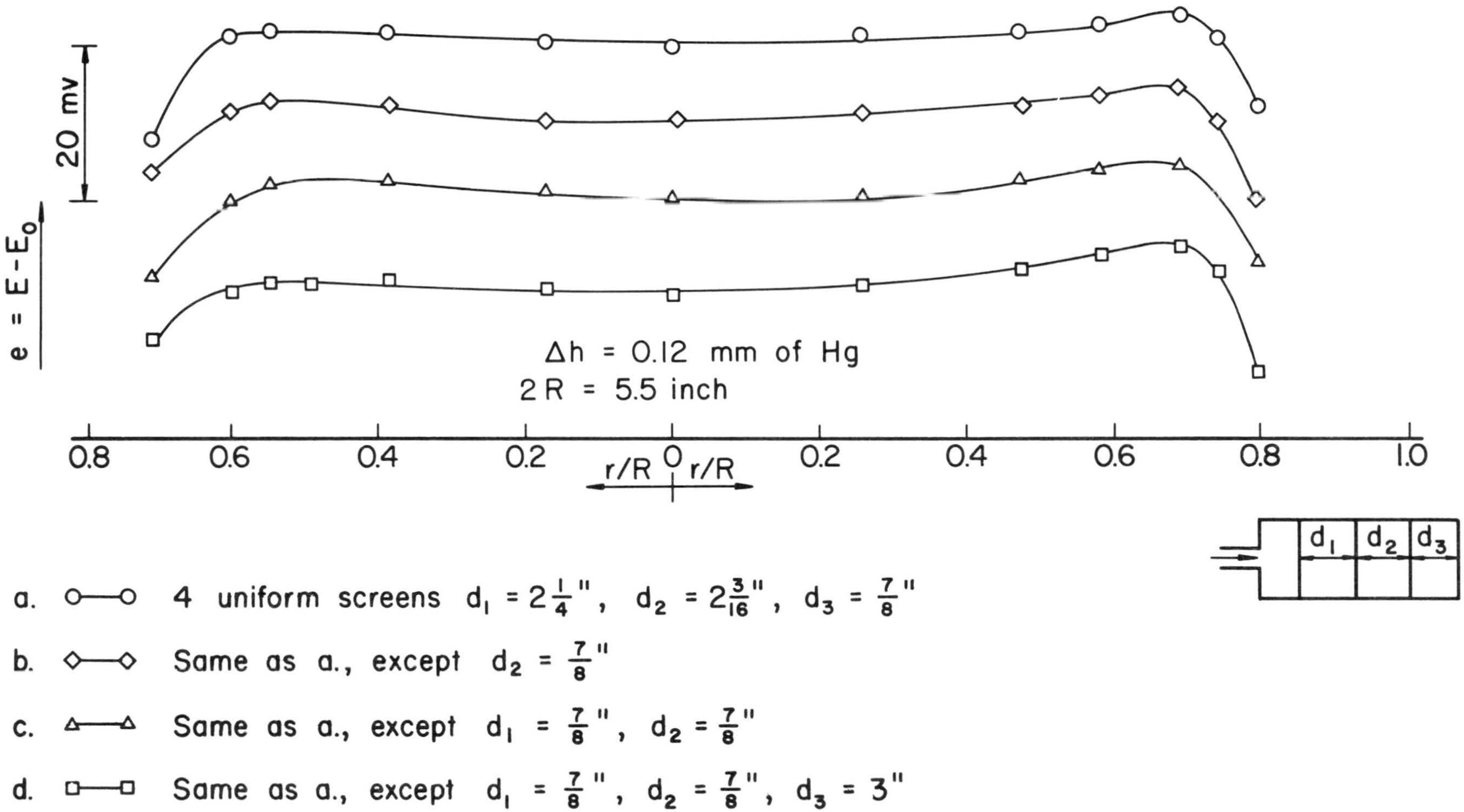

Figure 9. Velocity profiles in test section with four S-screens for variable distances between screens

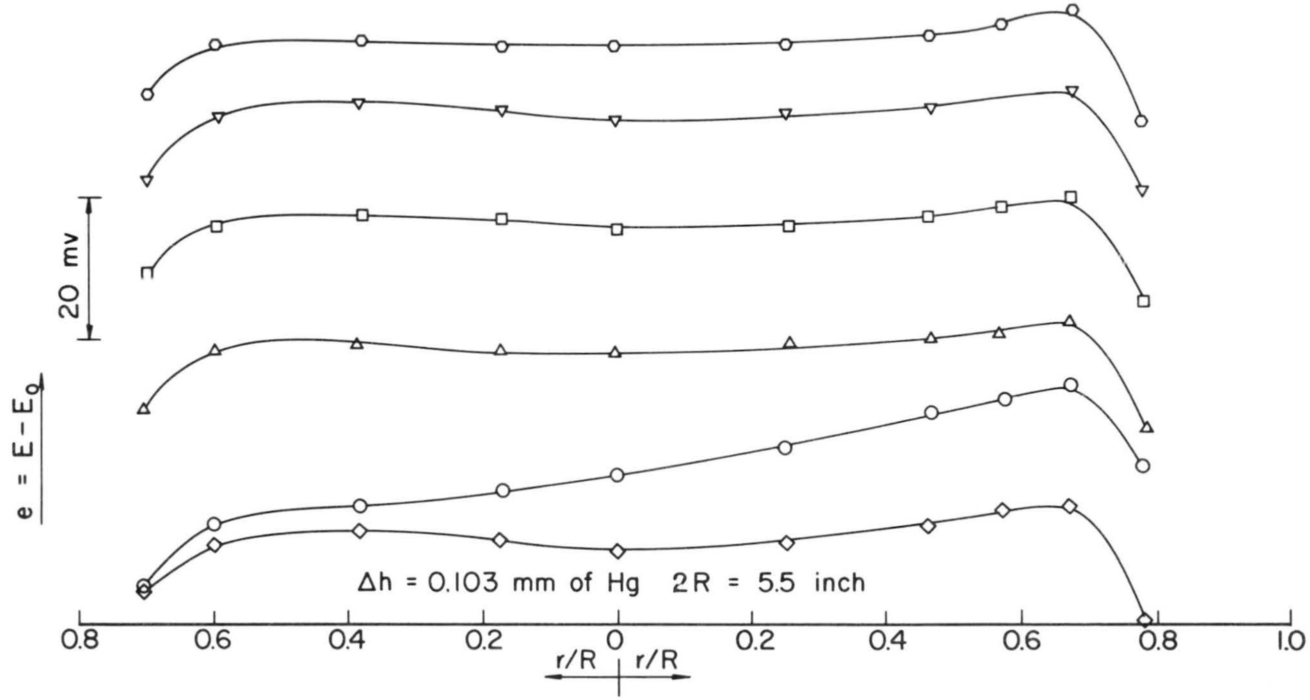

a. ◇—◇ Reference profile

b. ○—○ 4th screen turned 180° with respect to position in a.

c. △—△ Same as a., except 3rd screen turned 180°

d. □—□ Same as c., except 2nd screen turned 180°

e. ▽—▽ Same as c., except 1st screen turned 180°

f. ○—○ Same as c.

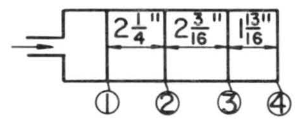

Figure 10. Velocity profiles in test section for various orientations of S-screens

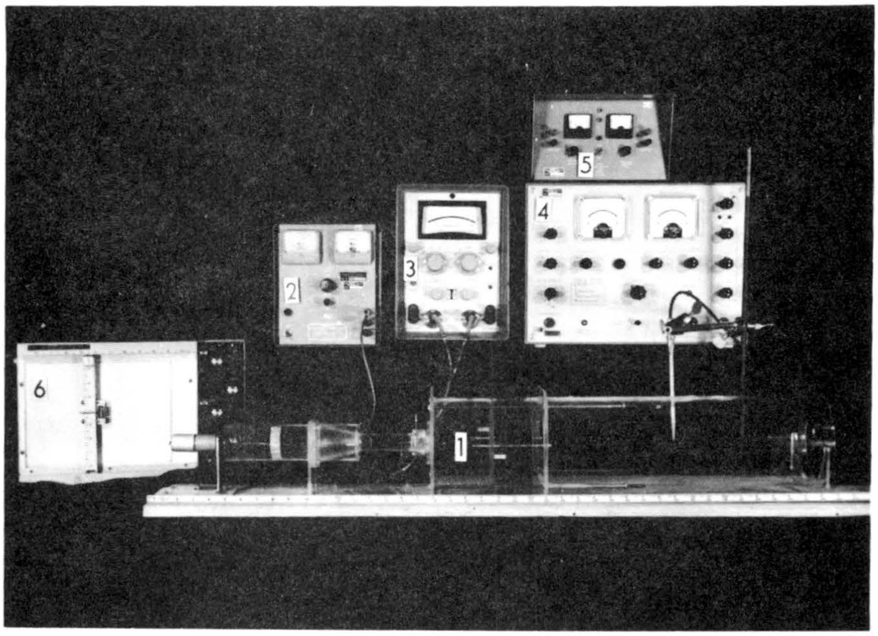

1. Micro-tunnel 2. Power supply of drive motor

3. Equibar pressure transducer 4. Disa hot-wire anemometer

5. Reference voltage power supply 6. Moseley x-y plotter

Figure 11. Instrumentations for micro-tunnel calibration

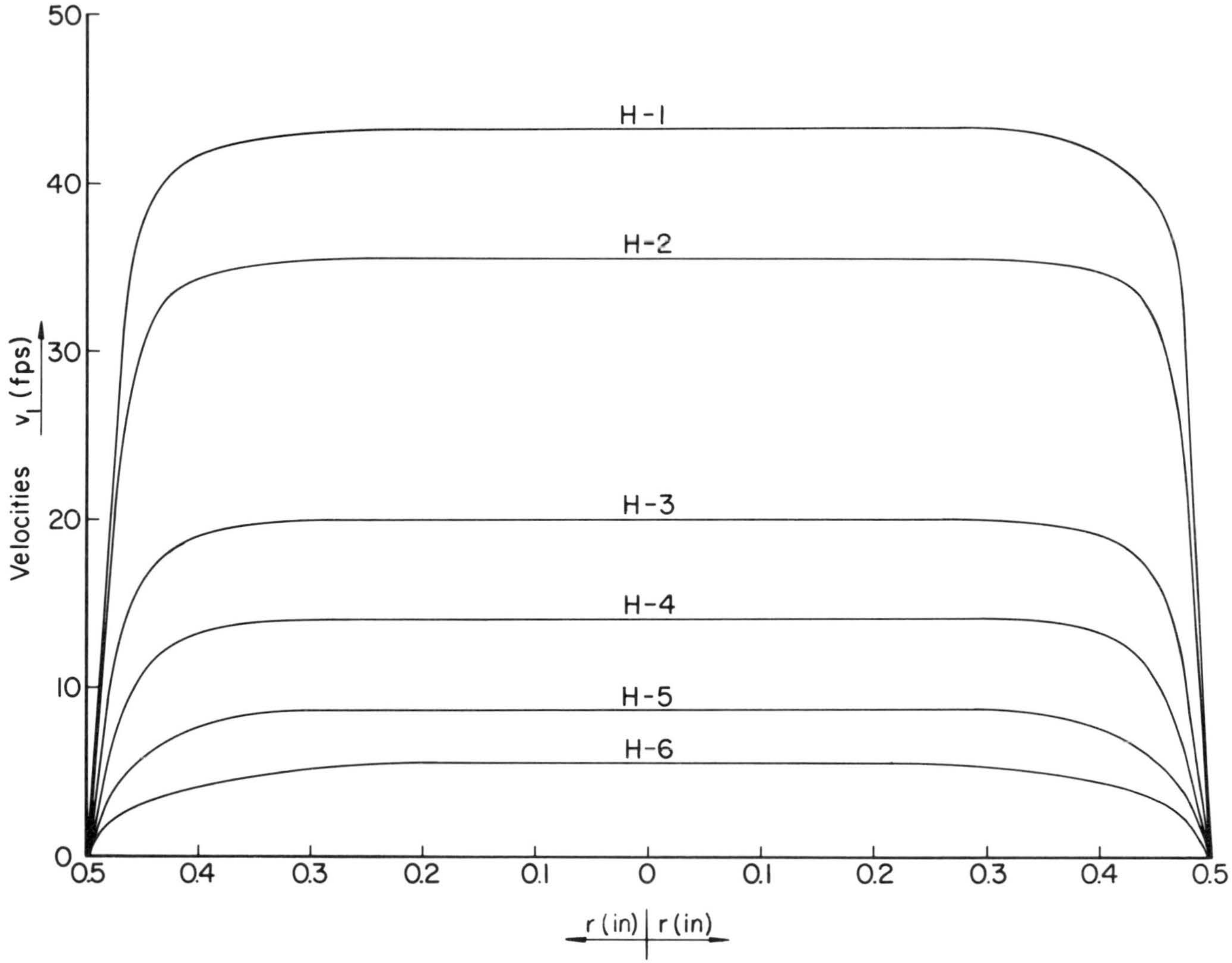

Figure 12. Vertical velocity profiles in the control section

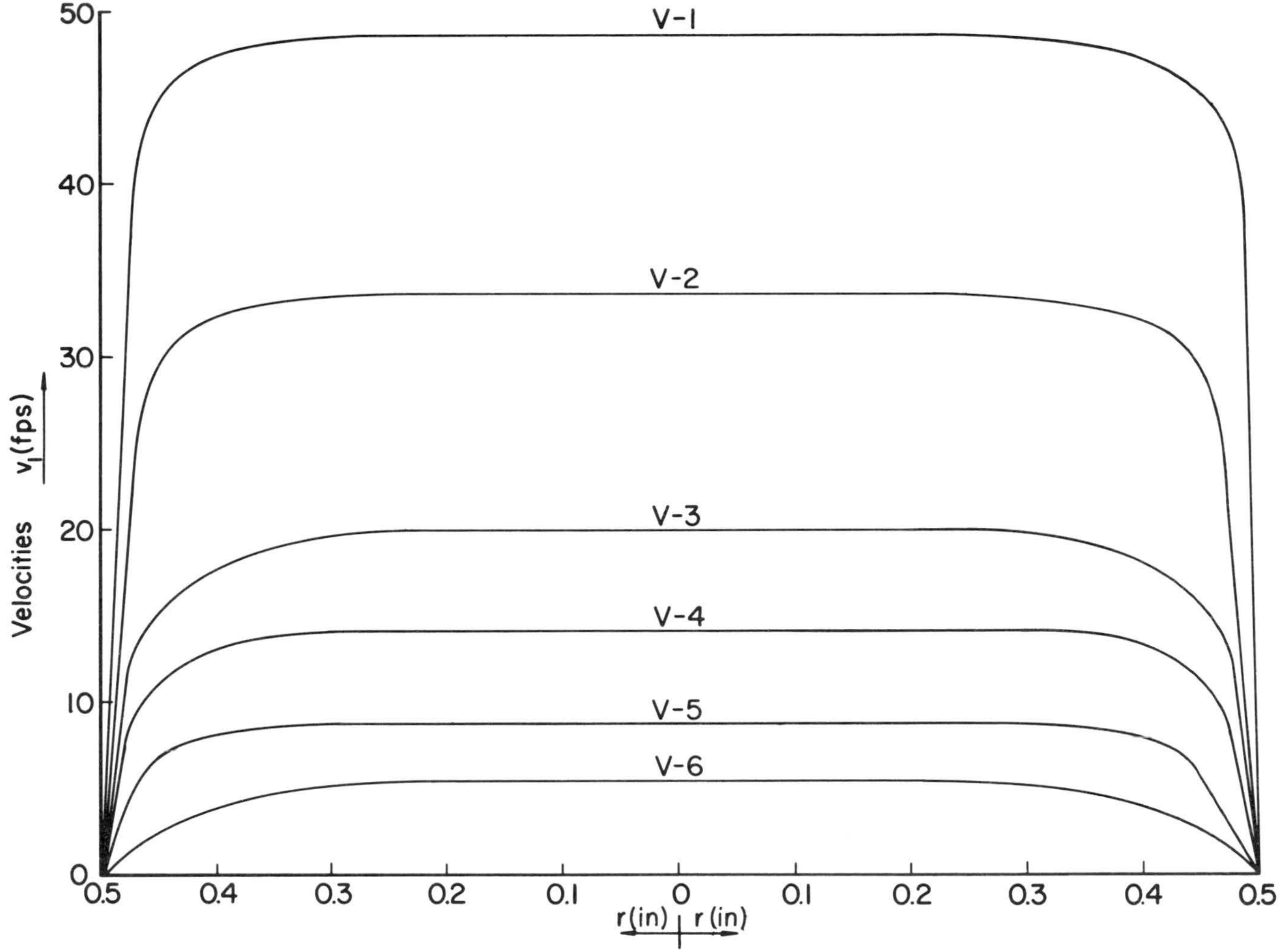

Figure 13. Horizontal velocity profiles in control section

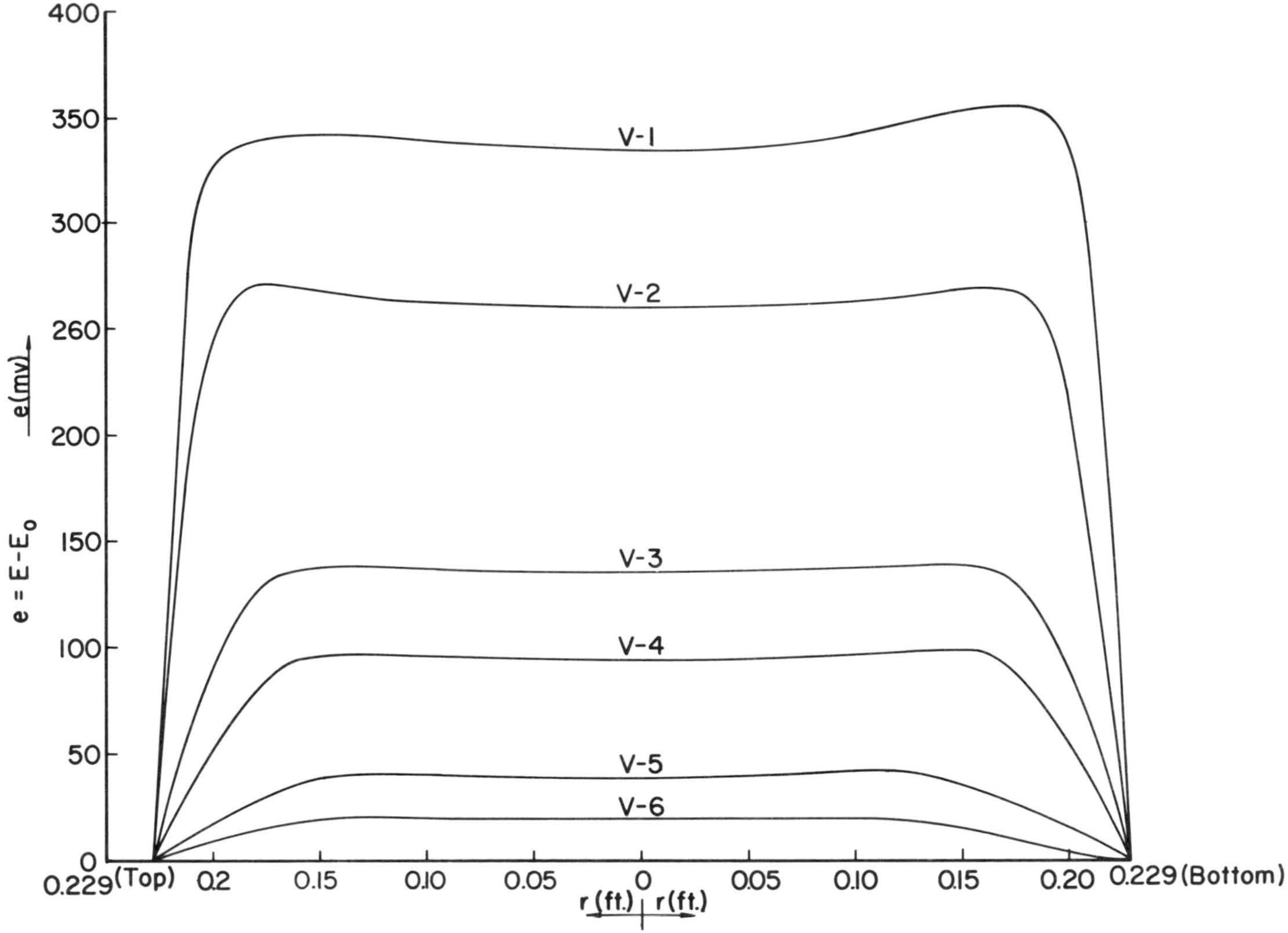

Figure 14. Vertical profiles of HWA output in test section

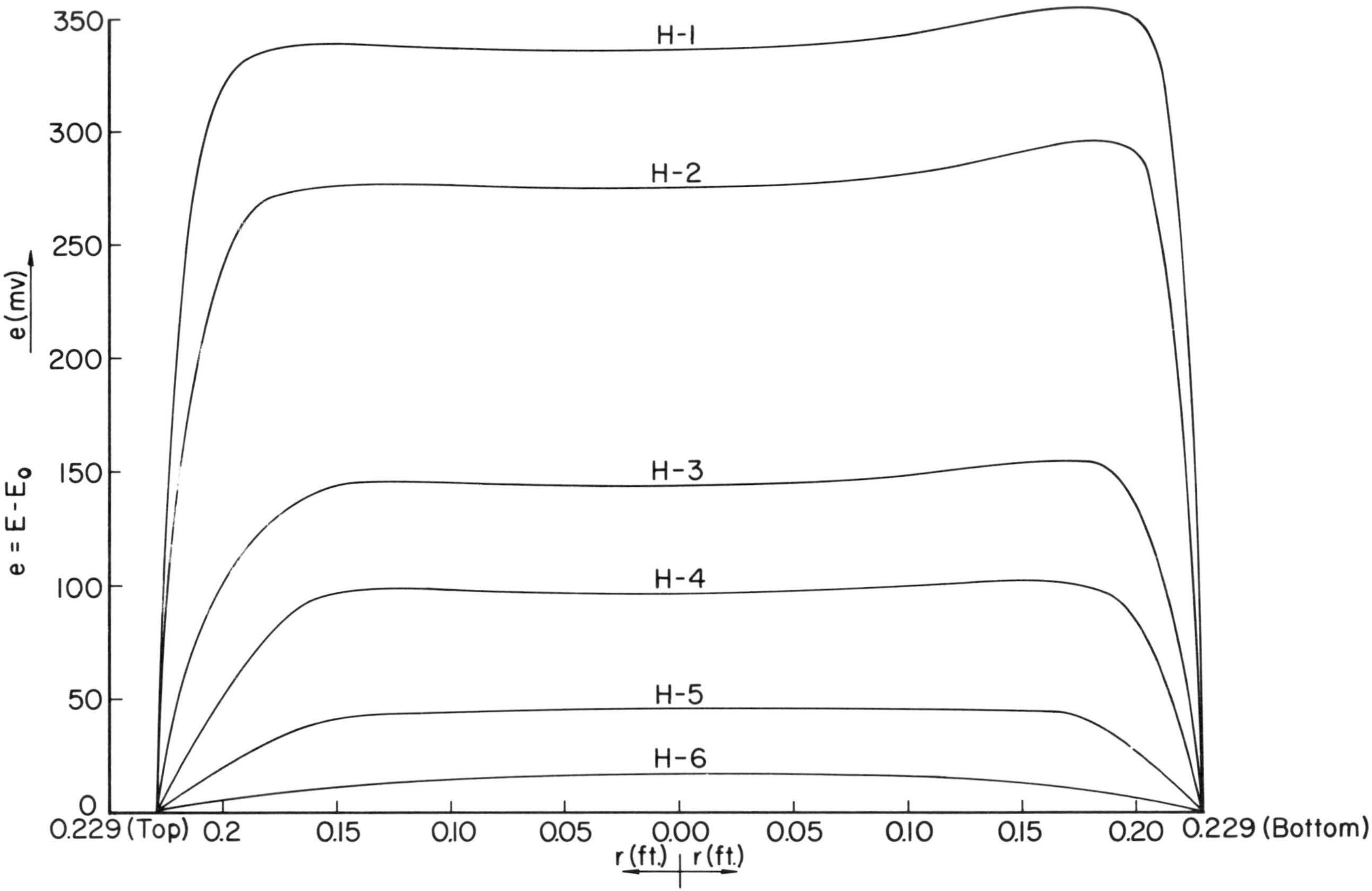

Figure 15. Horizontal profiles of HWA output in test section

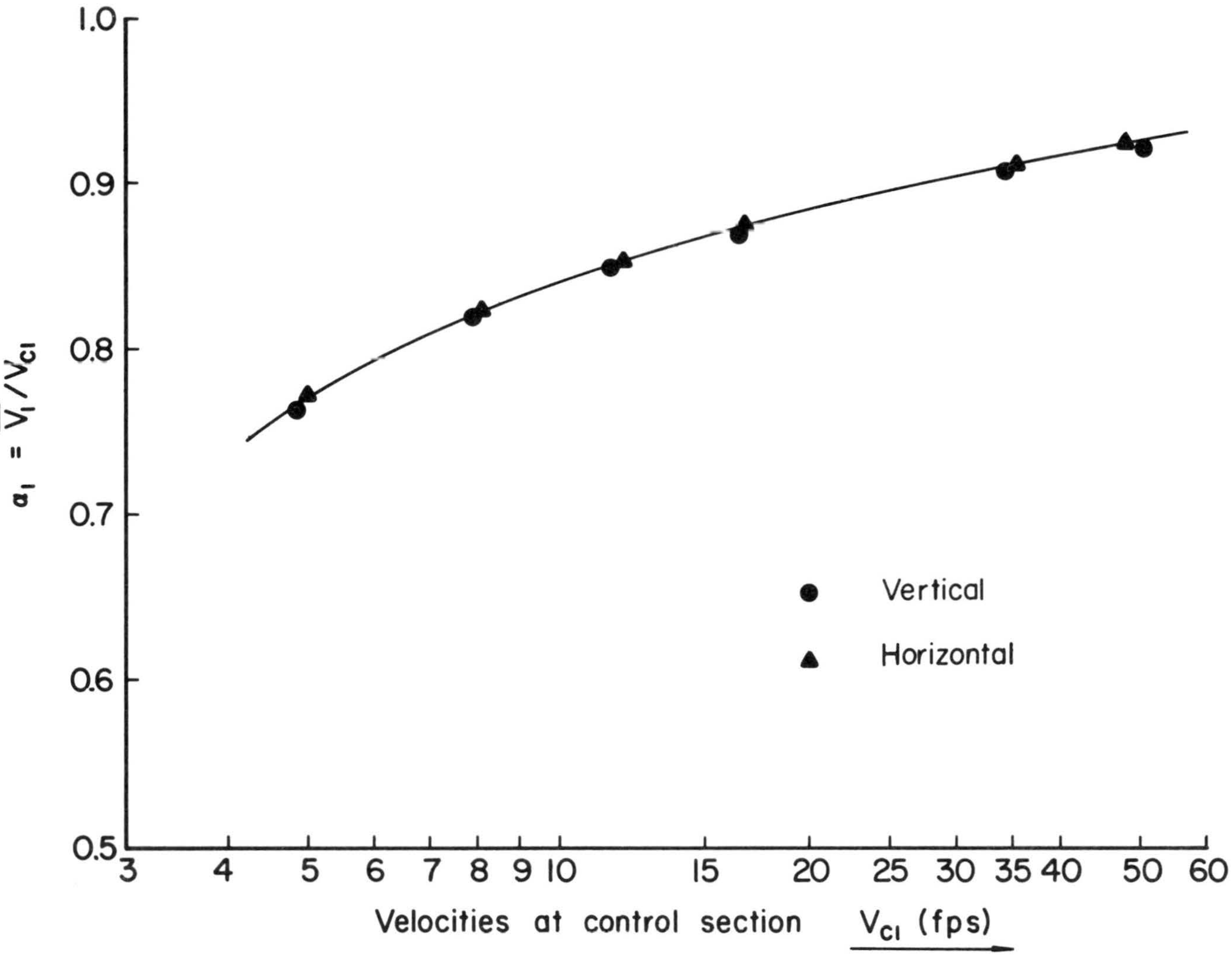

Figure 16. Values of α_1

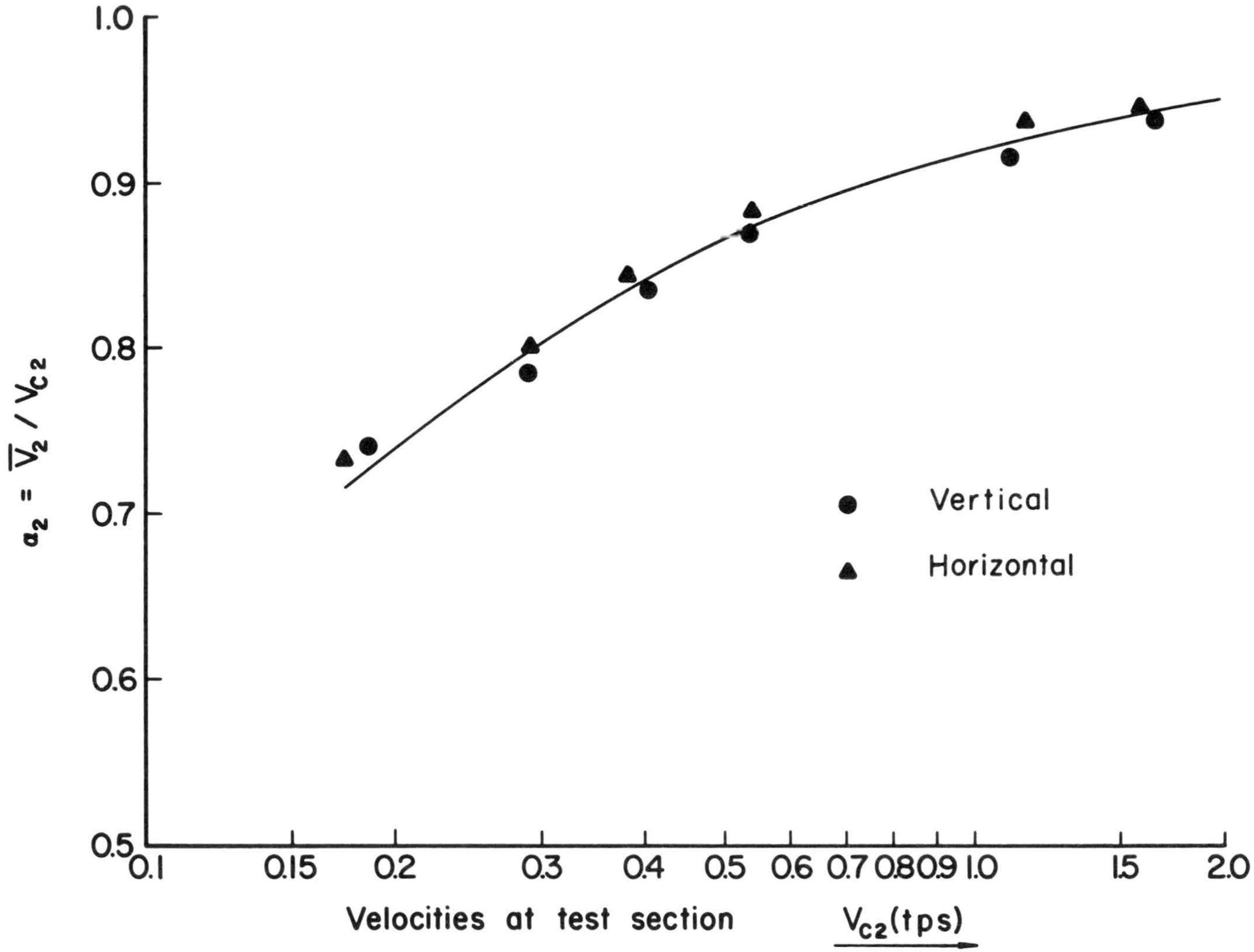

Figure 17. Values of α_2

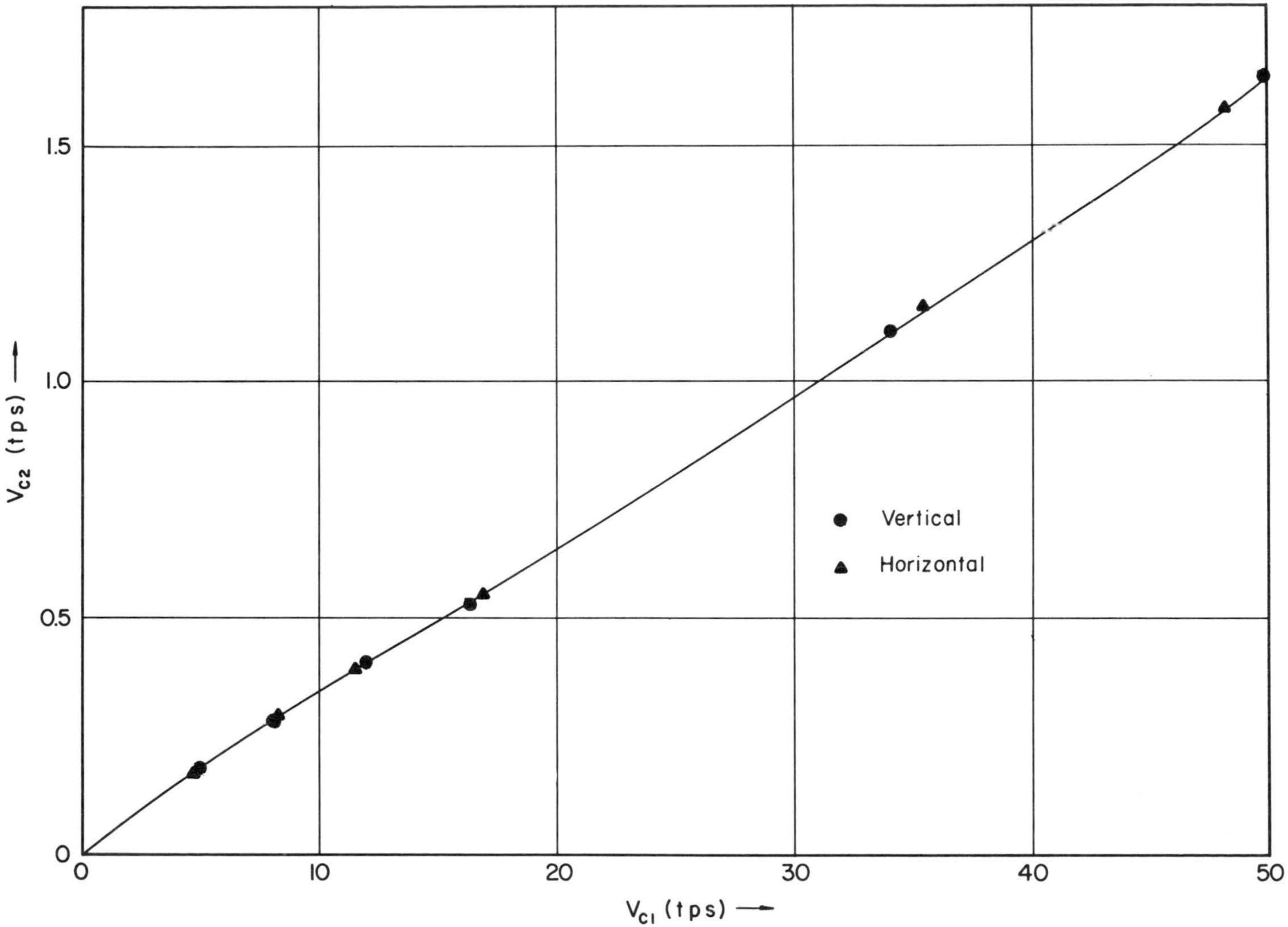

Figure 18. Calibration curve of the micro-tunnel

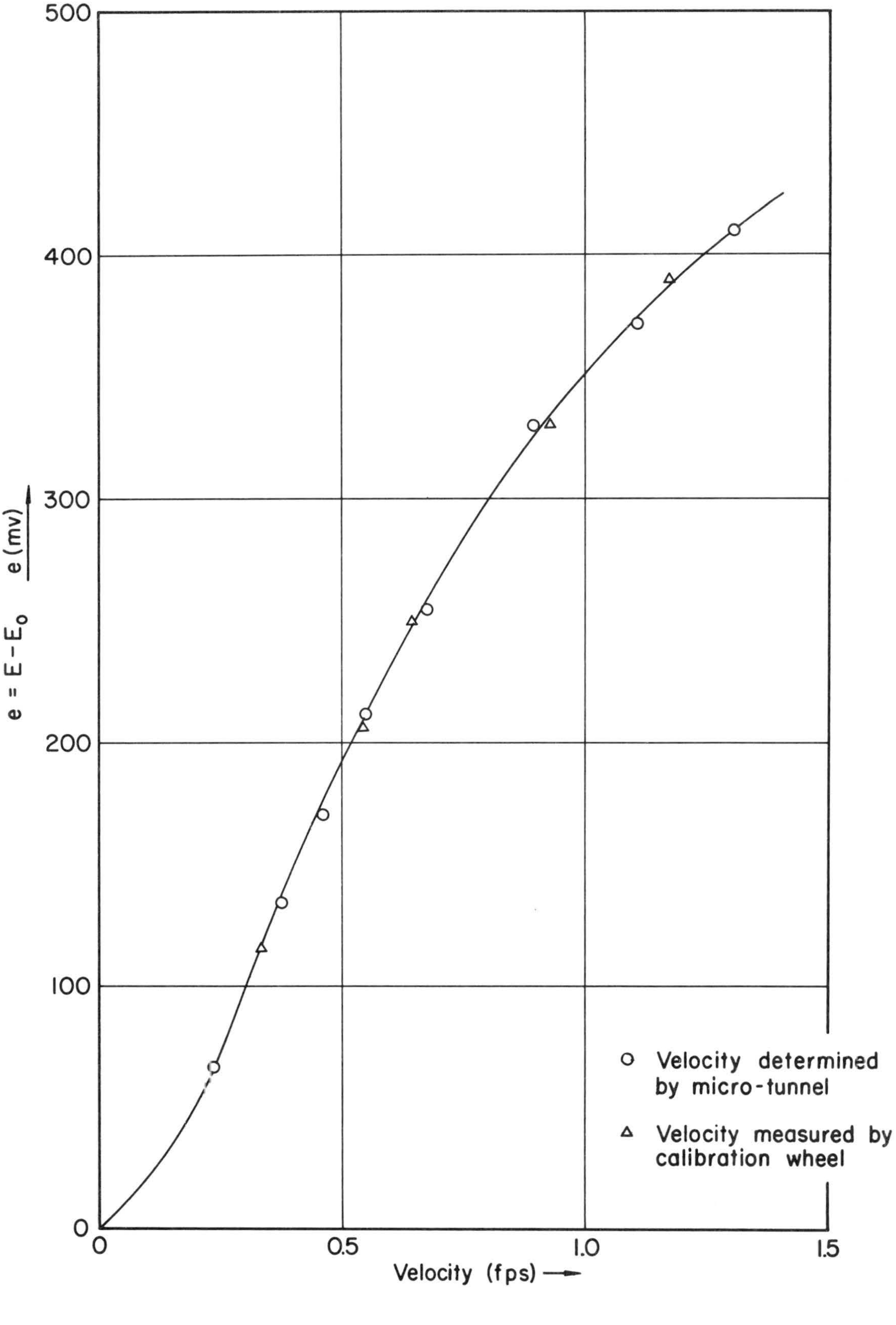

Figure 19. Check micro-tunnel calibration

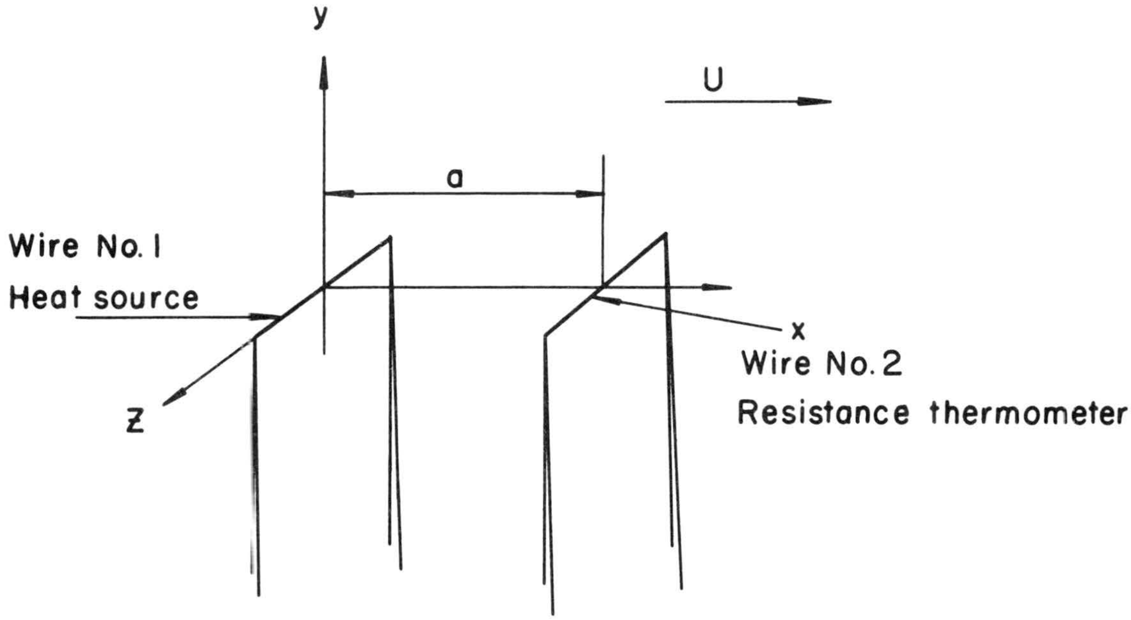

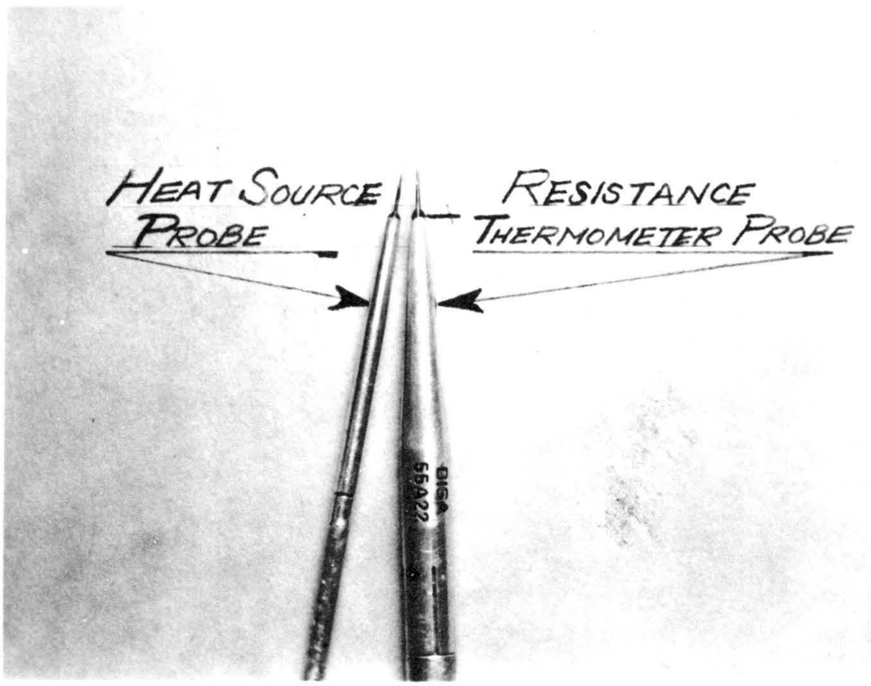

Figure 20. Sketch and photograph of the hot-spot anemometer probes

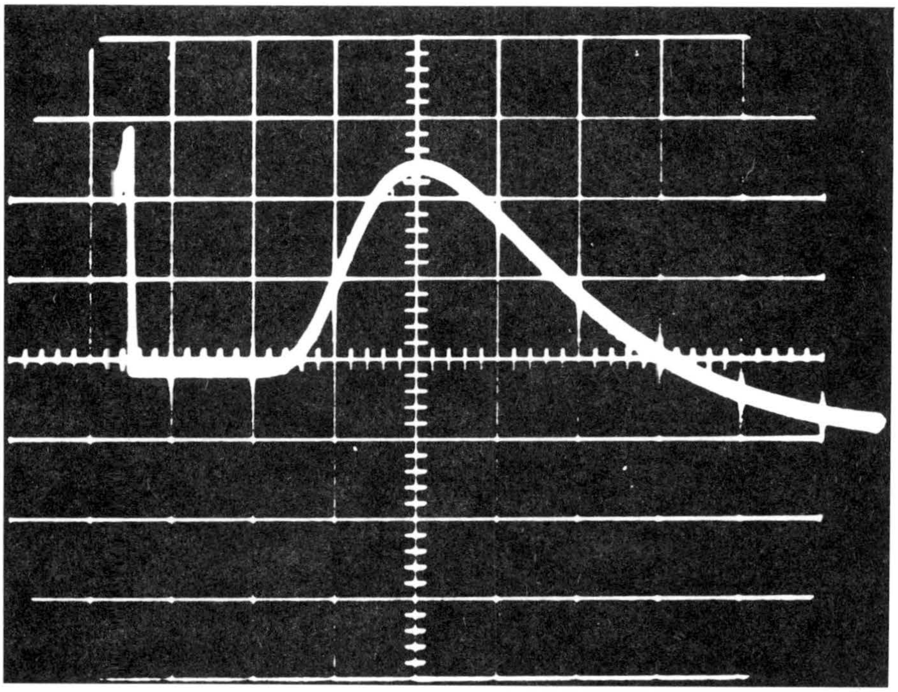

Scale Vertical { heating pulse 1 v/division; thermometer response 0.1 v/division }

Horizontal 5 ms/division

Figure 21a. Oscillogram of heating current pulse and subsequent response of amplified (1000 times) Pt.-thermometer

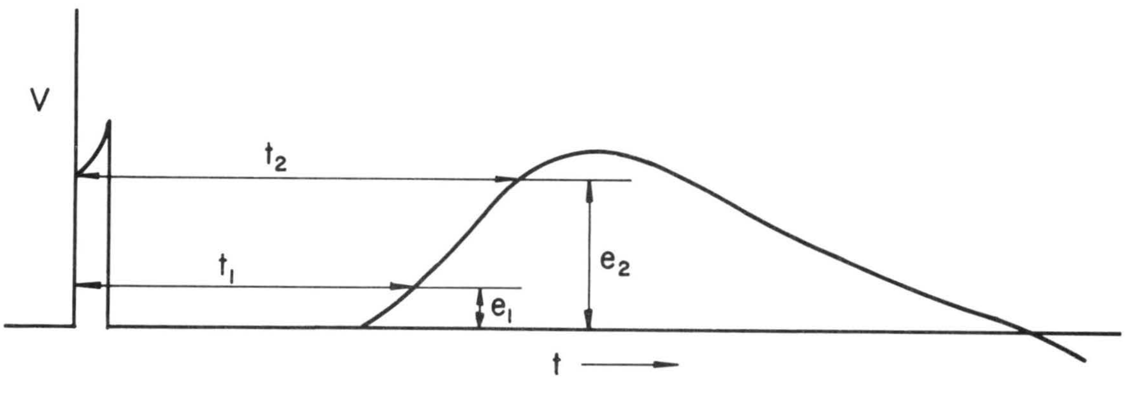

Figure 21b. Sketch of time measurement

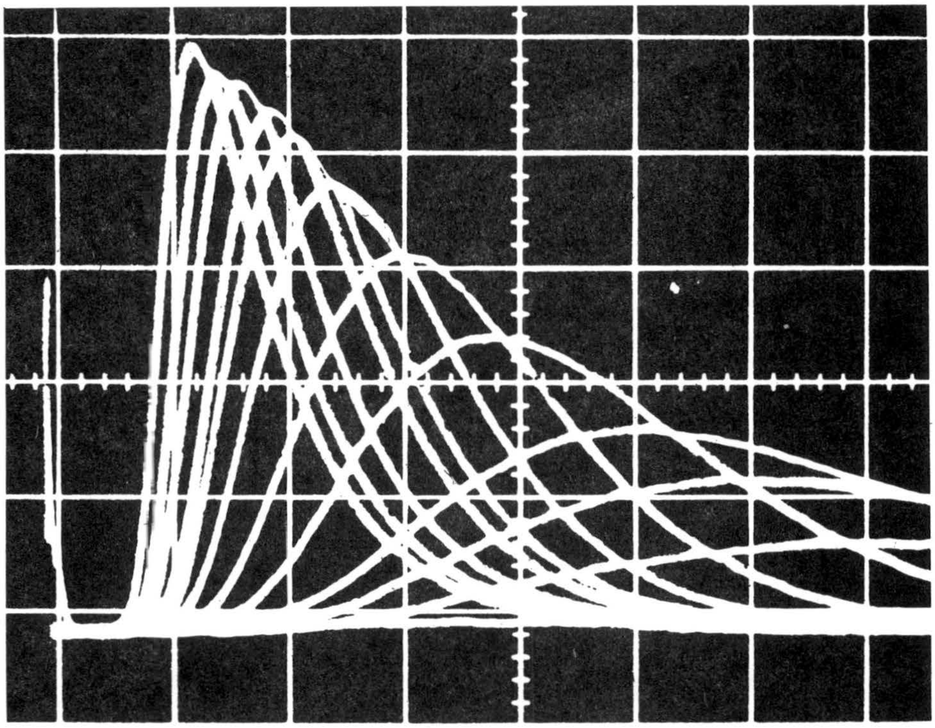

Scale	Vertical	pulse	1 v/division
		response	5 v/division
	Horizontal	5 ms/division	

Grain 10^3 a = 0.069 in

Figure 22. The resistance thermometer response for various velocities

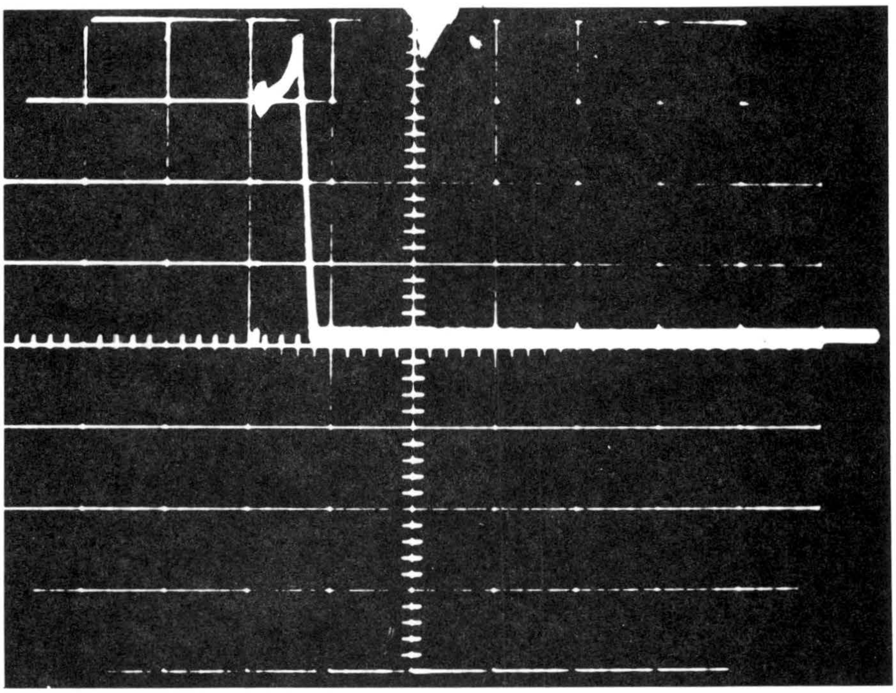

Scale Vertical 1 v/division

Horizontal 0.2 ms/division

Figure 23. Heating pulse

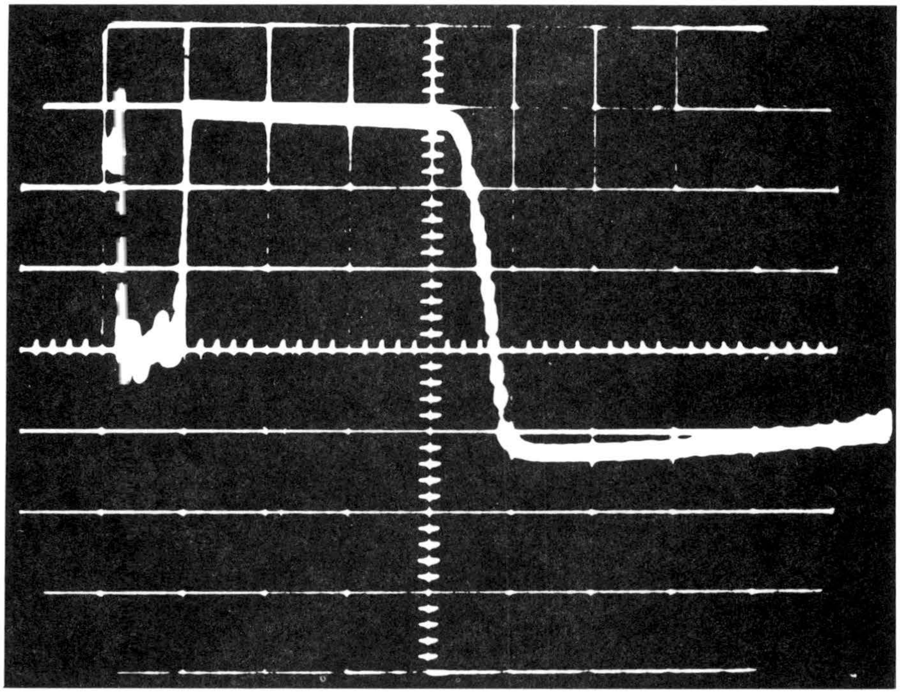

Scale	Vertical	{	pulse	1 v/division
			response	10 v/division
	Horizontal		10 ms/division	

Figure 24. A pulse and the correspondent response of the resistance thermometer (response amplified 10^6 times)

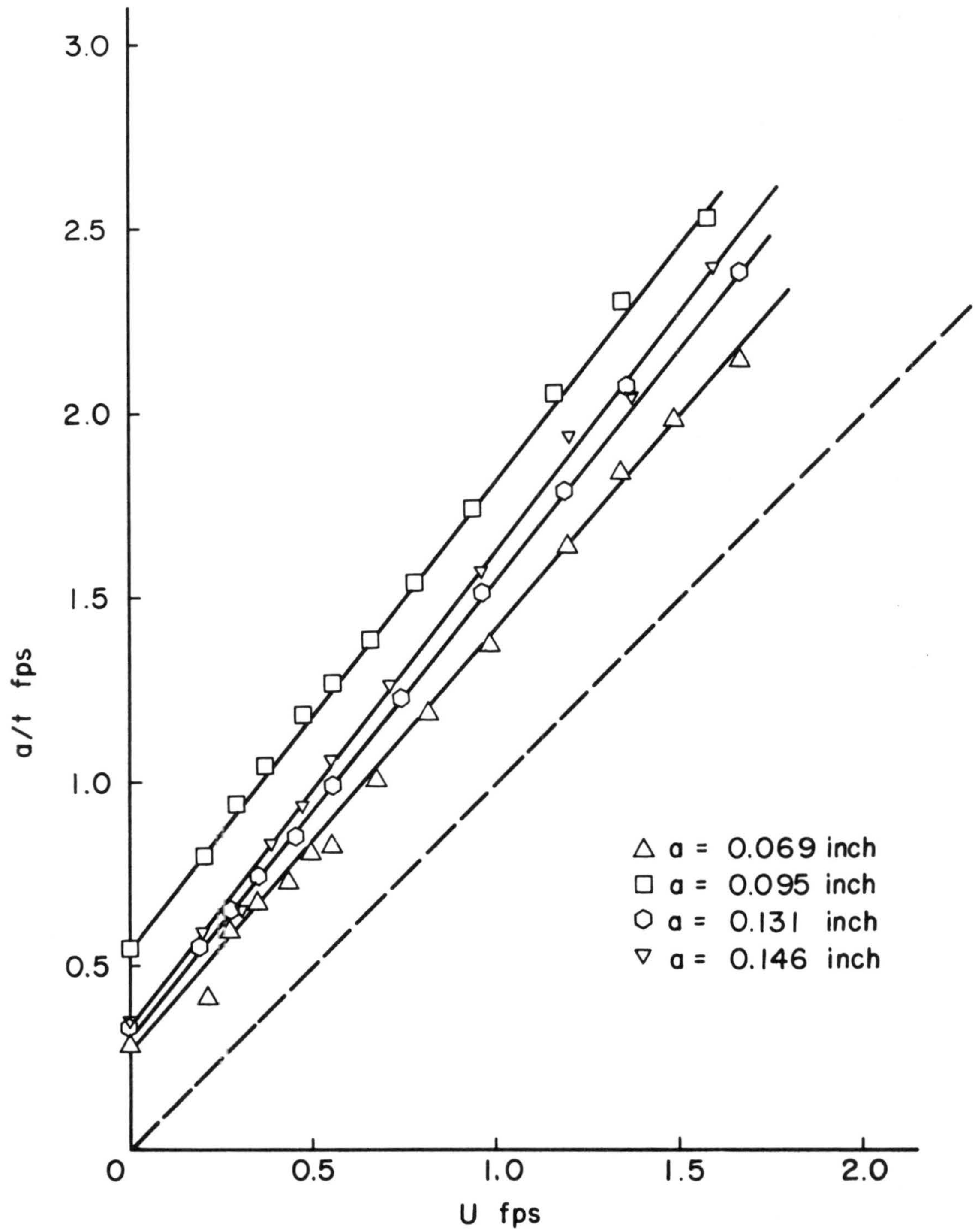

Figure 25. Hot spot anemometer results a/t vs. true velocity U

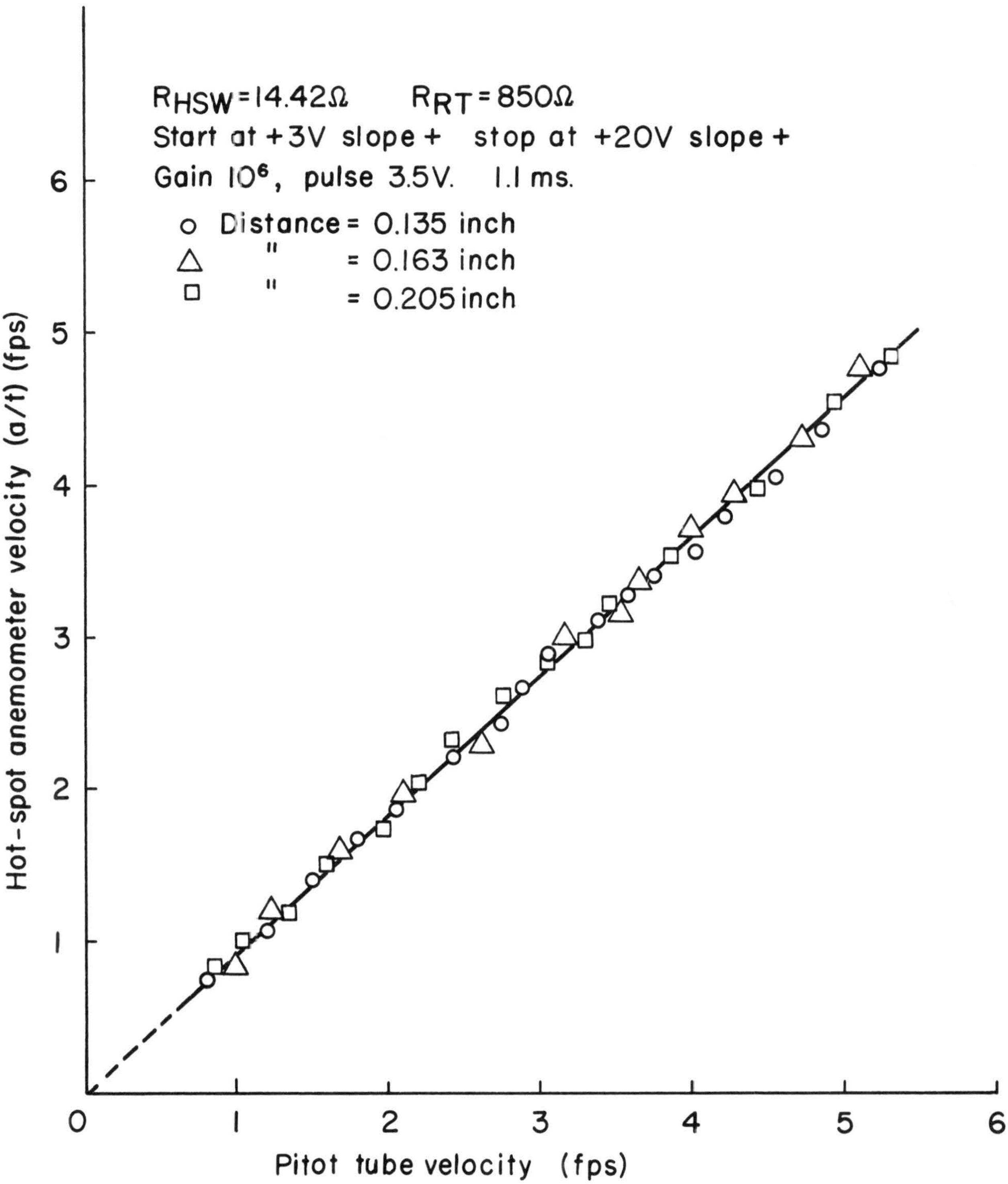

Figure 26. Calibration curve of HSA at large velocities

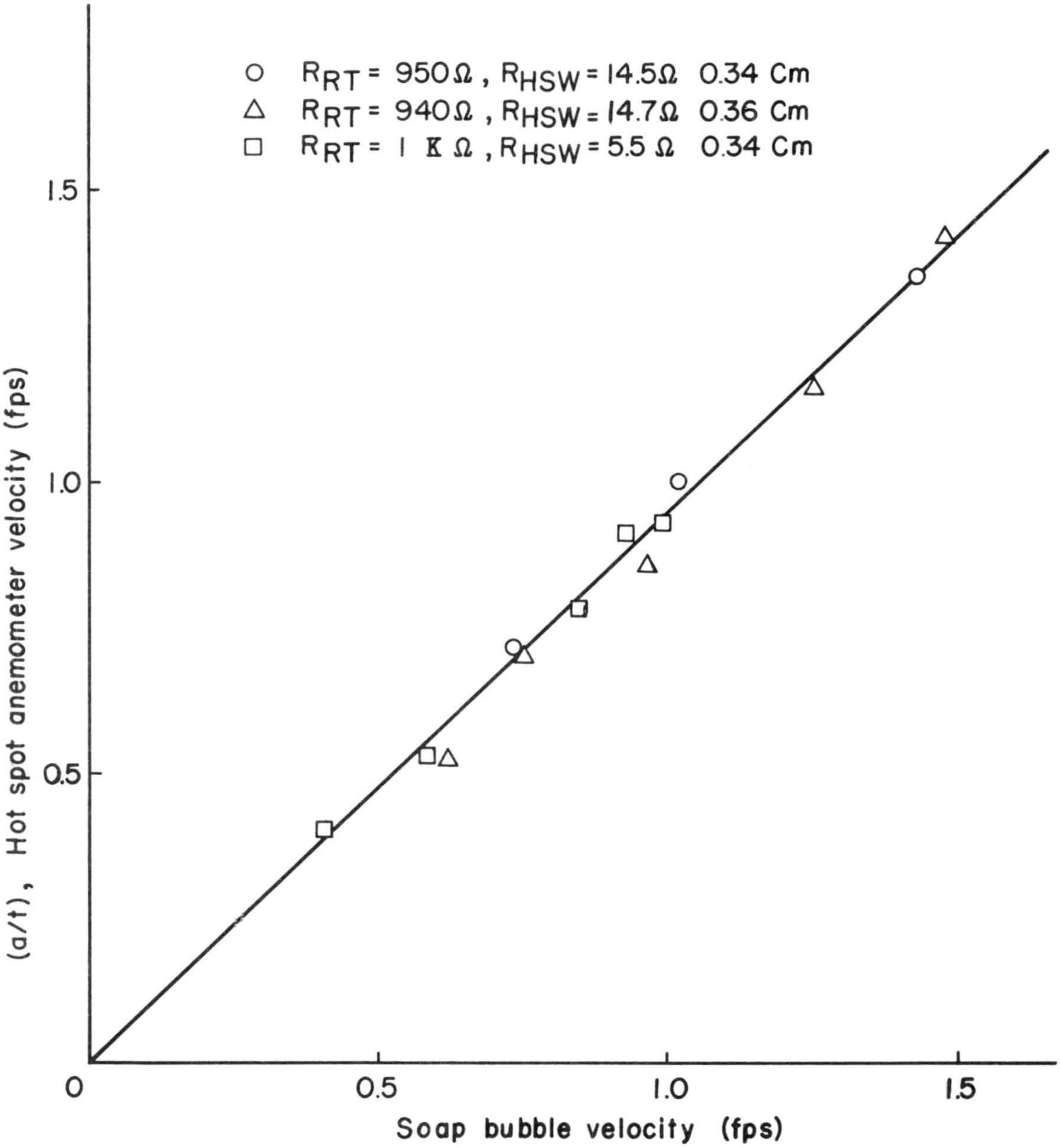

Figure 27. Calibration curve of HSA in large wind tunnel

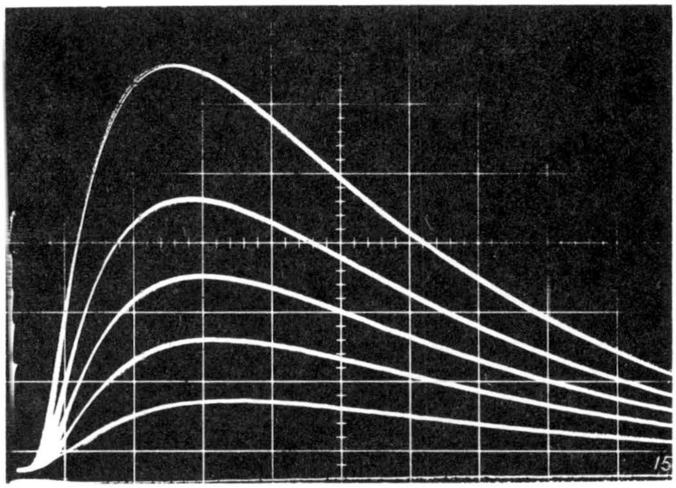

$R_{HSW} = 7.8\ \Omega$, duration of pulse = 0.15 ms

wire distance $y = 0.053$ in

Figure 28. Oscillograms of heating pulse and Pt-thermometer response with wires on same vertical and no flow

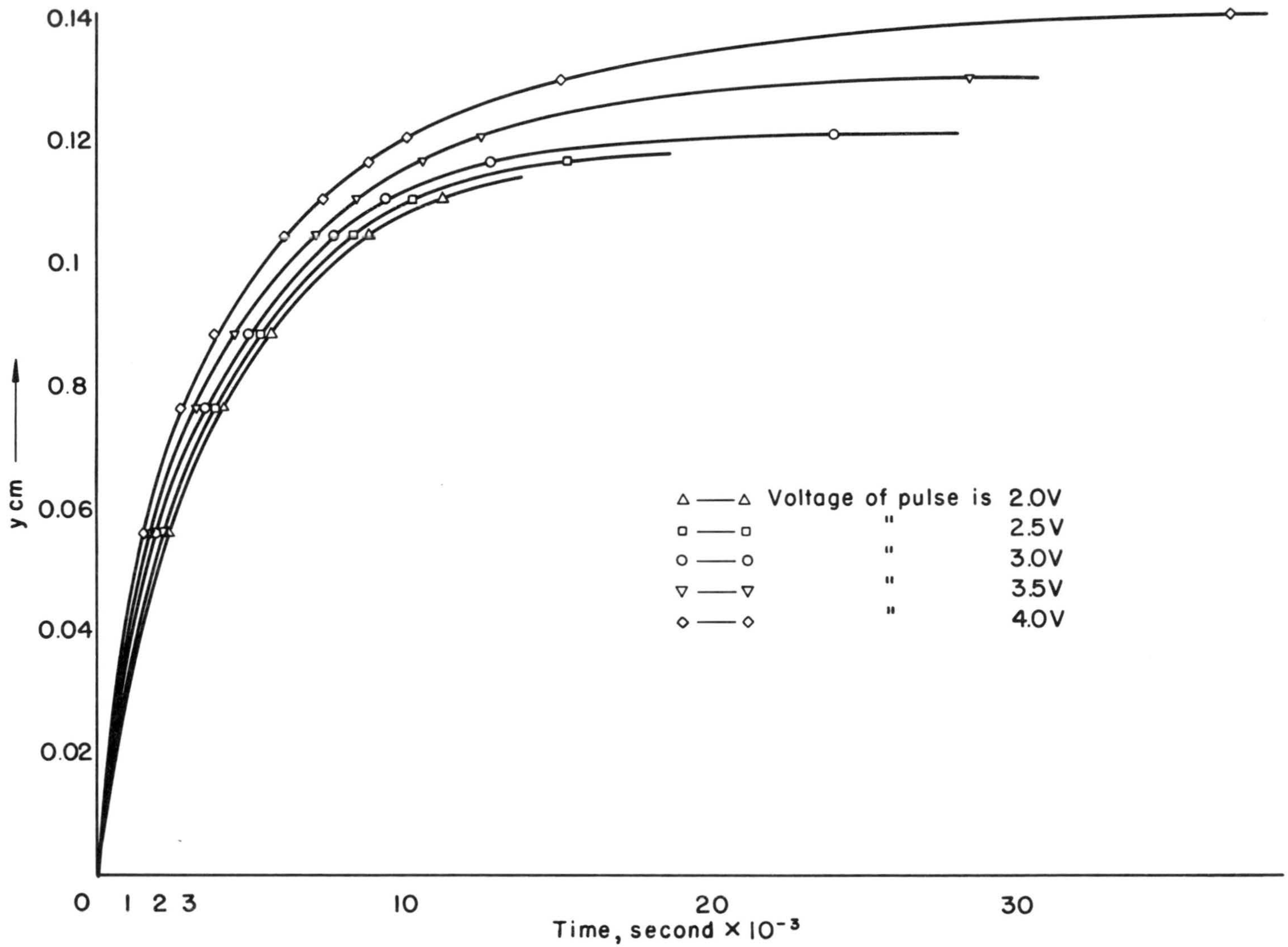

Figure 29. Rise time of heat cloud for various heat pulses

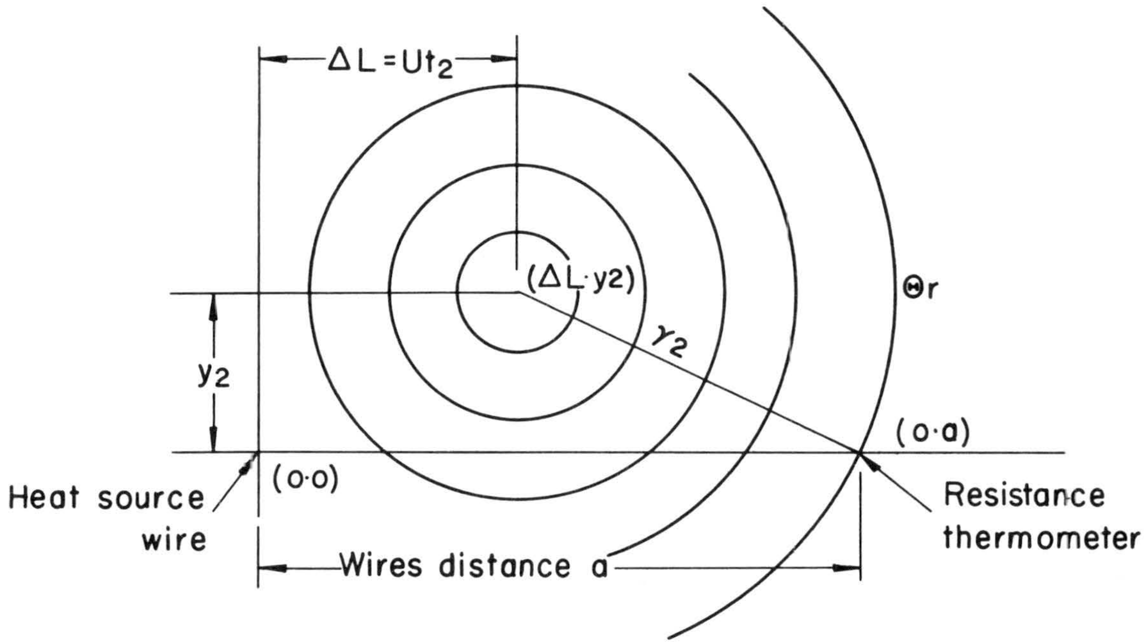

Figure 30a. A sketch of the heat pulse in flow

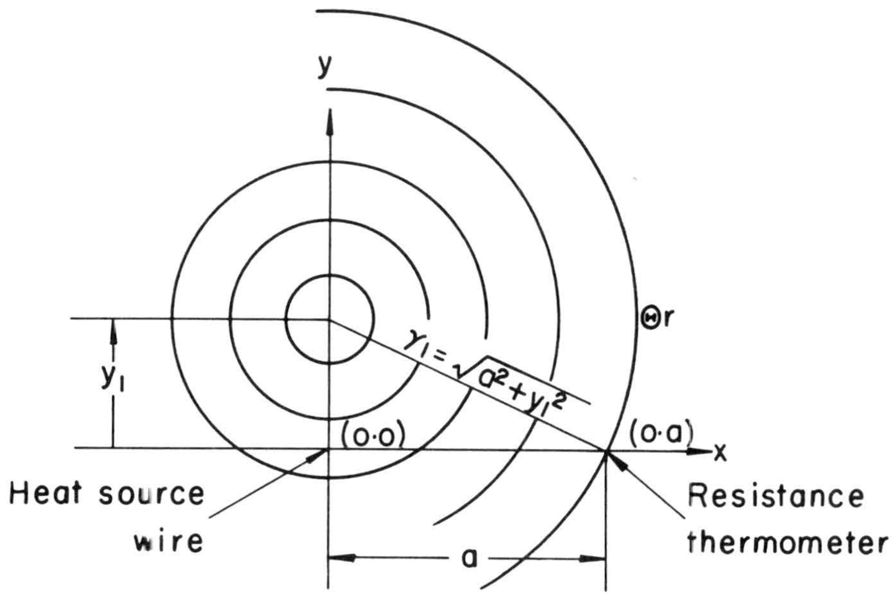

Figure 30b. Sketch of the heat pulse when U = 0

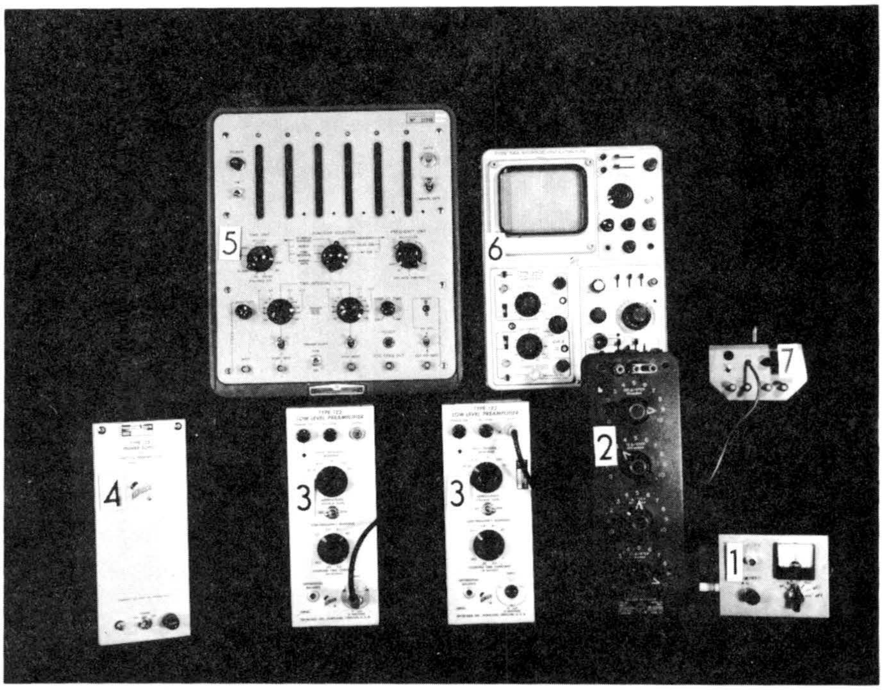

1. Pt-resistance thermometer bridge 2. Decade resistance
3. Amplifiers 4. Power supply of amplifiers 5. Counter
6. Dual beam storage oscilloscope 7. Current pulse generator

Figure 31. Instrumentations of HSA

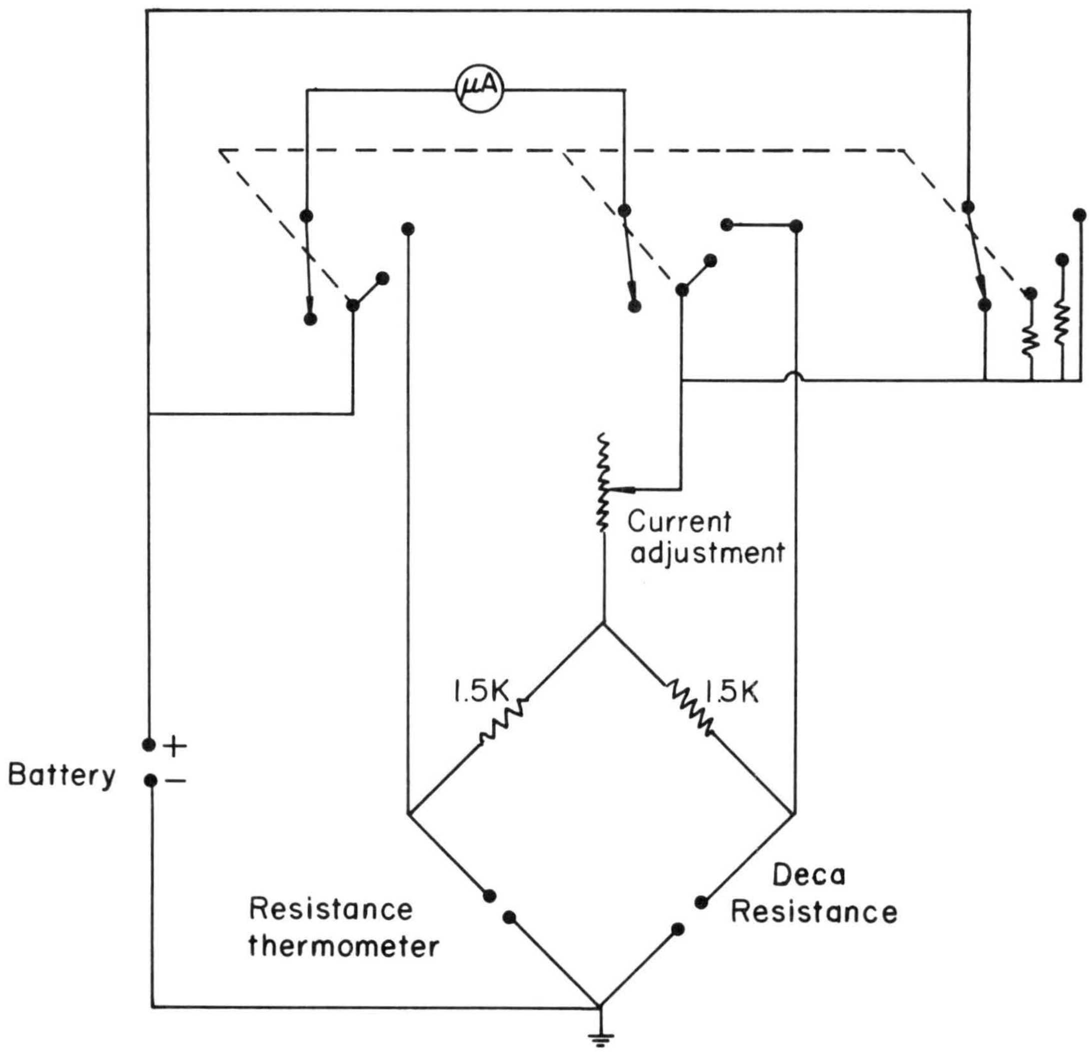

Figure 32. Circuit diagram of the bridge

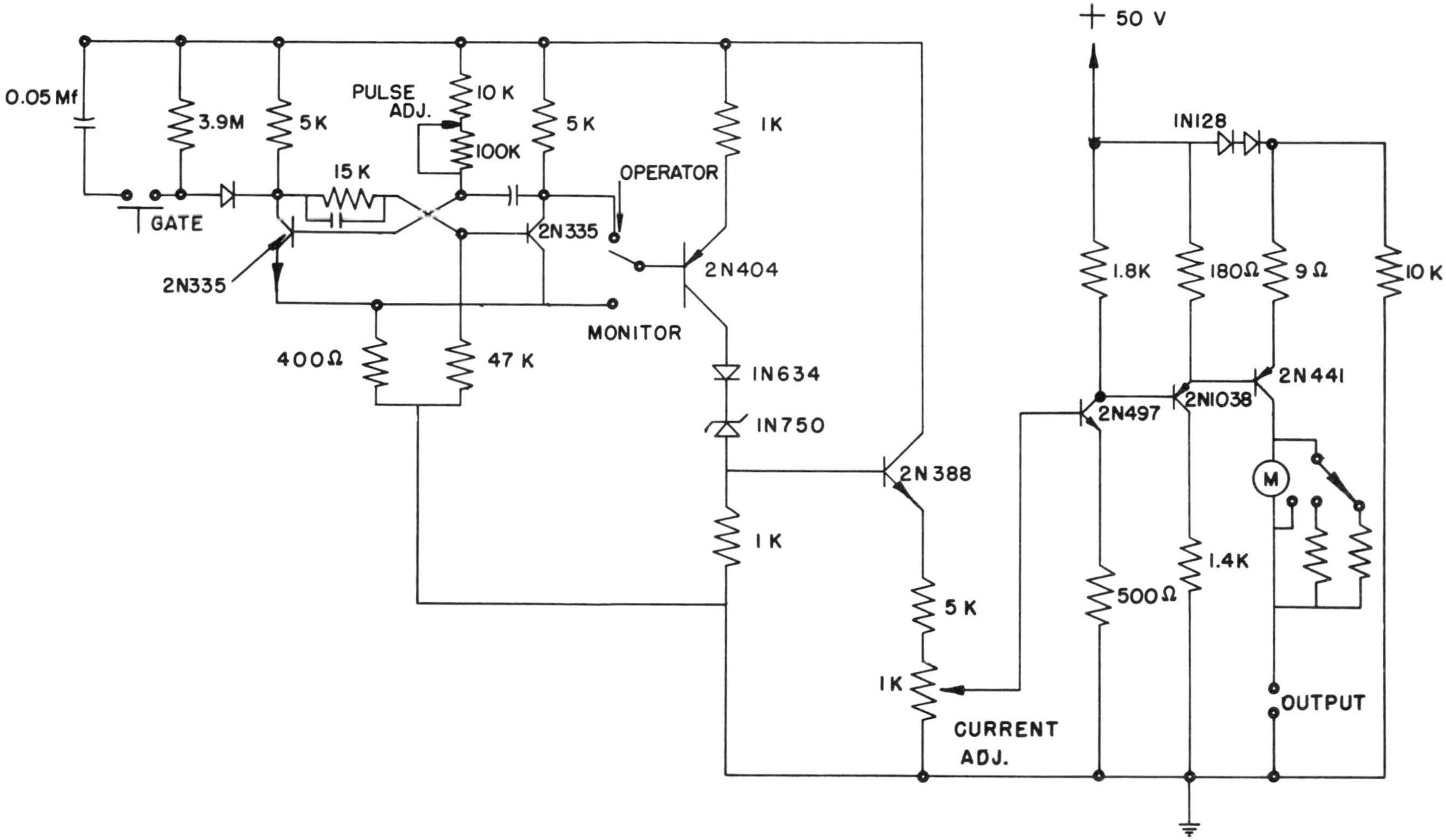

Figure 33. Circuit diagram of current pulse generator

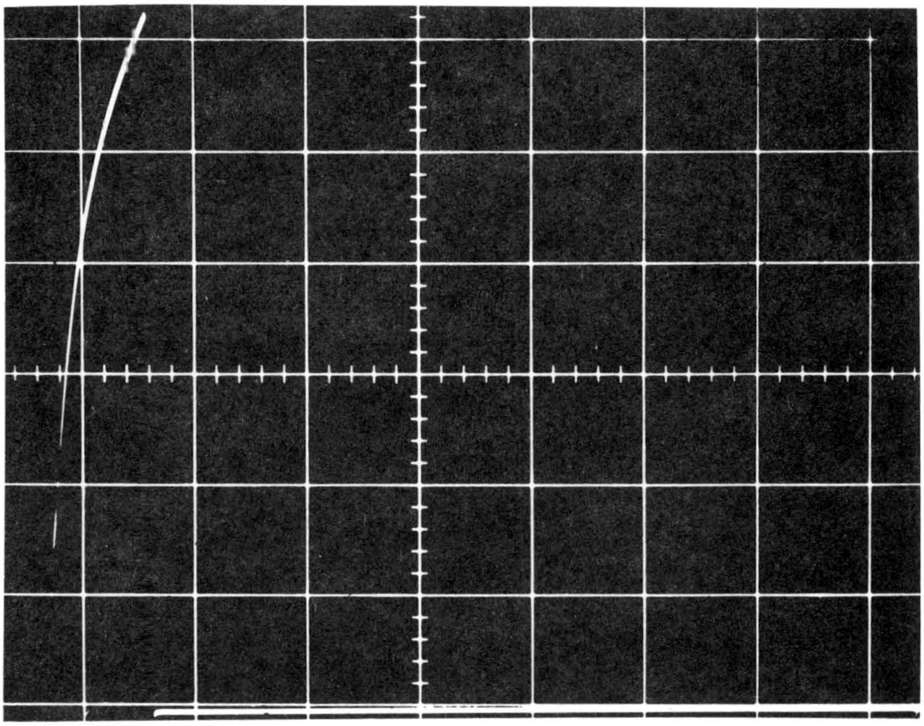

Scale Vertical 0.5 v/division

Horizontal 0.2 ms/division

Figure 34. Oscillogram of heat pulse

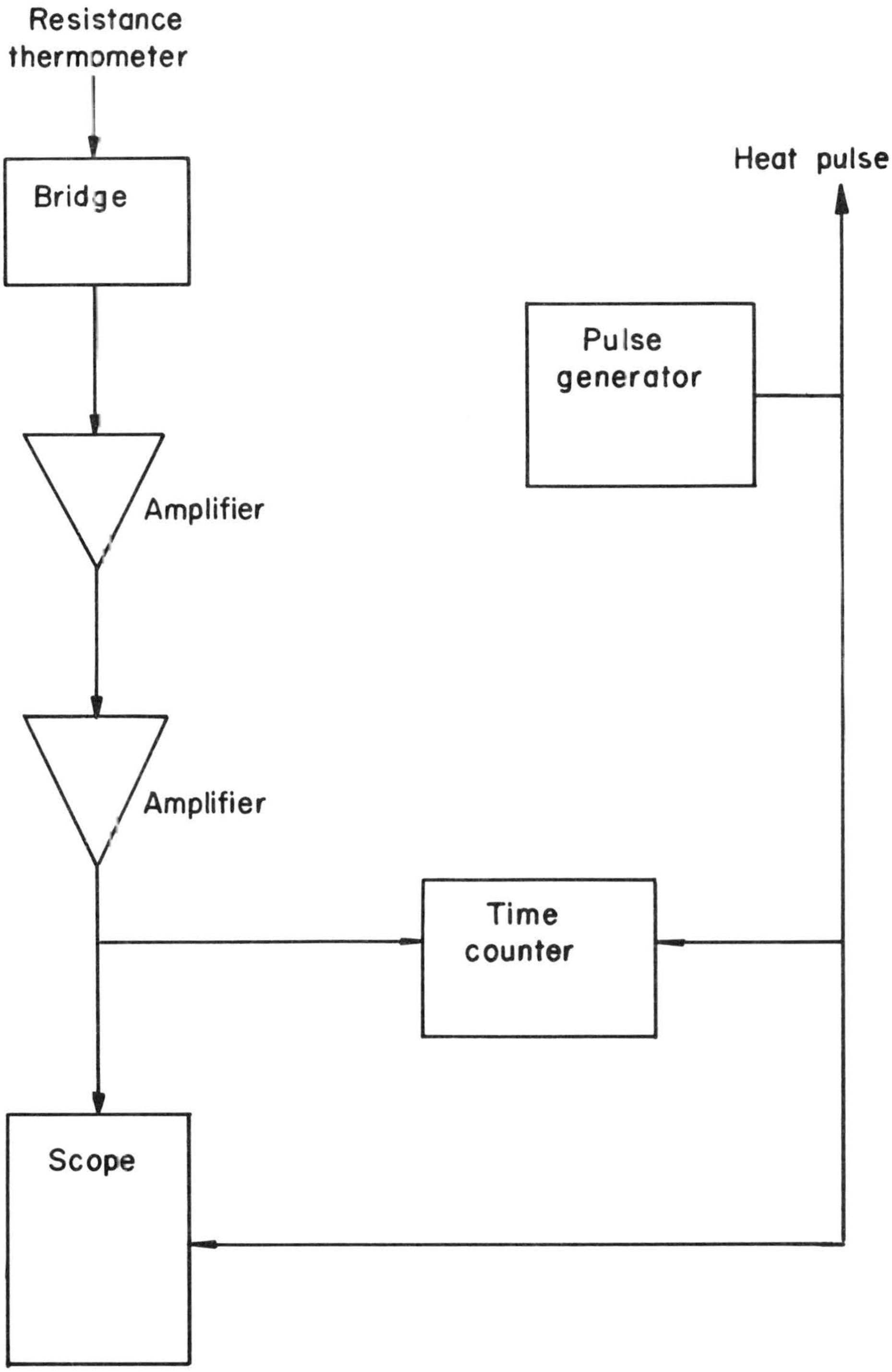

Figure 35. Block diagram of HSA

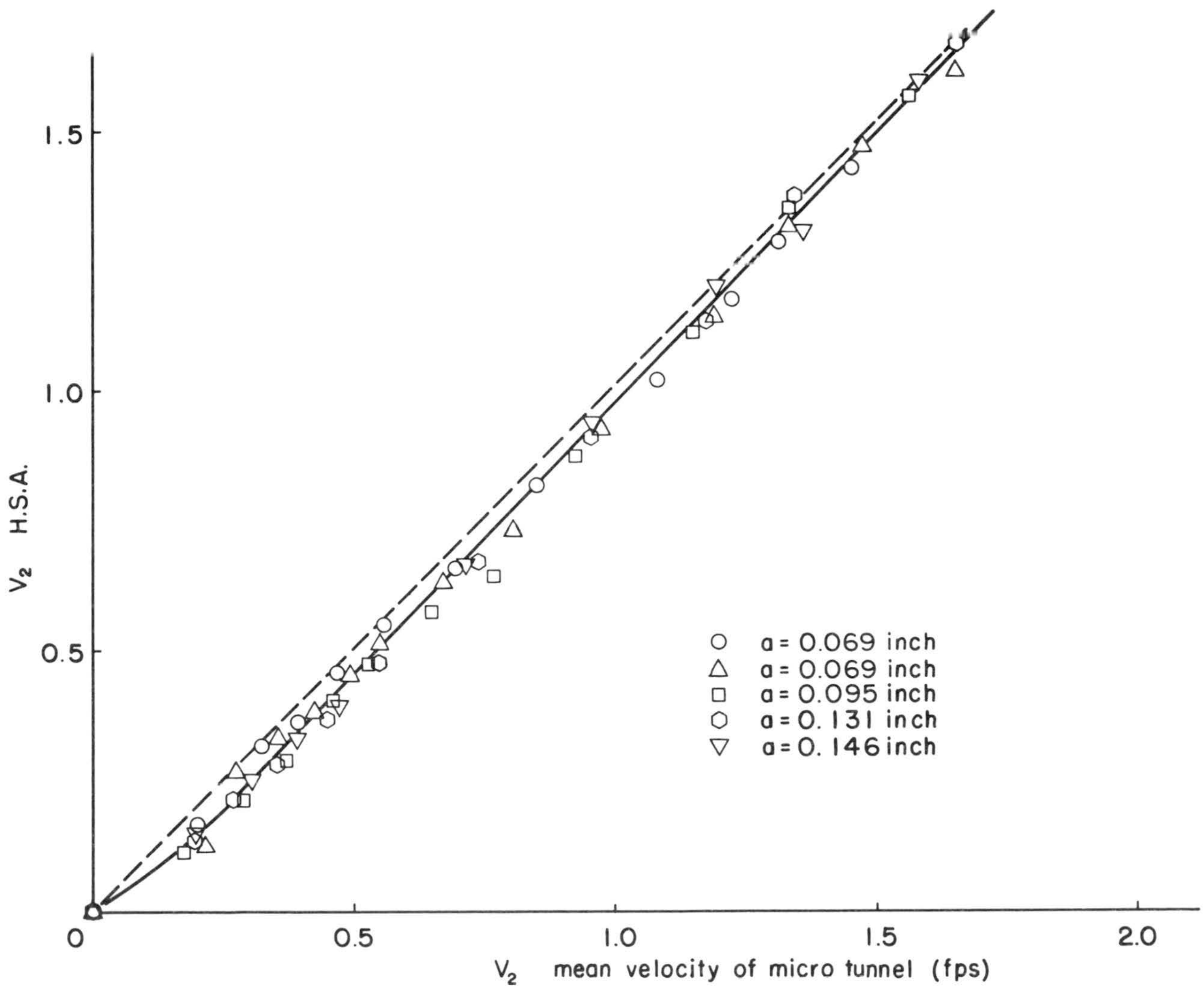

Figure 36. Corrected velocity determined from HSA vs. true velocity

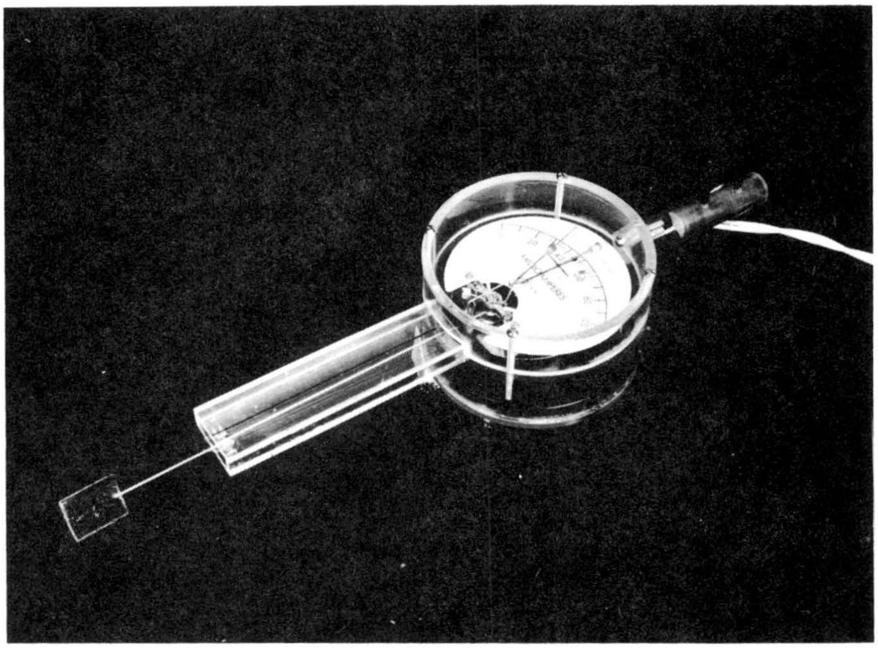

Figure 37. Drag anemometer

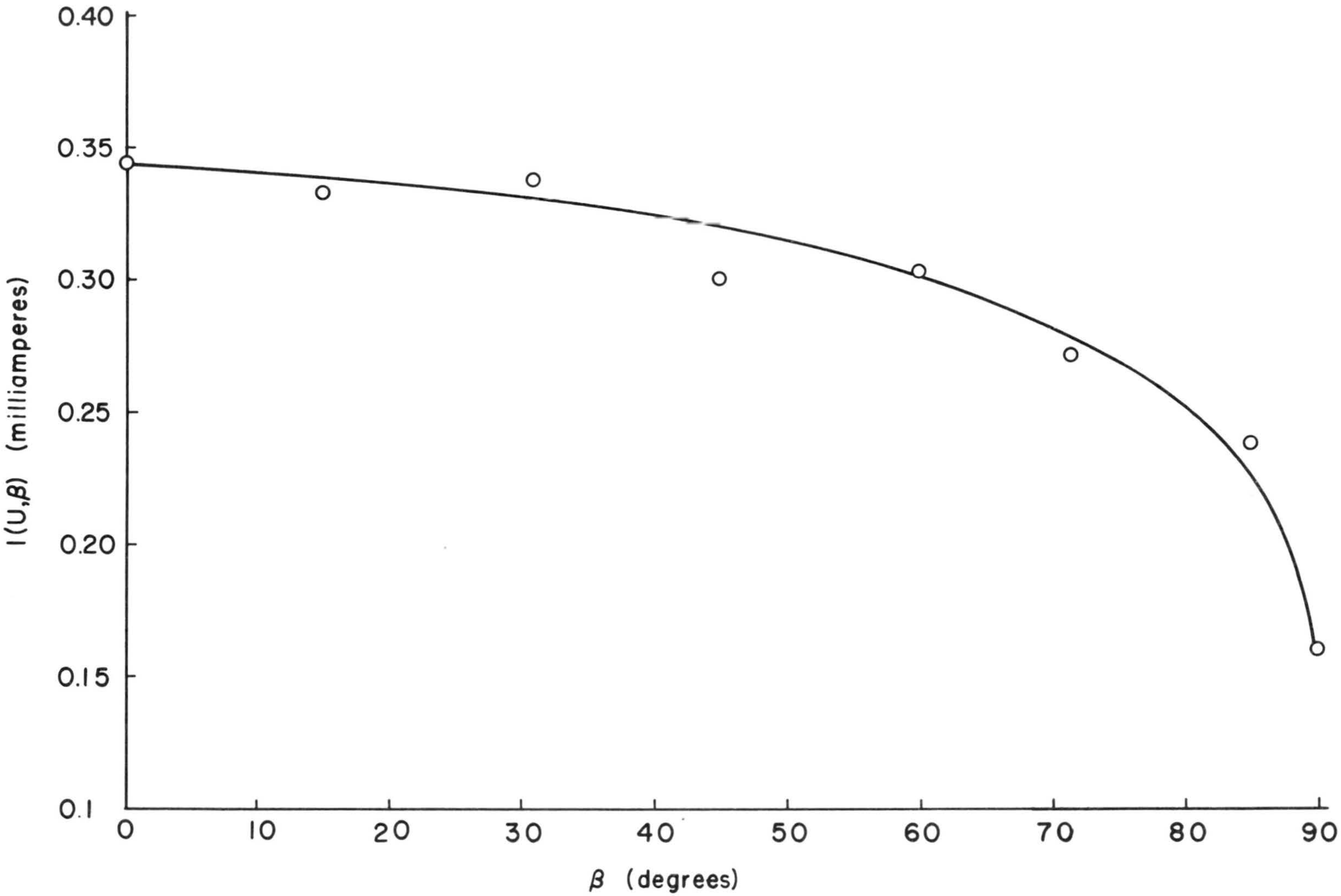

Figure 38. Directional measurement of drag anemometer in large wind tunnel

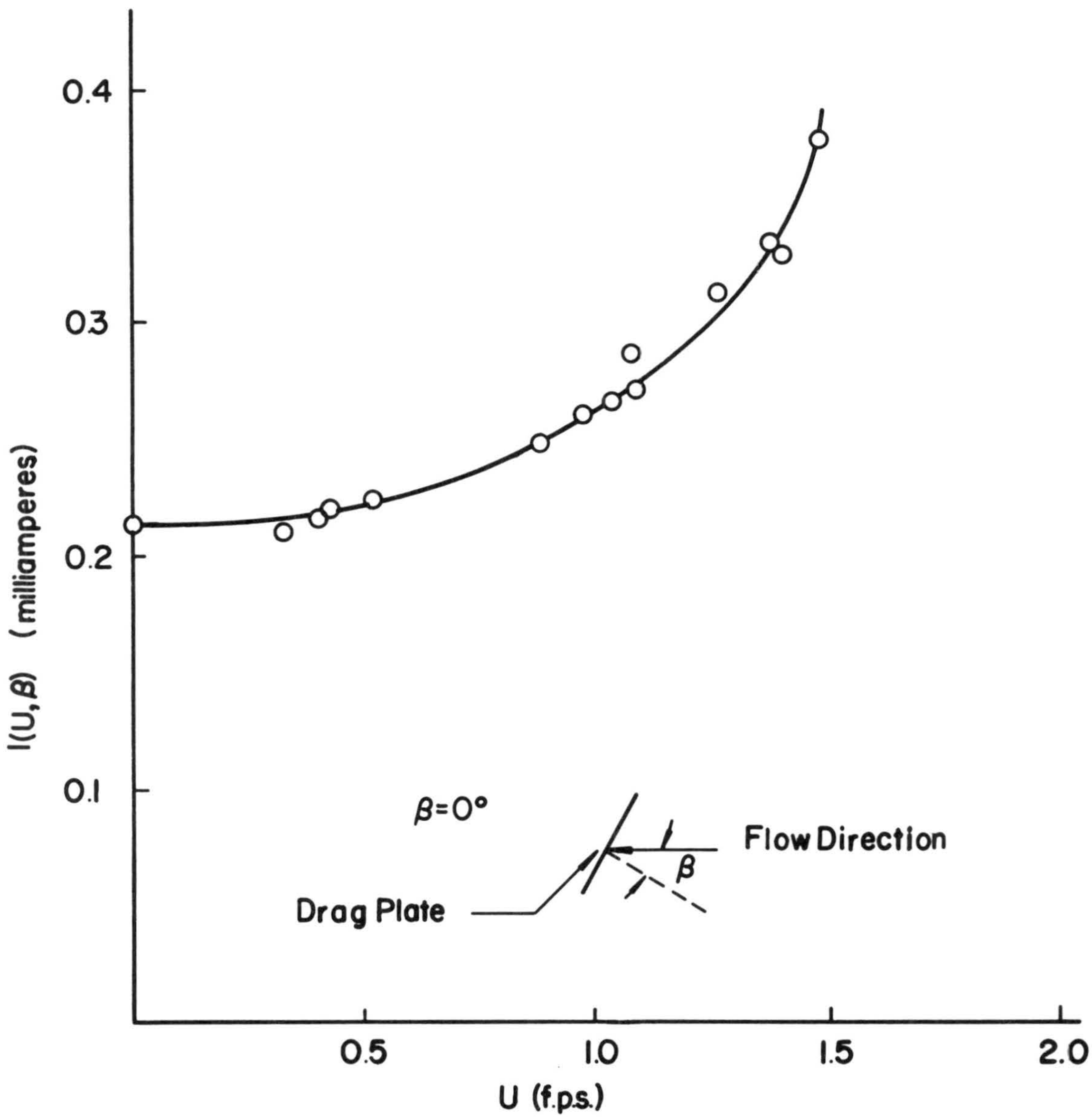

Figure 39. Calibration of drag anemometer in large wind tunnel U measured with hot-spot anemometer

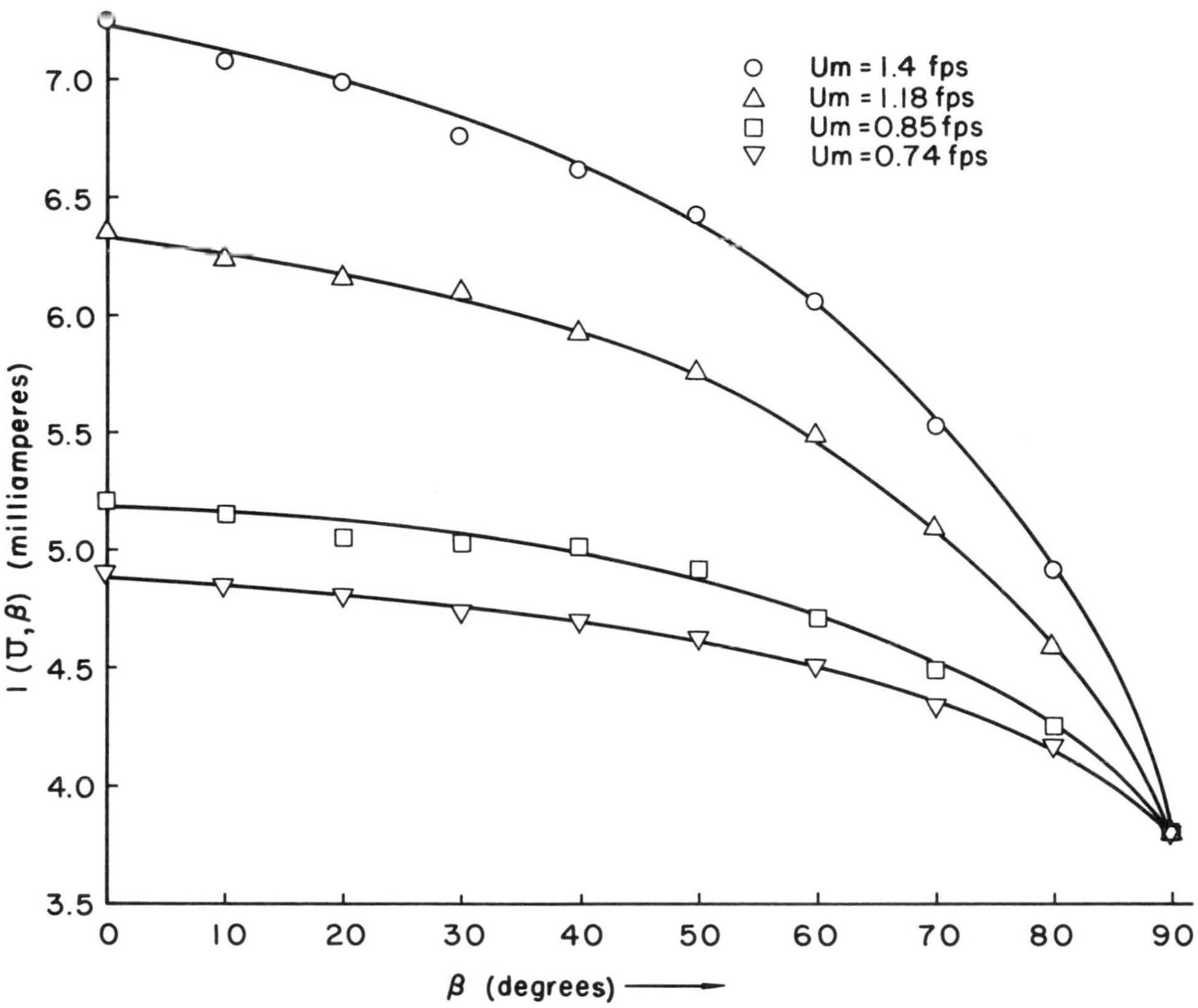

Figure 40. Directional measurement of drag anemometer in micro-wind tunnel

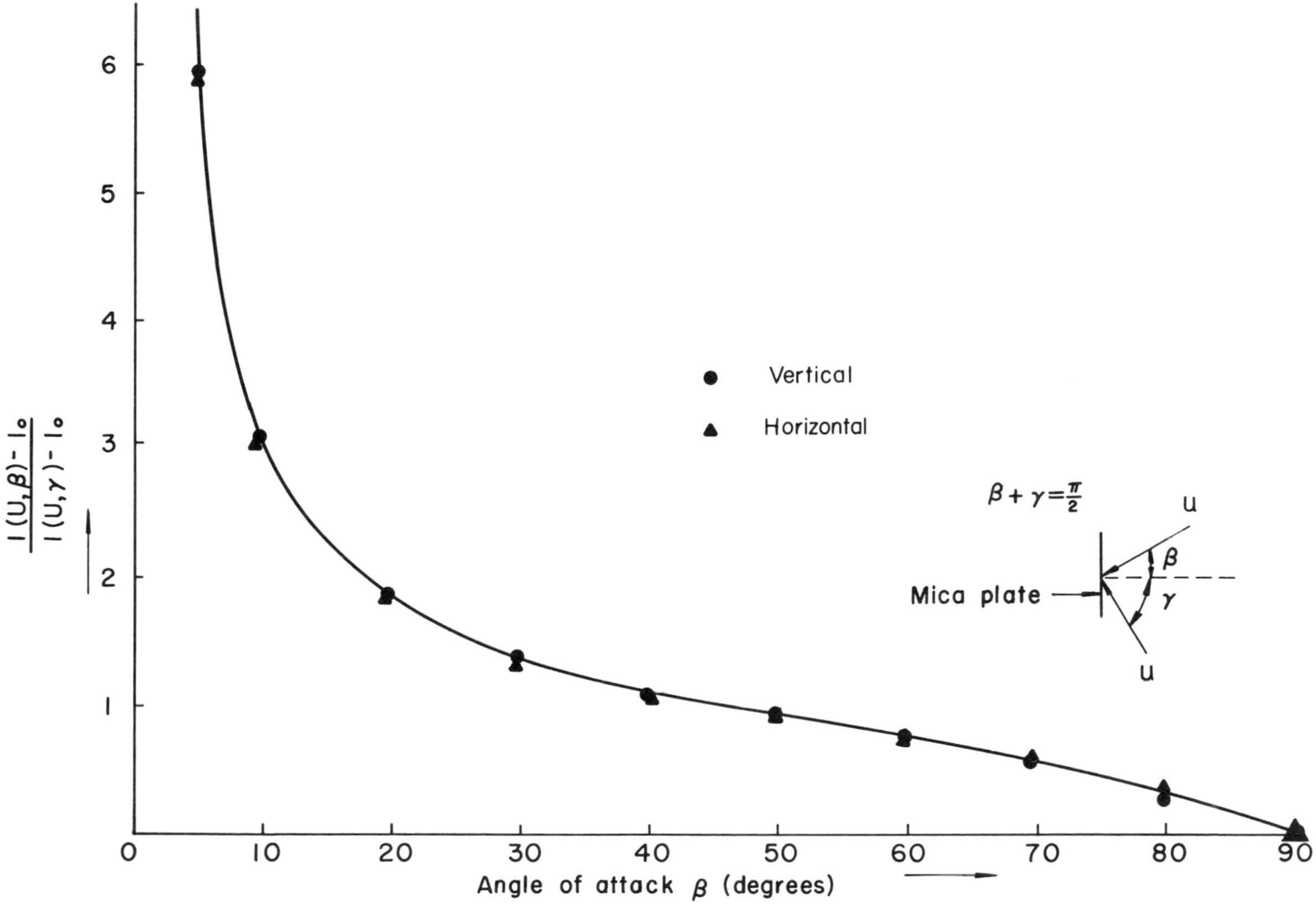

Figure 41. Universal curve $\dfrac{I(U,\beta) - I_o}{I(U,\frac{\pi}{2} - \beta) - I_o}$ vs. β

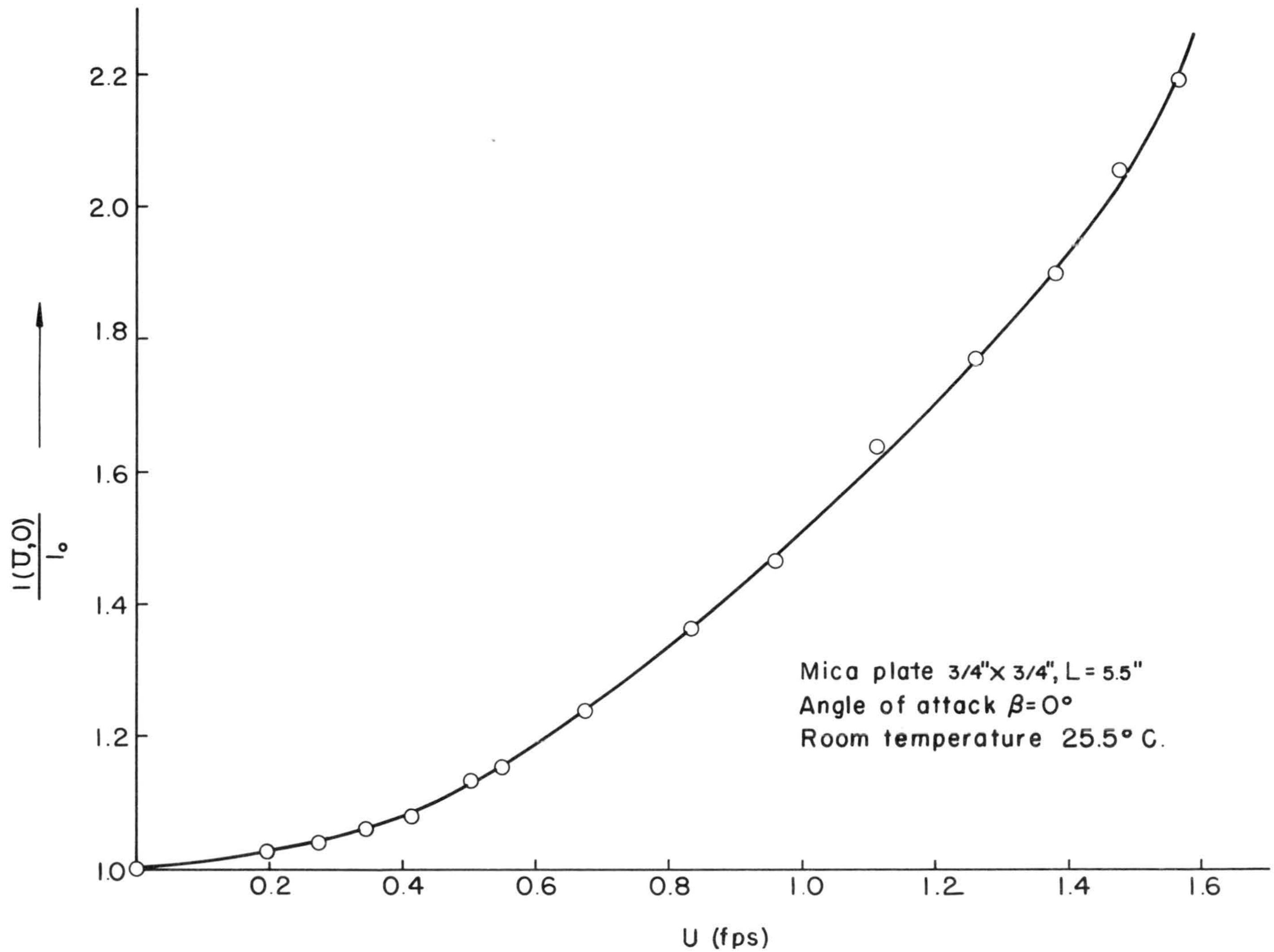

Figure 42. Calibration curve of drag anemometer

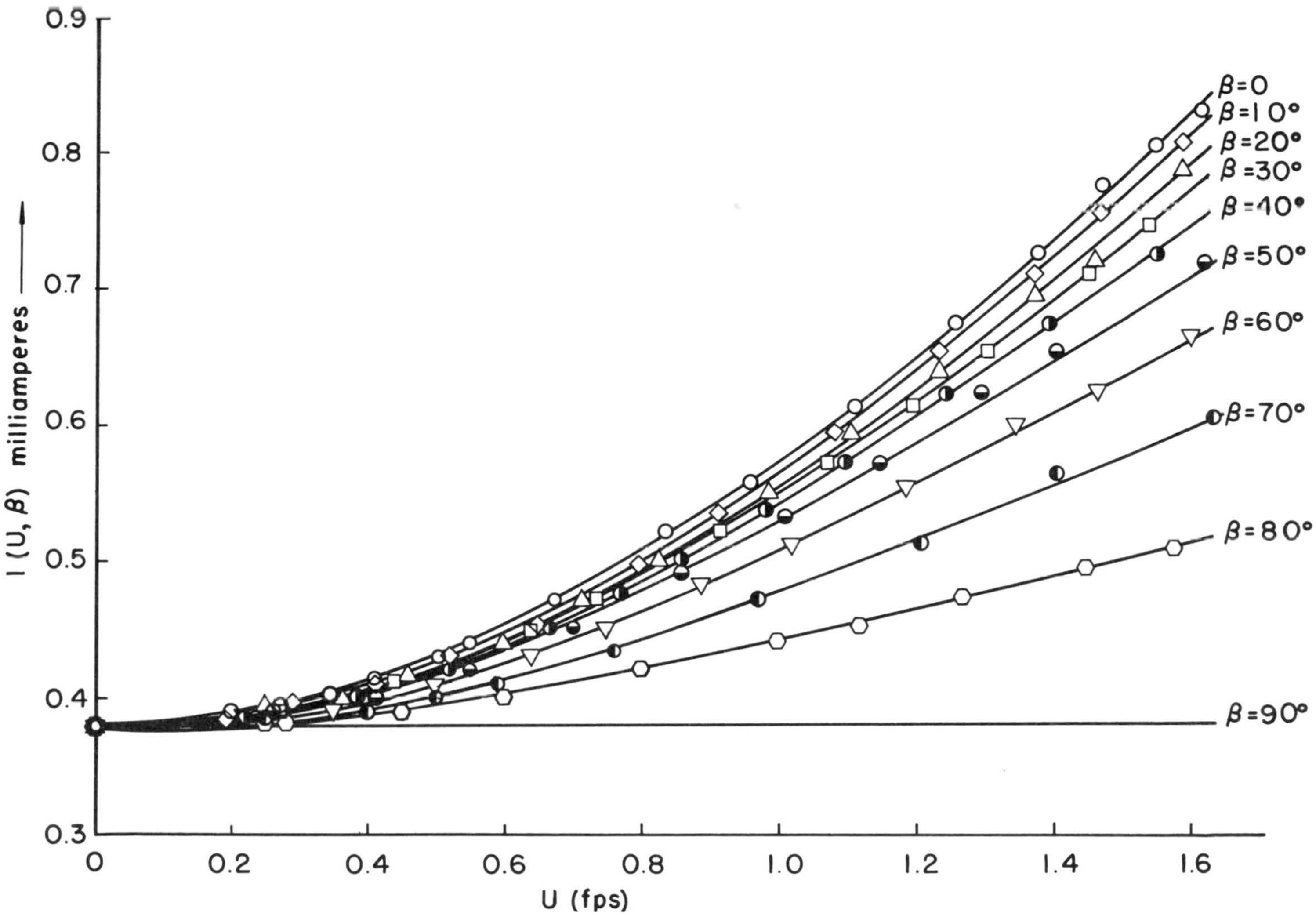

Figure 43. Calibration of drag anemometer for various β

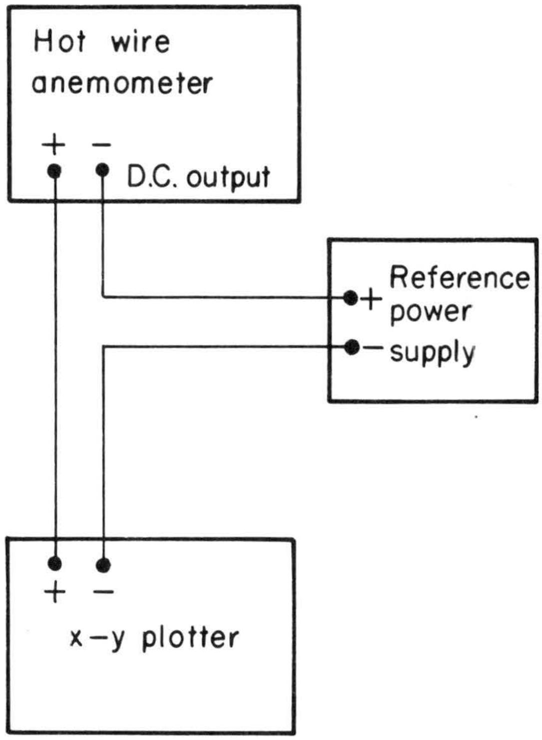

Figure 44. Block diagram of the bucking system

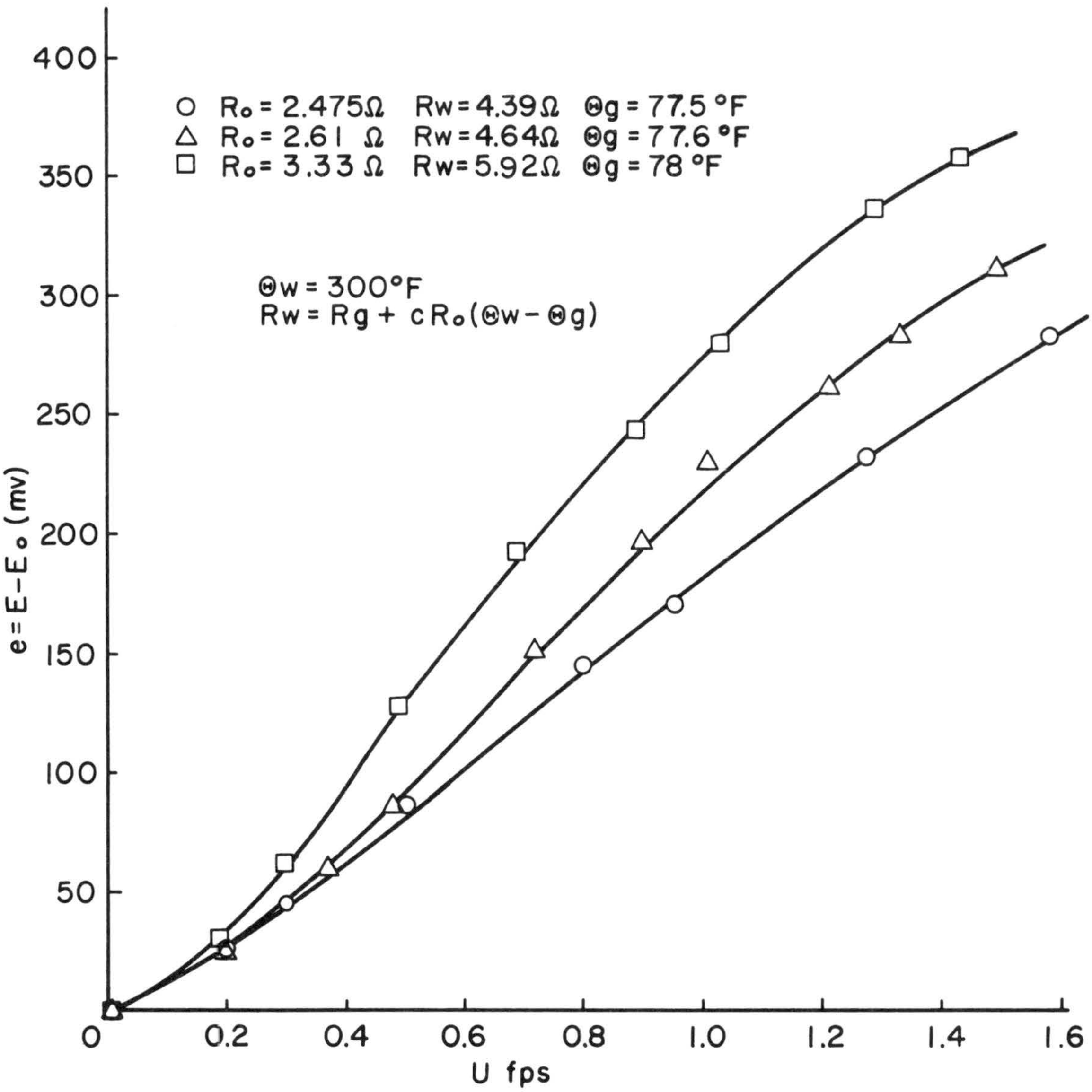

Figure 45. Calibration of HWA

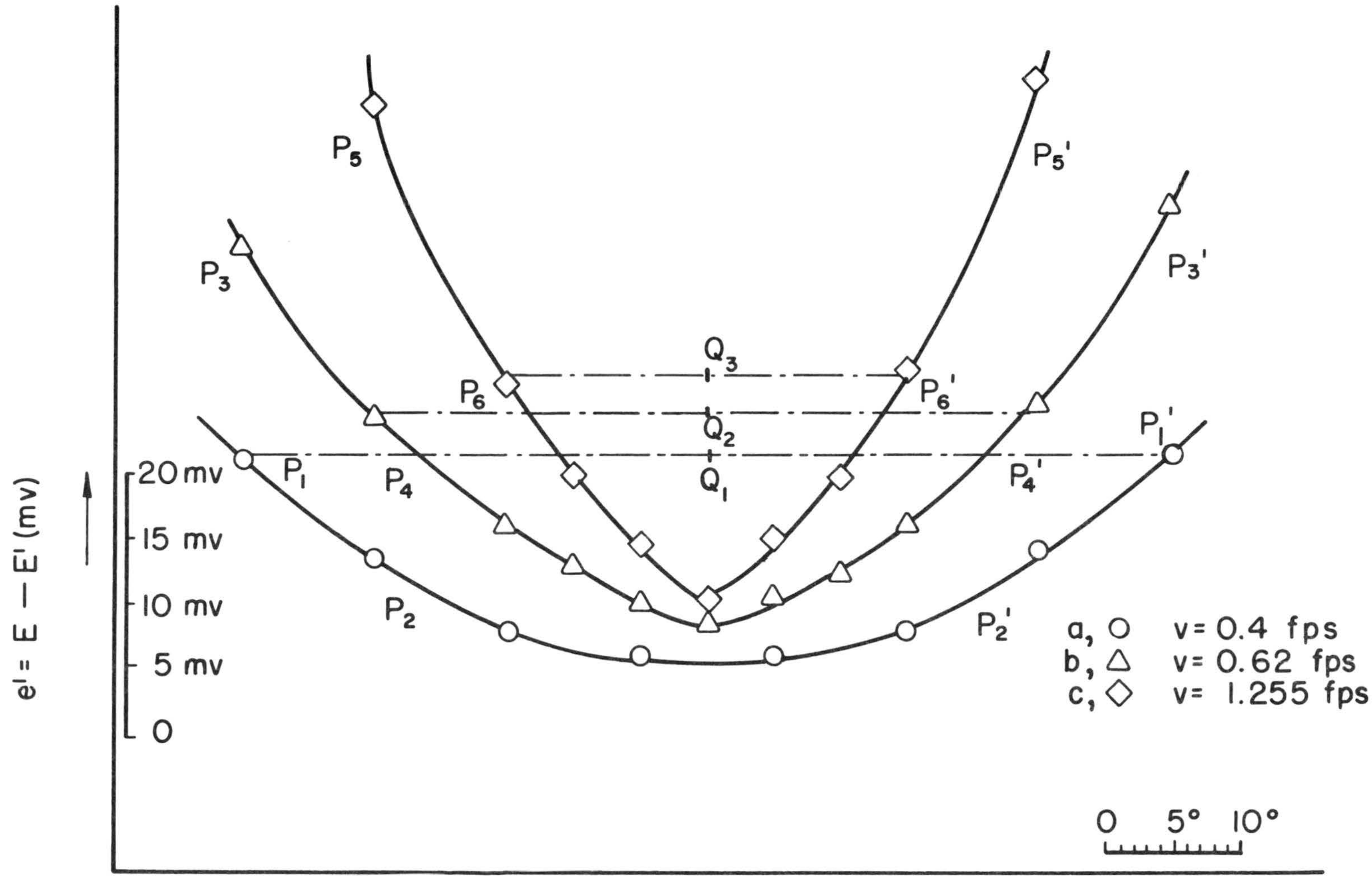

Figure 46. The directional measurement of HWA

BIBLIOGRAPHY

BIBLIOGRAPHY

1. Bauer, A. B., 1965, Direct measurement of velocity by hot-wire anemometry. AIAA Jour., Vol. 3 No. 6, 1189

2. Bradshaw, P., 1965, The effect of wind tunnel screens on nominally two-dimensional boundary layers. Jour. Fluid Mech. 22, 679-687.

3. Chao, J. L., and Sandborn, V. A., 1964, A resistance thermometer of transient temperature measurement. Fluid Mech. Paper No. 1, C.S.U. January.

4. Collins, D. C., and Williams, M. J., 1959, Two-dimensional convection from heated wires at low Reynolds numbers. Jour. of Fluid Mech., Vol. 6.

5. Head, M. R., and Surrey, N. N., 1965, Low-speed anemometer. Jour. of Scientific Instruments, Vol. 42, p.349, May.

6. Jokob, M., 1950, Heat transfer. Vol. 1, John Wiley and Son, Inc.

7. Kovasznay, L. S. G., 1946, Hot-wire investigation of the wake behind cylinders at low Reynolds numbers. Proc. Roy. Soc., (London), A 98, 174

8. Kramers, H., 1946, Heat transfer from spheres to flowing media.

9. Lin, J. T., and Binder, A., (to be published in 1967), Laboratory investigation of mountain lee waves. CSU C.E. Dept.

10. Plate, E. J., and Cermak, J. E., 1963, Micrometeorological wind tunnel facility. CSU C.E. Dept.

11. Sato, H., 1937, Non-linearity and inversion effects of hot-wire anemometer on the mean and fluctuating velocity measurements at low-wind speed. Rep. Inst. Sc. Technol Univ., Tokoyo,

Unclassified

Security Classification

DOCUMENT CONTROL DATA - R&D

(Security classification of title, body of abstract and indexing annotation must be entered when the overall report is classified)

1. ORIGINATING ACTIVITY (Corporate author) Fluid Mechanics Program, College of Engineering Colorado State University, Fort Collins, Colo.	2a. REPORT SECURITY CLASSIFICATION Unclassified 2b. GROUP

3. REPORT TITLE

ULTRA-LOW-SPEED ANEMOMETRY

4. DESCRIPTIVE NOTES (Type of report and inclusive dates)

Technical Report

5. AUTHOR(S) (Last name, first name, initial)

Kung, Robin J., and G. J. Binder

6. REPORT DATE	7a. TOTAL NO. OF PAGES	7b. NO. OF REFS
June 1967	114	11

8a. CONTRACT OR GRANT NO. DA-AMC-28-043-65-G20 b. PROJECT NO. 2246 c. d.	9a. ORIGINATOR'S REPORT NUMBER(S) CER66-67RJK49 9b. OTHER REPORT NO(S) (Any other numbers that may be assigned this report)

10. AVAILABILITY/LIMITATION NOTICES

Distribution of this document is unlimited.

11. SUPPLEMENTARY NOTES	12. SPONSORING MILITARY ACTIVITY
	U.S. Army Materiel Command

13. ABSTRACT

An investigation of low-speed (0-2 ft/sec) anemometers is presented. First the design, the characteristics and the calibration of a very low-speed micro wind tunnel are described. Then the principle, operation and performance of three different anemometers at these low speeds are discussed. These instruments are: 1) hot-spot anemometer, based on the measurement of the travelling time of a hot cloud, 2) drag anemometer which consists of a small plate mounted to the moving coil mechanism of a micro-ammeter, 3) constant temperature hot-wire anemometer. The comparison of the merits and disadvantages of these instruments shows that in most instances the hot-wire anemometer is superior to the two other anemometers.

DD FORM 1 JAN 64 1473

Unclassified

Security Classification

14. KEY WORDS	LINK A		LINK B		LINK C	
	ROLE	WT	ROLE	WT	ROLE	WT
Anemometer Wind tunnel Very-low velocities Theory Instrumentation Calibration Sensitivity Fluid mechanics						

INSTRUCTIONS

1. ORIGINATING ACTIVITY: Enter the name and address of the contractor, subcontractor, grantee, Department of Defense activity or other organization *(corporate author)* issuing the report.

2a. REPORT SECURITY CLASSIFICATION: Enter the overall security classification of the report. Indicate whether "Restricted Data" is included. Marking is to be in accordance with appropriate security regulations.

2b. GROUP: Automatic downgrading is specified in DoD Directive 5200.10 and Armed Forces Industrial Manual. Enter the group number. Also, when applicable, show that optional markings have been used for Group 3 and Group 4 as authorized.

3. REPORT TITLE: Enter the complete report title in all capital letters. Titles in all cases should be unclassified. If a meaningful title cannot be selected without classification, show title classification in all capitals in parenthesis immediately following the title.

4. DESCRIPTIVE NOTES: If appropriate, enter the type of report, e.g., interim, progress, summary, annual, or final. Give the inclusive dates when a specific reporting period is covered.

5. AUTHOR(S): Enter the name(s) of author(s) as shown on or in the report. Enter last name, first name, middle initial. If military, show rank and branch of service. The name of the principal author is an absolute minimum requirement.

6. REPORT DATE: Enter the date of the report as day, month, year; or month, year. If more than one date appears on the report, use date of publication.

7a. TOTAL NUMBER OF PAGES: The total page count should follow normal pagination procedures, i.e., enter the number of pages containing information.

7b. NUMBER OF REFERENCES: Enter the total number of references cited in the report.

8a. CONTRACT OR GRANT NUMBER: If appropriate, enter the applicable number of the contract or grant under which the report was written.

8b, 8c, & 8d. PROJECT NUMBER: Enter the appropriate military department identification, such as project number, subproject number, system numbers, task number, etc.

9a. ORIGINATOR'S REPORT NUMBER(S): Enter the official report number by which the document will be identified and controlled by the originating activity. This number must be unique to this report.

9b. OTHER REPORT NUMBER(S): If the report has been assigned any other report numbers *(either by the originator or by the sponsor)*, also enter this number(s).

10. AVAILABILITY/LIMITATION NOTICES: Enter any limitations on further dissemination of the report, other than those imposed by security classification, using standard statements such as:

(1) "Qualified requesters may obtain copies of this report from DDC."

(2) "Foreign announcement and dissemination of this report by DDC is not authorized."

(3) "U. S. Government agencies may obtain copies of this report directly from DDC. Other qualified DDC users shall request through
________________________."

(4) "U. S. military agencies may obtain copies of this report directly from DDC. Other qualified users shall request through
________________________."

(5) "All distribution of this report is controlled. Qualified DDC users shall request through
________________________."

If the report has been furnished to the Office of Technical Services, Department of Commerce, for sale to the public, indicate this fact and enter the price, if known.

11. SUPPLEMENTARY NOTES: Use for additional explanatory notes.

12. SPONSORING MILITARY ACTIVITY: Enter the name of the departmental project office or laboratory sponsoring *(paying for)* the research and development. Include address.

13. ABSTRACT: Enter an abstract giving a brief and factual summary of the document indicative of the report, even though it may also appear elsewhere in the body of the technical report. If additional space is required, a continuation sheet shall be attached.

It is highly desirable that the abstract of classified reports be unclassified. Each paragraph of the abstract shall end with an indication of the military security classification of the information in the paragraph, represented as *(TS)*, *(S)*, *(C)*, or *(U)*.

There is no limitation on the length of the abstract. However, the suggested length is from 150 to 225 words.

14. KEY WORDS: Key words are technically meaningful terms or short phrases that characterize a report and may be used as index entries for cataloging the report. Key words must be selected so that no security classification is required. Identifiers, such as equipment model designation, trade name, military project code name, geographic location, may be used as key words but will be followed by an indication of technical context. The assignment of links, rules, and weights is optional.

MINIMUM BASIC DISTRIBUTION LIST FOR USAMC SCIENTIFIC AND TECHNICAL REPORTS IN METEOROLOGY AND ATMOSPHERIC SCIENCES

Commanding General (1)
U. S. Army Materiel Command
Attn: AMCRD-RV-A
Washington, D. C. 20315

Commanding General (1)
U. S. Army Electronics Command
Attn: AMSEL-EW
Fort Monmouth, New Jersey 07703

Commanding General (1)
U. S. Army Test and Evaluation Command
Attn: NBC Directorate
Aberdeen Proving Ground, Maryland 21005

Commanding Officer (1)
U. S. Army Ballistics Research Laboratories
Attn: AMXBR-IA
Aberdeen Proving Ground, Maryland 21005

Chief, Atmospheric Physics Division (2)
Atmospheric Sciences Laboratory
U. S. Army Electronics Command
Fort Monmouth, New Jersey 07703

U. S. Army Munitions Command (1)
Attn: Irving Solomon
Operations Research Group
Edgewood Arsenal, Maryland 21010

Commanding Officer (1)
U. S. Army Dugway Proving Ground
Attn: Meteorology Division
Dugway, Utah 84022

Commanding Officer (1)
U. S. Army CDC, CBR Agency
Attn: Mr. N. W. Bush
Fort McClellan, Alabama 36205

Commanding General (1)
U. S. Army Test and Evaluation Command
Attn: AMSTE-EL
Aberdeen Proving Ground, Maryland 21005

Commandant (1)
U. S. Army Signal School
Attn: Meteorological Department
Fort Monmouth, New Jersey 07703

Assistant Chief of Staff for Force Development (1)
CBR Nuclear Operations Directorate
Department of the Army
Washington, D. C. 20310

Director (1)
Atmospheric Sciences Programs
National Sciences Foundation
Washington, D. C. 20550

Assistant Secretary of Defense (1)
Research and Engineering
Attn: Technical Library
Washington, D. C. 20301

R. A. Taft Sanitary Engineering Center (1)
Public Health Service
4676 Columbia Parkway
Cincinnati, Ohio

Dr. Hans A. Panofsky (1)
Department of Meteorology
The Pennsylvania State University
University Park, Pennsylvania

Commanding General (1)
U. S. Continental Army Command
Attn: Reconnaissance Branch ODCS for Intelligence
Fort Monroe, Virginia 23351

Commander (1)
Air Force Cambridge Research Laboratories
Attn: CRZW
1065 Main Street
Waltham, Massachusetts

President (1)
U. S. Army Artillery Board
Fort Sill, Oklahoma 73504

National Center for Atmospheric Research (1)
Attn: Library
Boulder, Colorado

Dr. J. E. Cermak, Head (15)
Fluid Mechanics Program
Colorado State University
Fort Collins, Colorado 80521

Author (1)

Chief of Research and Development (1)
Department of the Army
Attn: CRD/M
Washington, D. C. 20310

Commanding General (1)
U. S. Army Missile Command
Attn: AMSMI-RRA
Redstone Arsenal, Alabama 35809

Commanding General (1)
U. S. Army Natick Laboratories
Attn: Earth Sciences Division
Natick, Massachusetts 01762

Director, U. S. Army Engineer (1)
Waterways Experiment Station
Attn: WES-FV
Vicksburg, Mississippi 39181

Chief, Atmospheric Sciences Research Division (5)
Atmospheric Sciences Laboratory
U. S. Army Electronics Command
Fort Huachuca, Arizona 85613

Commanding Officer (1)
U. S. Army Frankford Arsenal
Attn: SMUFA-1140
Philadelphia, Pennsylvania 19137

Commandant (1)
U. S. Army Artillery and Missile School
Attn: Target Acquisition Department
Fort Sill, Oklahoma 73504

Commanding General (1)
U. S. Army Electronics Proving Ground
Attn: Field Test Department
Fort Huachuca, Arizona 85613

Commanding General (1)
U. S. Army Test and Evaluation Command
Attn: AMSTE-BAF
Aberdeen Proving Ground, Maryland 21005

Office of Chief Communications - Electronics (1)
Department of the Army
Attn: Electronics Systems Directorate
Washington, D. C. 20315

Chief of Naval Operations (1)
Department of the Navy
Attn: Code 427
Washington, D. C. 20350

Director (1)
Bureau of Research and Development
Federal Aviation Agency
Washington, D. C. 20553

Director of Meteorological Systems (1)
Office of Applications (FM)
National Aeronautics and Space Administration
Washington, D. C. 20546

Director (1)
Atmospheric Physics and Chemistry Laboratory
Environmental Science Services Administration
Boulder, Colorado

Andrew Morse (1)
Army Aeronautical Activity
Ames Research Center
Moffett Field, California 94035

Commanding Officer (2)
U. S. Army Cold Regions Research and Engineering Laboratories
Attn: Environmental Research Branch
Hanover, New Hampshire 03755

Mr. Ned L. Kragness (1)
U. S. Army Aviation Materiel Command
SMOSM-E
12th and Spruce Streets
Saint Louis, Missouri 63166

Commanding Officer, U. S. Army (1)
Artillery Combat Development Agency
Fort Sill, Oklahoma 73504

Commander, USAR Air Weather Service (MATS) (1)
Attn: AWSSS/TIPD
Scott Air Force Base, Illinois

Dr. John Bogusky (1)
7310 Cedardale Drive
Alexandria, Virginia 22308

Commanding General (1)
U. S. Army Combat Development Command
Attn: CDCMR-E
Fort Belvoir, Virginia 22060

Commanding General (1)
U. S. Army Munitions Command
Attn: AMSMU-RE-R
Dover, New Jersey 07801

Commanding Officer (1)
U. S. Army Ballistics Research Laboratories
Attn: AMXBR-B
Aberdeen Proving Ground, Maryland 21005

Director (2)
Atmospheric Sciences Laboratory
U. S. Army Electronics Command
Fort Monmouth, New Jersey 07703

Chief, Atmospheric Sciences Office (2)
Atmospheric Sciences Laboratory
U. S. Army Electronics Command
White Sands Missile Range, New Mexico 88002

Commanding Officer (1)
U. S. Army Picatinny Arsenal
Attn: SMUPA-TV-3
Dover, New Jersey 07801

Commanding Officer (1)
U. S. Army Communications - Electronics Combat Development Agency
Fort Monmouth, New Jersey 07703

Commanding General (1)
Deseret Test Center
Attn: Design and Analysis Division
Fort Douglas, Utah 84113

Commandant (1)
U. S. Army CBR School Micrometeorological Section
Fort McClellan, Alabama 36205

Assistant Chief of Staff for Intelligence (1)
Department of the Army
Attn: ACSI-DERSI
Washington, D. C. 20310

Officer in Charge (1)
U. S. Naval Weather Research Facility
U. S. Naval Air Station, Building 4-28
Norfolk, Virginia 23500

Chief, Fallout Studies Branch (1)
Division of Biology and Medicine
Atomic Energy Commission
Washington, D. C. 20545

Director (1)
U. S. Weather Bureau
Attn: Librarian
Washington, D. C. 20235

Dr. Albert Miller (1)
Department of Meteorology
San Jose State College
San Jose, California 95114

Mrs. Francis L. Wheedon (1)
Army Research Office
3045 Columbia Pike
Arlington, Virginia 22201

Commander (1)
Air Force Cambridge Research Laboratories
Attn: CRXL
L. G. Hanscom Field
Bedford, Massachusetts

Harry Moses, Asso. Meteorologist (1)
Radiological Physics Division
Argonne National Laboratory
9700 S. Cass Avenue
Argonne, Illinois 60440

Defense Documentation Center (20)
Cameron Station
Alexandria, Virginia 22314

Office of U. S. Naval Weather Service (1)
U. S. Naval Air Station
Washington, D. C. 20390

Dr. Gerald Gill (1)
University of Michigan
Ann Arbor, Michigan 48103